Acoustically Targeted Gene Delivery for Non-invasive Neuroengineering

Thesis by

Hongyi Richard Li

In Partial Fulfillment of the Requirements for

the degree of

Doctor of Philosophy

CALIFORNIA INSTITUTE OF TECHNOLOGY

Pasadena, California

2025

(Defended September 12, 2025)

Hongyi Richard Li
ORCID: 0000-0001-6970-0230

ACKNOWLEDGEMENTS

It all started in that windless summer night, when Steven Spielberg's Jurassic Park planted a seed of idea in a naive six-year-old from the fast-rising China, that was eagerly trying to catch up to the world. Besides the visual marvels, what struck the young kid the hardest was how the miniscule can leverage the immensity. The discovery as tiny as a mosquito can give rise to a prodigious enterprise; and the molecules as microscopic as DNA can instruct the resurrection of the largest living-thing ever walked on this planet. It is the ever-evolving science and technology that enables the minute to achieve greatness. Since then, the boy has developed a firm belief that even as a kid from a distant corner of the world, he could and should weave a noticeable mark on the fabric of this world, through the leverage of contribution in scientific and technological advancement.

Twenty-five years later, the boy is poised to defend his PhD degree, far from home, trying to weave a mark in his own life first. It has been a long march – and I am forever grateful for all those who have been part of the journey.

To begin with, I would like to extend my deepest gratitude for my advisor, Professor Mikhail Shapiro. Mikhail has been more than an academic advisor to me. My time at Caltech started with a bumpy ride of rotations. At the end of the long, dark tunnel, holding the torch to guide me through was Mikhail. He trusted in my potential—especially in times when I doubted myself—and this scene repeated itself many times in the following years, which eventually made this thesis possible. Mikhail is a man of focus and consistency; he is like a mirror, from which almost every academic can reflect on characters they lack. Persistence and organization were rare to me – but over the years Shapiro lab nurtured me on both. In moments of doubt, he offered clarity; in times of struggle, encouragement; and in achievement, genuine exhilaration. There have been too many occasions when I was cornered by failure, confusion, or success, joy, "what would Mikhail do?" always gives me an answer that keeps me going. I am glad that I was able to spend probably my most important formative years in a lab whose leader truly led by example, led by aspiration, led by vision. For all of this and more, I am deeply grateful. Thank you, Mikhail.

I am profoundly grateful to Professor Jerzy Szablowski, whose mentorship has been one of the most formative influences on my PhD journey. From the very beginning, during my rotation in his lab, Jerzy offered a space that was both intellectually demanding and deeply supportive—an environment that pushed me to grow at every level. He later became the major advisor on my thesis project, and his role in my development as a scientist, engineer, and thinker cannot be overstated. Jerzy not only taught me how to conduct rigorous research and pursue meaningful questions with technical precision, but also how to think critically, communicate clearly, and uphold the values that define good science. His feedback was always incisive, and his standards—unapologetically high—motivated me to rise to challenges I didn't always believe I could meet. But what made Jerzy's mentorship truly exceptional was that it went far beyond the scientific. Through his example, I learned what it means to be a reliable and thoughtful mentor: someone who is patient but exacting, honest yet encouraging. Jerzy taught me how to be a stern thinker: to avoid shortcuts, question assumptions, and hold myself to a standard that is internally driven rather than externally rewarded. He also modeled what it means to be a true technologist—someone who doesn't simply develop tools, but understands them deeply and builds with a sense of purpose, clarity, and long-term vision. Working with Jerzy has left an indelible mark on my academic and personal growth. His mentorship shaped not only the trajectory of my thesis, but also the foundation of how I hope to approach research, collaboration, and mentorship in the years to come. For his trust, his time, and his unwavering commitment to my growth, I offer my heartfelt thanks.

I am sincerely grateful to the mentors who first introduced me to the world of biomedical engineering and research during my undergraduate years. Dr. Sandor Kovacs sparked my fascination with biophysics and showed me the beauty of extracting meaning from physiological signals. Dr. Steve George welcomed me into the world of tissue engineering, where I first learned the value of precision, patience, and scientific curiosity at the bench. And Dr. Himadri Pakrasi guided me through the interdisciplinary challenges of synthetic biology and iGEM, where I discovered the excitement of building and collaborating on real-world research problems. Each of them offered me not just a project, but an opportunity—to

explore, to question, and to grow. Their mentorship helped shape my early identity as a researcher and set me on the path that led to this thesis.

I am deeply thankful to my friends and colleagues in the Shapiro Lab, whose camaraderie and collaboration made the journey of this thesis both intellectually stimulating and personally meaningful. Working alongside such talented, creative, and generous individuals has been a privilege. From late-night experiments to spontaneous whiteboard brainstorms, from shared frustrations to collective celebrations, the lab has been a constant source of support, inspiration, and joy. I am especially grateful for the spirit of teamwork and curiosity that defines the lab, and for the friendships that grew out of it—relationships that I know will last far beyond the scope of this thesis. In particular, I would like to express my gratitude to (in alphabetical order) Avinoam Bar-Zion, Pierina Barturen-Larrea, Marjorie Buss, Josh Chen, Ernesto Criado-Hidalgo, Ishaan Dev, Hongsun Guo, Baptiste Heiles, Robert Hurt, Zhiyang Jin, Ahyoung Kim, Hengyu Li, Ann Liu, Bill Ling, Liz Hughes, Kaiwen Luo, Dina Malounda, Rosmelle Melgar, Alen Pavlič, Julio Revilla, Erik Schrunk, Liang She, Hao Shen, Margaret Swift, Reid Vassallo, Di Wu, Akanksha Yadav, Yuxing Yao, and most importantly, my dear brother, George Daghlian. The Shapiro Lab has been more than just a workplace; it has been a community that has shaped me as a scientist and as a person.

I would be remiss not to thank my four furry companions—Biscuit, Cookie, Latte, and Oreo—who have been with me through the highs and lows of this long journey. Their quiet (and sometimes not-so-quiet) presence brought comfort during late-night writing sessions, endless debugging marathons, and moments of stress and solitude. Whether it was a well-timed purr, a warm nap on my lap, or an unapologetic walk across my keyboard, they reminded me to pause, breathe, and laugh. In their own way, they offered companionship, joy, and a sense of home that made even the most difficult days feel a little softer. I'm lucky to have shared this chapter of life with them.

With all the warmth in my heart, I want to thank my beloved wife, Daisy, whose unwavering support has carried me through every stage of this journey. For the past seven years, she has been my constant source of strength, balance, and encouragement—through late nights, long

experiments, unexpected setbacks, and moments of doubt. Her belief in me never wavered, even when I struggled to believe in myself. Daisy's patience, resilience, and quiet wisdom have grounded me, reminding me of what truly matters and why this work is worth doing. Her love has been my anchor and my light, and I could not have reached this milestone without her. She might not know a single I did here; she understands everything I did here - This thesis is as much hers as it is mine.

Above all, I am deeply grateful to my parents, whose vision, strength, and unconditional support have guided me throughout my life. When I made the bold decision to leave home at the age of 16 to pursue educational opportunities in the United States, they stood firmly behind me. It could not have been easy for them to watch their child embark alone on such an uncertain path so far from home, but their belief in my potential never wavered. Their courage matched my own, and their quiet sacrifices gave me the freedom to chase my aspirations without hesitation. They instilled in me a deep respect for learning, a commitment to perseverance, and the courage to embrace the unknown. Every step I've taken on this journey has been grounded in the values they taught me and the love they have never failed to give. I owe more to them than words can express.

Lastly, I would like to thank the marvelous era of our time. To all the engineers of our time, to all the entrepreneurs of our time, to all the technologists of our time. There is still plenty of room in the bottom, and there is still plenty of room up and above. It leaves us little time to contemplate the irreversible changes to the world we just made – the frontiers are forever inches ahead of us.

What a time to be alive.

Per Aspera Ad Astra.

ABSTRACT

Noninvasive, spatially targeted gene delivery to the brain holds tremendous promise for addressing some of the most pressing neurological and psychiatric conditions of our time, including Parkinson's disease, treatment-resistant epilepsy, obsessive-compulsive disorder, and addictions. While adeno-associated viruses (AAVs) are the leading vectors for gene therapy in the state of the art, their clinical translation is hindered by the need for invasive injections to achieve site-specific delivery in the brain. Over the past two decades, focused ultrasound blood-brain barrier opening (FUS-BBBO) has emerged as a compelling alternative — enabling targeted entry of biomolecules, nanoparticles, and even small viral vectors like AAVs from the bloodstream into the brain without surgical intervention. Yet, natural AAV serotypes have shown only modest success with this method, often displaying low transduction efficiency and undesirable off-target expression in peripheral organs.

To overcome these limitations, we have developed a new framework for acoustically targeted gene delivery — a noninvasive, spatially and cell-type-specific approach for delivering genetic material to the brain. In this thesis, I will describe how we harnessed high-throughput *in vivo* directed evolution to engineer AAV variants optimized for neuronal transduction specifically at the site of ultrasound targeting. In rodent models, these newly evolved vectors demonstrate significantly improved performance — achieving efficient, localized gene delivery to neurons while minimizing peripheral expression. Building on these successes, we advanced the platform toward clinical relevance by extending our evolutionary screening to non-human primates (NHPs). This allowed us to identify AAV variants with enhanced translational potential and establish a strong foundation for future studies in human clinical trials.

In the final part of this thesis, I will showcase how these engineered AAVs can be further empowered by combining them with acoustic reporter genes — specifically, gas vesicle (GV) proteins — enabling non-invasive imaging of molecular activity deep within the brain. Using this powerful platform, we have also developed a novel therapeutic strategy for treating opioid addiction, in which biomolecular ultrasound coalesces with chemogenetic

neuromodulation. Taken together, I hope to convince you that the technique of ultrasound-based acoustically targeted gene delivery, paired with engineered delivery vectors, unlocks a new frontier in non-invasive neurotherapeutics and brings us one step closer to precise, personalized neuroengineering in interfacing the human brain.

PUBLISHED CONTENT AND CONTRIBUTIONS

Li, H. R., Harb, M., Heath, J. E., Trippett, J. S., Shapiro, M. G., & Szablowski, J. O. (2024). Engineering viral vectors for acoustically targeted gene delivery. *Nature Communications*, 15(1). https://doi.org/10.1038/s41467-024-48974-y

H.L. conceived the study, performed the experiments, data analysis, and prepared the manuscript.

Rabut, C., Yoo, S., Hurt, R. C., Jin, Z., **Li, H. R.**, Guo, H., Ling, B., & Shapiro, M. G. (2020). Ultrasound technologies for imaging and modulating neural activity. *Neuron*, 108(1), 93–110. https://doi.org/10.1016/j.neuron.2020.09.003

H.L. participated in the writing of the manuscript and the preparation of figures.

Rabut, C., Daghlian, G. H., Barturen-Larrea, P., **Li, H. R.**, Bruegge, R. V., Jones, R. M., Malounda, D., Pinton, G. F., & Shapiro, M. G. (2024). Acoustic Tumor Paint for Real-Time Imaging, Surgical Guidance and Recurrence Monitoring of Brain Tumors with Ultrasound. *bioRxiv*. https://doi.org/10.1101/2024.12.22.629782

H.L. participated in experiments design, data collection and analysis, and the preparation of figures.

Vassallo, R., Ling, B., Criado-Hidalgo, E., Robinson, N., Schrunk, E., Liu, A., Daghlian, G., **Li, H. R.**, Swift, M. B., Mannar, D., Malounda, D., Goldenberg, S. L., Salcudean, S. E., Shapiro, M. G., Black, P. C., & Cox, M. E. (2025). A modular method for rapidly prototyping targeted gas vesicle protein nanoparticles (p. 2025.08.06.668980). *bioRxiv*. https://doi.org/10.1101/2025.08.06.668980

H.L. participated in data collection and analysis, and the preparation of figures.

TABLE OF CONTENTS

LIST OF ILLUSTRATIONS AND/OR TABLES

Number *Page*

Chapter 1

INTRODUCTION

The ability to interrogate and manipulate neural activity at brain-wide scales remains a critical frontier in neurotechnology. Conventional modalities such as electrophysiology and optical imaging, while offering high spatiotemporal resolution, are fundamentally constrained by tissue scattering, invasiveness, and limited depth penetration, which impede their scalability to whole-brain applications in both animal models and humans. Ultrasound, by contrast, exhibits advantageous propagation characteristics in biological tissue, with minimal scattering and attenuation, enabling penetration through the intact brain and, in some regimes, through the skull. Its intrinsic spatiotemporal resolution—on the order of ~100 μm and ~1 ms—makes it uniquely suited for noninvasive interrogation and modulation of large-scale neural dynamics. These physical advantages have catalyzed the development of a diverse set of ultrasound-based neurotechnologies, including functional ultrasound imaging (fUS) for high-resolution hemodynamic mapping, focused ultrasound (FUS) for targeted neuromodulation, and ultrasound-mediated blood-brain barrier opening for localized pharmacological delivery. Beyond these applications, recent advances in molecular engineering have enabled coupling of ultrasound to genetically defined neural populations, giving rise to novel approaches such as biomolecular acoustic reporters for functional imaging and sonogenetics for cell-type-specific neuromodulation. Collectively, these innovations position ultrasound as a versatile and scalable modality for brain-wide neural interfacing.

Sections of this chapter have been adapted from:

Rabut, C., Yoo, S., Hurt, R. C., Jin, Z., **Li, H. R.**, Guo, H., Ling, B., & Shapiro, M. G. (2020). Ultrasound technologies for imaging and modulating neural activity. *Neuron*, 108(1), 93–110. https://doi.org/10.1016/j.neuron.2020.09.003

1.1 Ultrasound: a Versatile Toolkit to Interfacing Neural Dynamics

Historically, major advances in neuroscience have been driven by the development of novel experimental methodologies. A broad array of techniques—including electrophysiological recording, histological analysis, optical imaging, magnetic resonance imaging (MRI), optogenetics, and chemogenetics—have each enabled new dimensions of insight into the structural and functional organization of neural circuits. Despite these advances, a critical methodological gap remains: existing tools largely fail to provide simultaneous access to neural activity and causality at brain-wide scales in behaving mammalian systems. This limitation poses a fundamental barrier to understanding distributed computations and long-range circuit dynamics underlying behavior. Furthermore, the majority of established modalities either require invasive access to the brain or rely on genetically encoded actuators and reporters, rendering them impractical or ethically untenable for application in humans. As a result, there remains an unmet need for technologies that can noninvasively monitor and modulate neural circuit dynamics across the entire brain with high spatiotemporal resolution, ideally in both animal models and human subjects.

The limitations of current neuroscience methods largely stem from the fundamental physical constraints that govern the interaction between different forms of energy and biological tissue (Marblestone et al., 2013; Piraner et al., 2017a). For example, extracellular electrical recordings of action potentials require electrodes to be positioned within ~200 μm of the target neurons, and the finite dimensions of electrode arrays impose trade-offs between spatial coverage and recording density *in vivo* (Marblestone et al., 2013). Optical techniques, which rely on visible or near-infrared light, are restricted by photon scattering, typically confining high-resolution imaging and stimulation to depths of less than ~1 mm in scattering

brain tissue (Ntziachristos, 2010). In the case of functional magnetic resonance imaging (fMRI), the inherently weak polarization of nuclear spins limits both signal-to-noise ratio and achievable spatial resolution. Noninvasive electromagnetic stimulation modalities, such as transcranial magnetic stimulation (TMS) or transcranial electric stimulation (tES), suffer from poor spatial specificity due to the diffusive nature of electric and magnetic field propagation through the skull and brain tissue. Nuclear imaging approaches employing radioactive probes are constrained by both the pharmacokinetics of tracer molecules and the spatial blurring introduced by positron emission or gamma decay path lengths. Finally, chemogenetic techniques, while cell-type specific, generally require invasive intracranial delivery to achieve anatomically localized control, thereby limiting their utility in large-scale or translational applications.

In contrast to other modalities, ultrasound (US) represents a form of mechanical energy that propagates efficiently through soft biological tissues with characteristic wavelengths on the order of ~100 μm at clinically relevant frequencies (Maresca et al., 2018a). This enables ultrasound-based techniques to image or deliver energy several centimeters into tissue with spatial resolution defined by the acoustic wavelength. Furthermore, the high propagation speed of sound in soft tissue (~1.5 km/s) supports temporal resolution on the sub-millisecond scale, a regime suitable for capturing fast physiological dynamics. These intrinsic advantages—deep tissue penetration, high spatiotemporal resolution, and favorable safety profile—have contributed to the widespread adoption of ultrasound imaging in clinical medicine. Its utility is further enhanced by its portability, real-time feedback capability, and relatively low cost compared to other imaging modalities. Beyond diagnostic applications, ultrasound is also unique among non-ionizing energy forms in its ability to be focused with millimeter-scale precision at depth. As a result, focused ultrasound (FUS) has emerged as a promising platform for noninvasive therapeutic interventions, including thermal ablation of tumors and targeted disruption of neural circuits, enabled by ongoing innovations in transducer array technology, phase control, and image-guided targeting systems (Escoffre and Bouakaz, 2016).

Over the past decade, ultrasound has rapidly gained prominence in neuroscience as the foundation for a suite of transformative technologies, spanning high-resolution hemodynamic imaging, molecular acoustic sensing, and noninvasive neuromodulation. While its entry into the field may appear abrupt, this recent wave of innovation is grounded in several decades of foundational advances in ultrasound physics, transducer engineering, and image reconstruction algorithms. These underlying technological developments have enabled the adaptation of ultrasound for neuroscience-specific applications, offering capabilities previously unattainable with conventional modalities. As the current ultrasound-based neurotechnologies quickly evolves, continued progress in acoustic hardware, computational modeling, contrast agent design, and non-invasive delivery are poised to further expand the landscape of brain imaging and modulation strategies.

1.2 Current Technologies for Neural Control and Gene Therapies in the Central Nervous System

Established molecular and physical neural intervention and gene therapy techniques include optogenetics, chemogenetics, ultrasonic neuromodulation or sonogenetics, and magnetogenetics. We will briefly discuss each of them below.

Optogenetics is among the most widely used methods for spatially- and cell type-selective control of neurons, but has significant limitations when applied to larger brain regions and larger animals. Light delivery usually requires invasive implantation of optical fibers, and it is often difficult to deliver enough light to cover the desired brain regions without damage or tissue heating (Pisanello et al., 2017 and Lin et al., 2013). As a result, multiple optical fibers may be required per region (Eriksson et al., 2022 and Stujenske et al., 2015), and the effects on brain function may be relatively modest (Zaaimi et al. 2022).

Classical chemogenetics tools allow neuromodulation to be performed without the need to deliver light or other physical stimuli. The most widely used class of chemogenetic constructs, designer receptors exclusively activated by designer drugs (DREADDs), are

GPCRs engineered to respond exclusively to a designer drugs (conventionally clozapine-N-oxide, or CNO). When DREADDs are expressed in specific neurons, this allows these neurons to be controlled by systemic administration of CNO with kinetics on the scale of minutes to hours (Armbruster et al. 2007). Recent work showed that CNO may act through back-metabolism into clozapine, which activates DREADDs at sub-clinical doses, suggesting that clozapine itself could be a selective chemogenetic effector with scope for clinical translation (Weston et al. 2019). Additional classes of chemogenetic receptors based on ion channels (Auffenberg et al. 2016) and GPCRs (Podewin et al. 2018) offer different kinetics and the potential to multiplex (Vardy et al., 2015 and Upright & Baxter, 2020). However, one of the major challenges in using chemogenetic tools is how to deliver the genes encoding them to relevant brain regions. The limited diffusion of virus from a single injection means that multiple injections are needed to cover a brain region in larger animals. Recent work in macaques involved ~50 viral injections per animal in the orbitofrontal cortex (Magnus et al., 2019).

Ultrasonic neuromodulation using frequencies of 250 kHz to a few MHz has been shown to directly elicit motor activity and electrical signals in several species (Yoo et al., 2022, Song et al., 2023, Lee et al., 2018, and Kamimura et al., 2016). However, we recently found that some of this activation could be due to indirect auditory effects (Sato et al, 2018). While it is believed that ultrasound can also produce direct modulation, this possibility and its underlying mechanisms are still under investigation. In contrast, the FUS-BBBO mediated nanotherapeutic gene delivery paradigm operates via a well-defined mechanism. In addition, other pharmacological methods coupled to ultrasound have been proposed. In one, focused ultrasound blood-brain barrier opening is followed (within ~ 1 hr) by systemic injection of GABA, which enters the brain at the site of opening to inhibit activity (Todd et al., 2019). In another, FUS is used to release propofol from circulating nanodroplets, resulting in local short-term inhibition (Airan et al., 2017). Compared to focused ultrasound blood-brain barrier opening mediated gene delivery, these methods do not require genetic modification. However, they require the application of FUS concomitantly with, or immediately prior to, behavioral testing, which burdens the experimental design, especially in larger animals

where accurate FUS requires MRI guidance. The same applies to emerging "sonogenetic" approaches (Yang et al. 2021). In addition, the inhibition produced by GABA and propofol is not cell type-selective.

Magnetogenetics uses magnetic fields, which can also be applied non-invasively. Several groups have reported technologies in which magnetic nanoparticles are used in combination with magnetic fields to activate temperature- or mechano-sensitive ion channels (Unda et al., 2024, Durent et al. 2017, and Hernández-Morales et al., 2024). However the mechanisms of fully genetic magnetogenetics are uncertain (Munshi et al. 2018), and actuation requires sophisticated equipment to apply the magnetic fields. The gene delivery techniques developed in our project could in the future be used in combination with magnetogenetic receptors.

1.3 Focused Ultrasound Enables Delivery of Targeted Nanotherapeutics and Neuromodulation

Ultrasound has been used as a tool for enhancing the targeted delivery of nanoscale therapeutic agents, leveraging its capacity to modulate tissue permeability, induce physical transformations in engineered delivery vehicles, and drive convective transport of materials across biological barriers. These mechanisms have been exploited to achieve spatially localized delivery of small molecules, nanoparticles, and viral vectors to a variety of tissues, including tumors (Nelson et al., 2002, Dromi et al., 2007, and Rapoport et al. 2019), the gastrointestinal tract (Schoellhammer et al., 2015), ocular tissues (Zderic et al., 2002), skeletal muscle (Dayton et al., 1999), and the central nervous system (Hynynen et al., 2001). In particular, focused ultrasound (FUS) has shown promise in transiently disrupting the blood-brain barrier (BBB), thereby enabling otherwise-impermeable agents to access neural tissue. The field has witnessed rapid growth, supported by a broad body of work that has been synthesized in recent comprehensive reviews covering ultrasound-mediated delivery across diverse contexts (Escoffre et al. 2015 and Mullick Chowdhury et al. 2017).

Targeted delivery to the brain presents a particularly formidable challenge due to both its complex cellular architecture and the presence of physiological barriers. The central nervous system (CNS) is organized into anatomically discrete regions, each comprising a heterogeneous array of cell types—including diverse neuronal subpopulations—that often lack unique molecular identifiers despite carrying out vastly different functions. For instance, morphologically similar neuronal phenotypes may mediate motor control, sensory processing, or higher-order cognition, depending on their anatomical localization and circuit connectivity. This functional heterogeneity underscores the necessity of both spatial and cellular specificity in brain-targeted interventions. Compounding this challenge is the blood-brain barrier (BBB), a specialized endothelial interface that tightly regulates molecular trafficking into the CNS. The BBB effectively excludes the vast majority of systemically administered compounds, including nanomaterials and biologics, thereby limiting the utility of conventional drug delivery strategies. Even when localized BBB disruption is achieved, further targeting precision is required to selectively engage desired cell types within the affected brain region (Lochhead & Thorne, 2011, Patel et al., 2011, Curtis et al., 2016 and Moyaert et al., 2023).

These challenges can be addressed by combining nanomaterials with focused ultrasound blood-brain barrier opening (FUS-BBBO). Focused ultrasound blood-brain barrier opening (FUS-BBBO) is a technique developed over the past ~20 years with the potential to overcome these limitations by providing a route to noninvasive, site-specific nanoparticle (including transgene-delivering vehicle) delivery to the brain (Thévenot et al., 2012, Wang et al., 2014, and Alonso et al., 2013, and Szablowski et al., 2018). In FUS-BBBO, ultrasound is focused through an intact human skull (Rezai et al., 2020 and Lipsman et al., 2018) to transiently loosen tight junctions in the BBB and allow for the passage of molecules from the blood into the targeted brain site (**Fig. 1-1a**). FUS-BBBO can target intravenously administered nanoparticles such as AAVs to millimeter-sized brain sites or cover large regions of the brain without tissue damage. These capabilities place FUS-BBBO in contrast with intracerebral injections, which are invasive and deliver genes to a single 2-3 millimeter-sized region per injection (Eldridge et al., 2015 and Upright & Baxter, 2020), consequently

requiring a large number of brain penetrations to cover major regions (e.g. an epileptogenic focus). At the same time, the spatial targeting capability of FUS-BBBO differentiates it from the use of spontaneously brain-penetrating engineered AAV serotypes, which lack spatial specificity (Chan et al., 2017). FUS-BBBO has been successfully used to open the BBB in human patients (Rezai et al., 2020 and Lipsman et al., 2018) and is moving toward FDA approval for indications focused on cross-BBB delivery of small molecules and biologics (**Fig. 1-1b**). Pioneering applications of this technology include the treatment of brain cancer (Carpentier et al., 2016) and neurodegenerative diseases (Lipsman et al., 2018, Baseri et al., 2012, and Burgess et al., 2015).

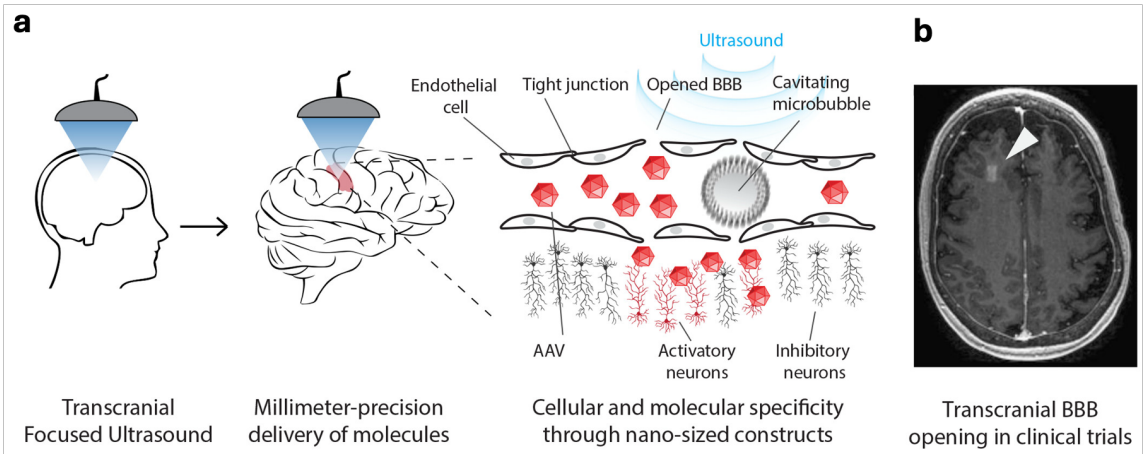

Figure 1-1 Ultrasound enhanced and triggered transport into the brain. (**a**) The human body contains thousands of types of molecules in different tissues. Restricting the region of delivery to a small subset of cells by focused ultrasound-enhanced delivery reduces off-target effects in nontargeted tissues. By combining ultrasound specificity with molecular engineering it is possible to both target the specific sites within the body and specific cells within the targeted site. Such specificity can be achieved by localized delivery of molecular constructs (AAV viral vectors, nanoparticles, proteins, small molecules) through the BBB into the brain. When microbubbles are injected into the bloodstream and insonated, they begin to oscillate (cavitate) and loosen tight junctions in the BBB, transiently, locally, and safely, improving transport from blood into the brain tissue. (**b**) Example of ultrasoundenhanced molecule delivery to the brain. The arrowhead points to the area of the BBB opened with ultrasound to allow the passage of a small molecule MRI contrast agent.

To integrate the spatial precision afforded by focused ultrasound (FUS) with the molecular, cell-type, and temporal specificity enabled by genetic engineering, we recently developed a method for noninvasive neuromodulation known as acoustically targeted chemogenetics, or ATAC (**Fig. 1-2a, b**) (Szablowski et al., 2018). This approach leverages FUS-induced blood-brain barrier opening (FUS-BBBO) to selectively deliver adeno-associated viral (AAV) vectors into specific brain regions (**Fig. 1-2c**). Upon transduction, these vectors drive the expression of engineered receptors in genetically specified neuronal populations, enabling remote control of their activity via a systemically administered, otherwise inert, brain-permeable small molecule (Sternson & Roth, 2014). AAV vectors, with diameters of approximately 20 nm, are well-suited for delivery following FUS-BBBO without inducing tissue damage and can be administered at doses sufficient to transduce over 50% of neurons in targeted regions (**Fig. 1-2d**). Cellular specificity is achieved through promoter-driven expression of the transgene, allowing for restriction to particular neuronal subtypes—such as excitatory glutamatergic neurons or dopaminergic neurons—depending on the promoter used (Dittgen et al., 2004). In the ATAC framework, the genetic payload consists of a designer G-protein coupled receptor (GPCR) that has been chemogenetically engineered to be unresponsive to endogenous ligands and selectively activated by a synthetic agonist. Following a single FUS-BBBO procedure and a subsequent several-week period for gene expression, the transduced neuronal population remains responsive to ligand administration for months (Szablowski et al., 2018), enabling temporally precise, repeatable, and noninvasive modulation of brain activity via peripheral drug delivery. In a proof-of-concept study,28 we used ATAC to noninvasively inactivate the mouse hippocampus (**Fig. 1-2d**) and inhibit the formation of associative memories (**Fig. 1-2e**).

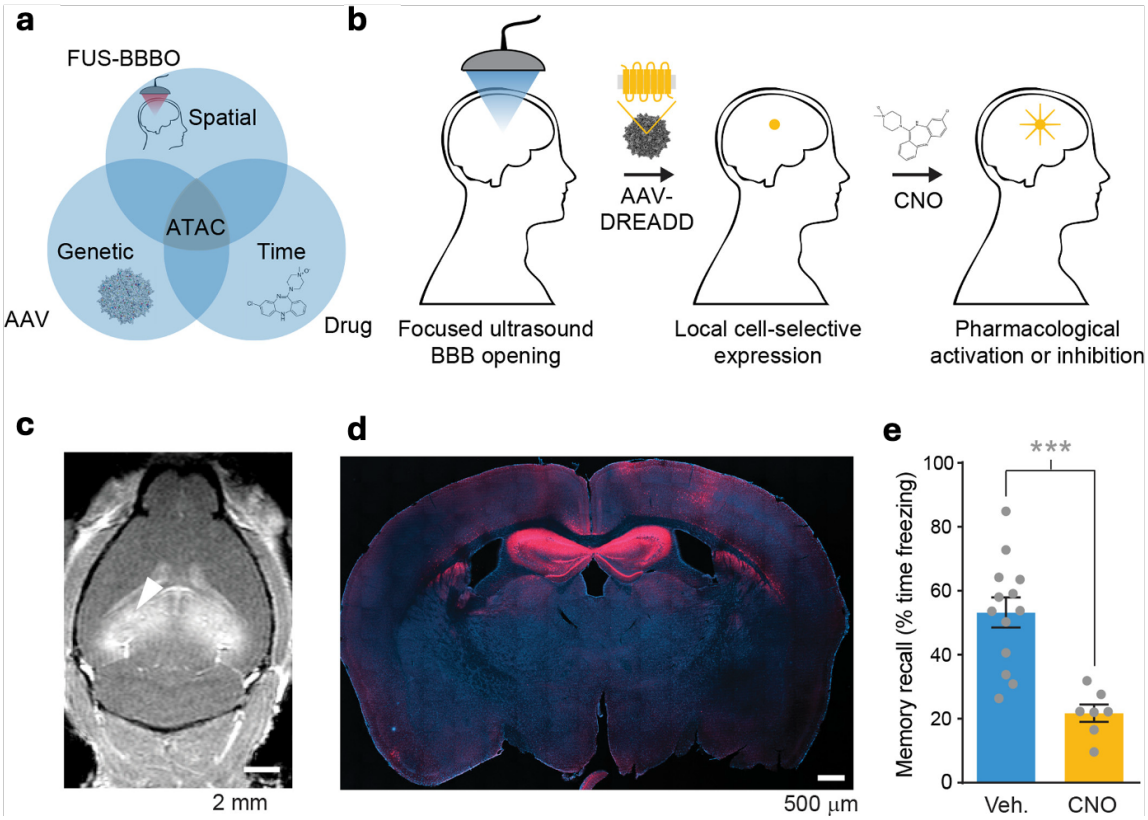

Figure 1-2 Acoustically targeted chemogenetics (ATAC). (**a**) ATAC combines FUS-BBBO, viral vector gene delivery, and chemogenetics to achieve fully noninvasive spatially, genetically, and temporally specific control cells in the brain. (**b**) In the ATAC process MRI-guided focused ultrasound reversibly opens the BBB to deliver viral vectors carrying chemogenetic receptors that can be activated specifically by a BBB-permeable ligand. (**c**) Safe and noninvasive opening of the BBB with FUS in hippocampus which was used to deliver viral vectors carrying DNA with a cell specific promoter and a chemogenetic receptor. The BBB opening is visualized by extravasation of gadolinium contrast agent in a T1-weighted MRI. (**d**) Gene expression of engineered chemogenetic receptors that respond to a specific BBB-permeable drug, as visualized by immunostaining (red). (**e**) The expression of engineered receptors allows subsequent pharmacological control of specific neurons and resulting behavior, such as memory recall.

1.4 Clinically Translatable Ultrasound-mediated Gene Therapy and Neural Control Entail Engineered Acoustically Targeted Gene Delivery

In proof-of-concept studies, FUS-BBBO has been used in rodents to introduce AAVs encoding reporter genes such as GFP (Thévenot, E. et al., 2012 and Wang et al., 2015), growth factors (Karakatsani et al., 2019) and optogenetic receptors. In our work, the delivery of chemogenetic receptors to the hippocampus provided the ability to modulate memory formation (Szablowski et al., 2018). Despite its promise, three critical drawbacks currently limit the potential of FUS-BBBO in research and therapy applications. First, while the BBB effectively prevents non-FUS-targeted regions of the brain from transduction by systemically administered AAV, peripheral organs allow AAV entry and consequently receive a high dose of the virus, which can lead to toxicity (*Nature Biotechnology*, 2020). Second, the relative inefficiency of AAV entry at the site of FUS-BBBO leads to the requirement of high doses of systemic AAVs, on the order of ~10^{10} viral particles per gram of body weight. While this magnitude has been used in recent clinical trials, it drives higher peripheral transduction and adds to the cost of potential therapies. Third, efficient delivery of AAV typically requires acoustic parameters below, but close to (Wang et al., 2015 and Sun et al., 2015), the threshold for brain tissue damage, reducing the margin for error in interventional planning.

These limitations arise from the fact that wild-type serotypes of AAV did not evolve to cross physically loosened biophysical barriers and are therefore not optimal for this purpose. In this project, we will address these limitations by developing new AAV serotypes specifically optimized for FUS-BBBO delivery. Capsid engineering techniques (Li & Samulski, 2020) in which mutations are introduced into viral capsid proteins have been used to enhance gene delivery properties such as tissue specificity (Chan et al., 2017, Gray et al., 2013, Tervo et al., 2016, and Li et al., 2024), immune evasion (Maheshri et al., 2006), or axonal tracing (Tervo et al., 2016). However, they have not yet been used to optimize viral vectors to work in conjunction with physical delivery mechanisms. Evidently, clinically translatable ultrasound-mediated gene therapy and neuromodulation is entailing engineered acoustically targeted gene delivery to the brain.

1.5 Thesis Organization

In the previous introduction section, we have recognized unmet needs of neurological gene therapy and neuromodulation in the brain, along with the limitations of the state of the art in today's neuroengineering technologies. To overcome these limitations, we have developed a new framework for acoustically targeted gene delivery — a noninvasive, spatially and cell-type-specific approach for delivering genetic material to the brain. In *Chapter 2*, I will describe how we harnessed high-throughput *in vivo* directed evolution to engineer AAV variants optimized for neuronal transduction specifically at the site of ultrasound targeting. In rodent models, these newly evolved vectors demonstrate significantly improved performance — achieving efficient, localized gene delivery to neurons while minimizing peripheral expression. Building on these successes, in *Chapter 3*, I will illustrate how we advanced the platform toward clinical relevance by extending our evolutionary screening to non-human primates (NHPs). This allowed us to identify AAV variants with enhanced translational potential and establish a strong foundation for future studies in human clinical trials.

In the final part of this thesis, in *Chapter 4*, I will showcase how these engineered AAVs can be further empowered by combining them with acoustic reporter genes — specifically, gas vesicle (GV) proteins — enabling noninvasive imaging of molecular activity deep within the brain. Using this powerful platform, we have also developed a novel therapeutic strategy for treating opioid addiction, in which biomolecular ultrasound coalesces with chemogenetic neuromodulation. Taken together, I hope to convince you that the technique of ultrasound-based acoustically targeted gene delivery, paired with engineered delivery vectors, unlocks a new frontier in noninvasive neurotherapeutics and brings us one step closer to precise, personalized neuroengineering in the human brain.

Chapter 2

PER VECTOREM, MENS SANATUR: ENGINEERING VIRAL VECTORS FOR ACOUSTICALLY TARGETED GENE DELIVERY

Sections of this chapter have been adapted from:

Li, H. R., Harb, M., Heath, J. E., Trippett, J. S., Shapiro, M. G., & Szablowski, J. O. (2024). Engineering viral vectors for acoustically targeted gene delivery. *Nature Communications*, 15(1). https://doi.org/10.1038/s41467-024-48974-y

2.1 Abstract

Targeted gene delivery to the brain is a critical tool for neuroscience research and has significant potential to treat human disease as therapeutic means. However, the site-specific delivery of common gene vectors such as adeno-associated viruses (AAVs) is typically performed via invasive injections, which limit its applicable scope of research and clinical applications. Alternatively, focused ultrasound blood-brain-barrier opening (FUS-BBBO), performed noninvasively, enables the site-specific entry of AAVs into the brain from systemic circulation. However, when used in conjunction with natural AAV serotypes, this approach has limited transduction efficiency and results in substantial undesirable transduction of peripheral organs. Here, we use high throughput in vivo selection to engineer new AAV vectors specifically designed for local neuronal transduction at the site of FUS-BBBO. The resulting vectors substantially enhance ultrasound-targeted gene delivery and neuronal tropism while reducing peripheral transduction, providing a more than ten-fold improvement in targeting specificity in two tested mouse strains. In addition to enhancing the only known approach to noninvasively target gene delivery to specific brain regions,

these results establish the ability of AAV vectors to be evolved for specific physical delivery mechanisms.

2.2 Introduction

Gene therapy is one of the most promising emerging approaches to treating human disease. Recently, a number of gene therapies were approved for clinical use to treat diseases such as blindness (Russell et al., 2017), muscular dystroprthehy (Mendell et al., 2017), and metabolic disorders (Gaudet et al., 2012) with Adeno-Associated Viral vectors (AAVs). Gene therapy could also potentially target brain disorders. Unfortunately, gene delivery to the brain remains a major challenge. The typical approach for the administration of such gene therapies involves a surgical injection directly into the brain parenchyma, which is invasive. Other studies show it may also be possible to achieve brain-wide gene delivery with systemic (Duque et al., 2009, Chan et al., 2017, and Deverman et al., 2016) or intrathecal injections (Gray et al., 2013). However, these approaches, while noninvasive, lack spatial precision and thus cannot target regionally defined neural circuits.

Focused ultrasound blood-brain barrier opening (FUS-BBBO) has the potential to overcome these limitations by providing a route to noninvasive, site-specific gene delivery to the brain (Alonso et al., 2013; Szablowski et al., 2018; Thévenot et al., 2012; and Wang et al., 2014, 2017). In FUS-BBBO ultrasound is focused through an intact skull (Lipsman et al., 2018; and Rezai et al., 2020) to transiently loosen tight junctions in the BBB and allow for the passage of AAVs from the blood into the targeted brain site. Other mechanisms of FUS-BBBO could include increased transcytosis (Sheikov et al., 2004) and decreased levels of efflux transporters (McMahon et al., 2017). FUS-BBBO can target intravenously administered AAVs to millimeter-sized brain sites or cover large regions of the brain without apparent tissue damage in the tested timeframes (Felix et al., 2021; and Nouraein et al., 2023). These capabilities place FUS-BBBO in contrast with intraparenchymal injections, which are invasive and deliver genes to a single 2–3 millimeter-sized region per injection (Eldridge et al., 2015; and Upright & Baxter, 2020), requiring a large number of brain penetrations to

cover larger regions of interest. At the same time, the spatial targeting capability of FUS-BBBO differentiates it from the use of spontaneously brain-penetrating engineered AAV serotypes which lack spatial specificity (Chan et al., 2017). In proof of concept studies, FUS-BBBO has been used in rodents to introduce AAVs encoding reporter genes such as GFP (Kofoed et al., 2022; Nouraein et al., 2023; Thévenot et al., 2012; and Wang et al., 2014), growth factors (Karakatsani et al., 2019), and optogenetic receptors (Wang et al., 2017). The delivery of chemogenetic receptors to the hippocampus provided the ability to modulate memory formation (Szablowski et al., 2018).

Despite its promise, three critical drawbacks currently limit the potential of FUS-BBBO in research and therapy applications. First, the BBB effectively limits the transduction of systemically administered naturally occurring AAVs in non-FUS-targeted regions. peripheral organs have endothelia that allow AAV entry and consequently receive a high dose of the virus, which could lead to toxicity ("High-dose AAV Gene Therapy Deaths," 2020). Second, the relative inefficiency of AAV entry at the site of FUS-BBBO have led published studies to use doses that were higher than those needed for direct intraparenchymal injections, which in the clinic typically range from 10^{10} to 10^{12} viral genomes (VGs) per site injected, compared to 10^{12}–10^{14} VGs per kilogram of body weight for intravenous route (Hudry & Vandenberghe, 2019). In our previous work, to achieve transduction efficiency comparable to such injections at 5×10^{8} VGs, we used 10^{10} VGs per gram of body weight intravenously with FUS-BBBO (Szablowski et al., 2018). The AAV9 doses used in other FUS-BBBO studies to date have ranged from 5×10^{8} to 1.67×10^{10} VGs per gram of body weight (Hsu et al., 2013; Kofoed et al., 2022; Szablowski et al., 2018; Thévenot et al., 2012; Wang et al., 2014; and McMahon et al., 2021). Lowering the viral doses would reduce the chances of peripheral toxicity, and the costs of potential therapies (Hudry & Vandenberghe, 2019).

We reasoned that these limitations arise from the fact that wild-type serotypes of AAV did not evolve to cross physically loosened biophysical barriers and are therefore not optimal for this purpose. We hypothesized that we could address these limitations by developing new

engineered viral serotypes specifically optimized for FUS-BBBO delivery. Capsid engineering techniques (Li & Samulski, 2020) in which mutations are introduced into viral capsid proteins have been used to enhance gene delivery properties such as tissue specificity (Chan et al., 2017; Deverman, B. E. et al. 2016; Marsic et al., 2014; Ojala et al., 2017; and Powell et al., 2016), immune evasion (Maheshri et al., 2006; and Ojala et al., 2017), or axonal tracing (Maheshri et al., 2006; Tervo et al., 2016; and Ojala et al., 2017). However, they have not yet been used to optimize viral vectors to work in conjunction with specific physical delivery mechanisms.

To test our hypothesis, we performed in vivo selection of mutagenized AAVs in mice in conjunction with FUS-BBBO (**Fig. 2-1**) by adapting a recently developed Cre-recombinase-based screening methodology (Deverman et al., 2016; Tervo et al., 2016; and Ojala et al., 2017). We identified 5 viral capsid mutants with enhanced transduction at the site of FUS-BBBO and not in the untargeted brain regions. We then performed detailed validation experiments comparing each of these mutants to the parent wild-type AAV, revealing a significant increase in on-target transduction efficiency, increased neuronal tropism, and a marked decrease in off-target transduction in peripheral organs, with an overall performance improvement of more than 10-fold. These results demonstrate the evolvability of AAVs for specific physical delivery methods.

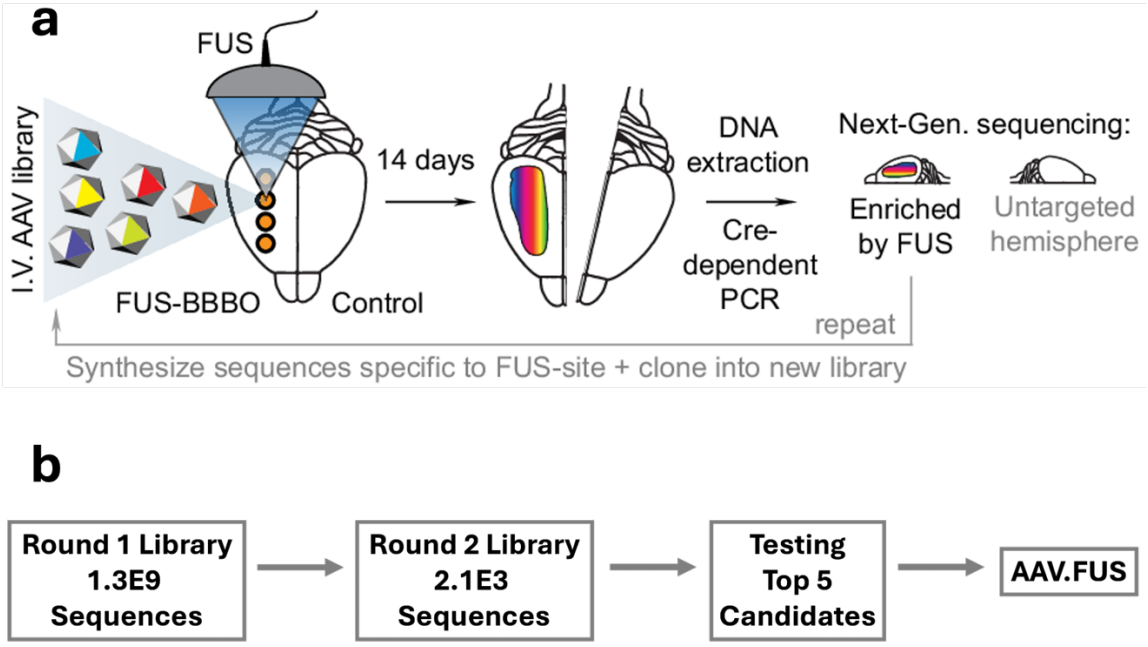

Figure 2-1 Screening methodology for generation of an AAV for improved site-specific noninvasive gene delivery to the brain. (**a**) Summary of the high-throughput screening and selection process. AAV library is administered intravenously (I.V.) and delivered to one brain hemisphere through FUS-BBBO. After 14 days mice are euthanized, their brain harvested, and the DNA from selected hemispheres is extracted. The DNA is then amplified by Cre-dependent PCR that enriches the viral DNA modified by Cre. In our case, neurons expressed Cre exclusively, and the Cre-dependent PCR enriched viral DNA of AAVs that transduced neurons. We subjected the obtained viral DNA to next-generation sequencing for the targeted hemisphere (round 1) or both targeted and control hemispheres (round 2). The process is then repeated for the next round (steps exclusive to round 2 indicated by the gray text). (**b**) Overall, 1.3 billion clones were screened in the first round, and 2098 clones in the second round of selection. Out of these clones, we selected 5 that were tested in low-throughput to yield AAV.FUS.3—a vector with enhanced FUS-BBBO gene delivery.

2.3 High-throughput *in vivo* Screening for AAVs with Efficient FUS-BBBO Transduction

To identify new AAV variants with improved FUS-BBBO-targeted transduction of neurons, we generated a library of viral capsid sequences containing insertions of 7 randomized amino acids between residues 588 and 589 of the AAV9 capsid protein (**Fig. 2-2a, b**). Such 7-mer insertions have been widely used to engineer AAVs with new properties (Chan et al., 2017; Deverman, B. E. et al. 2016; Li & Samulski, 2020; Maheshri et al., 2006; Marsic et al., 2014; Ojala et al., 2017; Powell et al., 2016; and Tervo et al., 2016). We chose AAV9 as a starting point due to its use in previous FUS-BBBO studies (Szablowski et al., 2018; Thévenot et al., 2012; and Wang et al., 2014) and superior transduction compared to other naturally occurring AAV serotypes (Kofoed et al., 2022).

To make the screening more efficient, we employed recombination-based AAV selection (Chan et al., 2017; and Ojala et al., 2017). This approach uses a Cre recombinase inside the cells to invert a fragment of the vector's DNA. (**Fig. 2-2a**). Because Cre is only present inside the cells, this approach allows for the identification of capsid variants that can enter the cells and deliver their DNA to the nucleus. These Cre-inverted DNA sequences can then be detected by PCR using primers specific to the inverted section of the DNA (**Fig. 2-2b**). Here, we used transgenic mice that expressed Cre in neurons, to select for AAVs with improved neuronal transduction (Chan et al., 2017; Deverman, B. E. et al. 2016; and Tervo et al., 2016).

To ensure we selected for AAVs transduced specifically within the FUS-BBBO-targeted areas we started with a library of 1.3×10^9 AAV candidates delivered to one hemisphere with FUS-BBBO (**Fig. 2-1a, b**). We then extracted the viral DNA that was delivered to the targeted hemisphere, and re-screened the extracted variants again to quantify specificity and efficiency of FUS-BBBO-mediated transduction. We targeted 4 sites within one hemisphere using magnetic resonance imaging (MRI) guidance, and confirmed the successful BBB opening through imaging of gadolinium contrast agent extravasation (**Fig. 2-3a**). We employed FUS parameters below tissue damage limits (Baseri et al., 2010; and Szablowski et al., 2018) (0.33 MPa at 1.5 MHz, 10 ms pulse length, 1 Hz repetition frequency, 0.22 µl

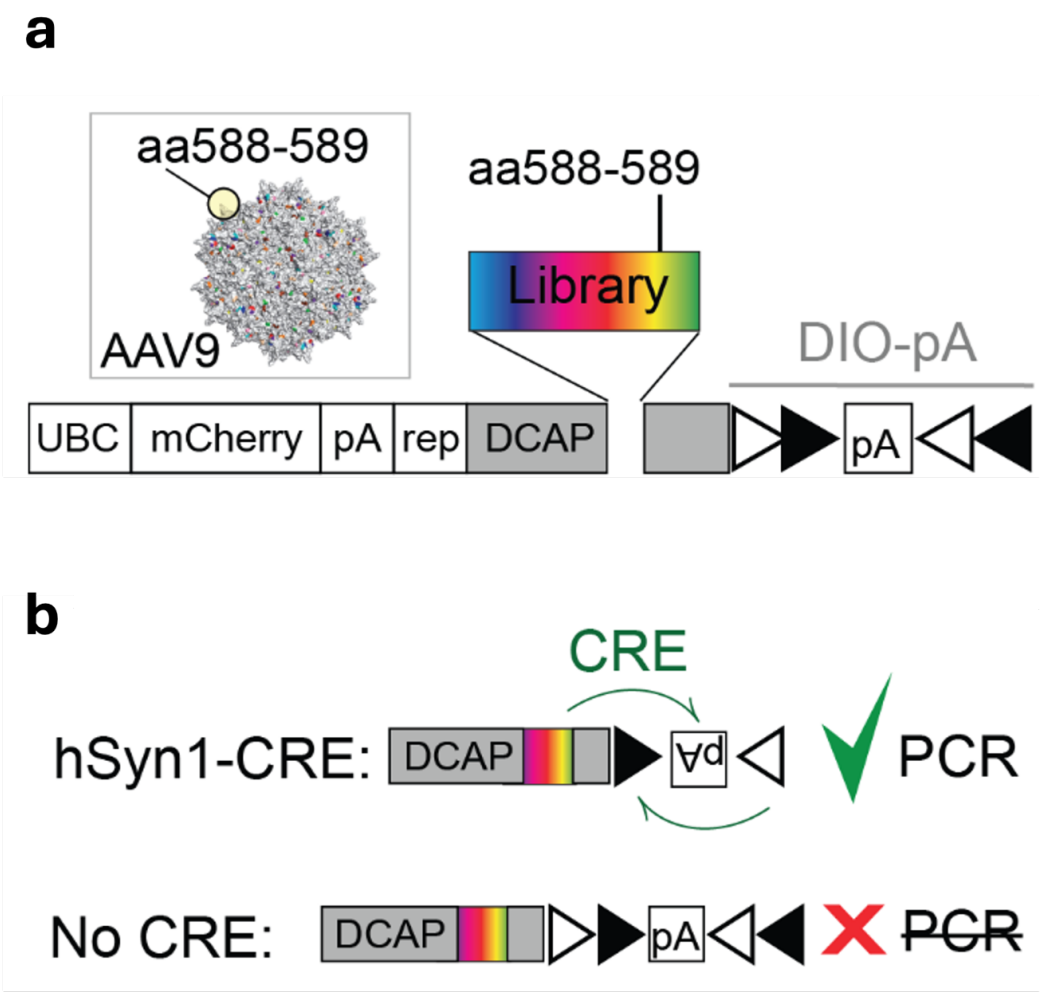

Figure 2-2 Construction of the AAV library and CRE-dependent PCR. (**a**) Randomized 21-basepair DNA fragment was inserted into the AAV9 capsid between amino acids 588 and 589, which resides at the exterior of an AAV capsid (inset). AAV capsid was produced within the AAV genome allowing for recovery of the capsid sequenced from transduced cells. The capsid coding sequence was followed by a polyA (pA) sequence flanked by a double-inverted floxed open reading frame (DIO). (**b**) The DIO sequence can be recombined and inverted in the presence of Cre enzyme. That sequence inversion can then be detected using PCR. Therefore, the DNA from AAVs that transduced cells expressing Cre can be amplified using a PCR reaction. In our study, we used hSyn1-Cre mice which express Cre selectively in neurons, and thus, we selected for neuron-transducing AAVs.

dose of microbubbles per gram of body weight). The AAV libraries were delivered intravenously (IV) immediately following FUS application to the brain at a dose of at a dose of 6.7×10^9 VGs per gram of body weight. We then allowed for 2 weeks of expression, euthanized the mice for tissue collection. Immediately after, we extracted the viral DNA from the brain and used Cre-dependent PCR amplification to selectively amplify the Cre-modified viral DNA, with a goal of finding AAVs selectively transducing neurons. We then sequenced the obtained DNA with next-generation sequencing (NGS) of the region of the 7-mer insertion and selected the 2098 most abundant sequences for subsequent evaluation. This screen selected for AAVs which could enter the neurons. However, these variants could not be quantitatively compared at this stage, due to large number of vectors in library compared to the total administered dose. As a result, each AAV clone existed in the library in a small copy number preventing statistically meaningful comparisons between each AAV candidates.

Instead, to quantitatively compare our 2098 down-selected capsid variants, we re-synthesized and packaged them as a new AAV library at a dose of 1.3×10^9 viral genomes per gram of body weight, corresponding to ~$1.5–3 \times 10^7$ viral genomes of each clone being injected into each mouse. In each of the two hSyn-CRE mice, we injected the AAV library intravenously and opened the BBB in one hemisphere using MRI-guided FUS as in round 1. Two weeks after treatment, we performed a series of procedures on each mouse. First, we removed the brain and separated the two hemispheres. We then extracted DNA from both the hemisphere that was targeted by the FUS and the hemisphere that was not. The DNA extract was amplified by the CRE-dependent PCR to enrich for viral genomes that transduced neurons. After FUS-BBBO delivery, DNA extraction, CRE-dependent PCR, and NGS, we recovered 1433 sequences.

To identify the most improved candidates, we examined their copy number in each hemisphere (**Fig. 2-3b**). To identify AAVs that selectively transduced sites that underwent FUS-BBBO, we first looked for variants that were at least 100-fold more represented in the targeted hemisphere relative to the untargeted hemisphere. From this list, we further selected candidates for which the 100-fold difference was maintained in both mice. To ensure that the

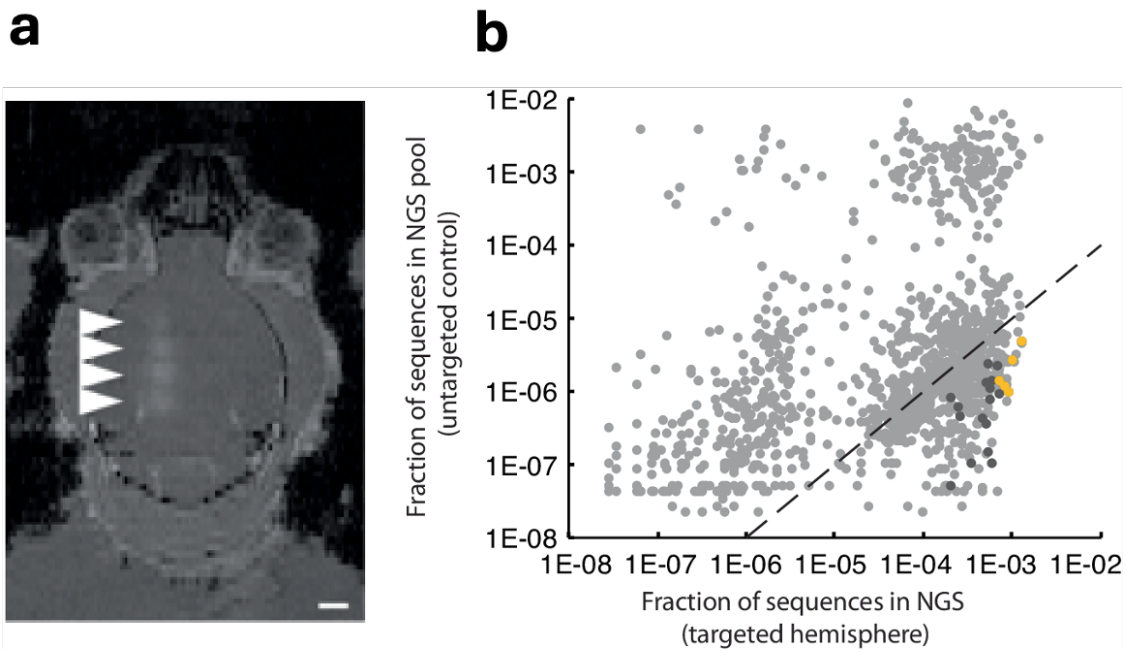

Figure 2-3 High throughput screening yields vectors with improved FUS-BBBO gene delivery. (**a**) An MRI image showing mouse brain with 4 sites opened with FUS-BBBO in one hemisphere. The bright areas (arrowheads) indicate successful BBB opening and extravasation of the MRI contrast agent Prohance into the brain. This BBB opening was used for delivery of the AAV library. (**b**) Sequencing results of round 2 of screening show a fraction of NGS reads within the DNA extracted from brains of Syn1-Cre mice subjected to FUS-BBBO and injected with a focused library of 2098 clones. Each dot represents a unique capsid protein sequence, and the position on each axis corresponds to the number of times the sequence was detected in the FUS-targeted and untargeted hemispheres. Markers below the dotted line represent sequences that on average showed 100-fold higher enrichment in the targeted hemisphere as compared to the control hemisphere. Dark gray dots represent 22 clones that are enriched in the FUS targeted hemispheres at least 100-fold in every tested mouse and DNA sequence encoding the 7-mer insertion peptide. Additional 13 clones had zero detected transduction in the untargeted hemisphere and could not be presented on the log-log plot. Yellow dots represent 5 clones (AAV.FUS.1-5) selected for low-throughput testing. Due to the use of a logarithmic plot, clones that had zero copies detected in either of the hemispheres are not shown. Data from one male and one female mouse.

sequences were not the result of sequencing error, we selected candidates that were found with two alternative codon sequences corresponding to its 7-mer peptide. In the end, 35 sequences met these criteria (dark gray symbols in **Fig. 2-3b**). Among these FUS-BBBO-specific variants, we chose the 5 most common sequences, which we hypothesized would code for AAV capsids with the most efficient neuronal transduction. We re-synthesized these sequences (**Table. 2-1**), cloned them into the AAV9 capsid between amino acids 587–588, and packaged them for detailed evaluation, naming them AAV.FUS 1 through 5.

Candidate	7-mer insert
AAV.FUS.1	AGNTSDR
AAV.FUS.2	ATDAYNK
AAV.FUS.3	WSEGGQP
AAV.FUS.4	SVGSADP
AAV.FUS.5	VRMEGEV

Table 2-1 Amino-acid sequences inserted into AAV9 capsid to obtain AAV.FUS.1- 5 vectors.

2.4 AAV.FUS Candidates: Enhanced Transduction of Neurons in Targeted Brain Regions & Reduced Transduction of Peripheral Organs

An ideal AAV vector for ultrasound-mediated gene delivery to the brain would efficiently transduce targeted neurons while avoiding the transduction of peripheral tissues, such as the liver which is highly transduced by the naturally-occurring AAV serotypes (Zincarelli et al., 2008). Additionally, such a vector should only transduce the brain at the FUS-targeted sites. Of the natural AAV serotypes, AAV9 is most commonly used in FUS-BBBO because it transduces neurons at the ultrasound target with relatively high specificity and efficiency compared to untargeted brain regions (Kofoed et al., 2022; Szablowski et al., 2018; Thévenot et al., 2012; and Wang et al., 2017). However, AAV9 also shows peripheral transduction and is typically administered at doses higher than those used in direct intraparenchymal injection (Kofoed et al., 2022; Szablowski et al., 2018; and Thévenot et al., 2012), leaving room for improvement. To evaluate our engineered vectors, we used AAV9 as a benchmark and an internal control for each tested animal.

We performed FUS-BBBO while intravenously co-administering each AAV.FUS candidate alongside AAV9 in individual comparison experiments at 1E10 VGs per gram of body weight. Consequently, each mouse had an internal control where the injected volume, targeted brain site, and the efficiency of FUS-BBBO were identical for both serotypes, leaving the efficiency of the vector as the independent variable. To quantify the transduction efficiency, we encoded the fluorescent proteins mCherry and EGFP in AAV9 and each AAV.FUS variant, respectively, under a cell-type nonselective CaG promoter (Jun-Ichi et al., 1989). After 2 weeks of expression, we counted the numbers of mCherry and EGFP-expressing cells within the sites of FUS-BBBO. We established the reliability of this quantification method by comparing cell counts in the brain for co-administered AAV9-EGFP and AAV9-mCherry (**Fig. 2-4**).

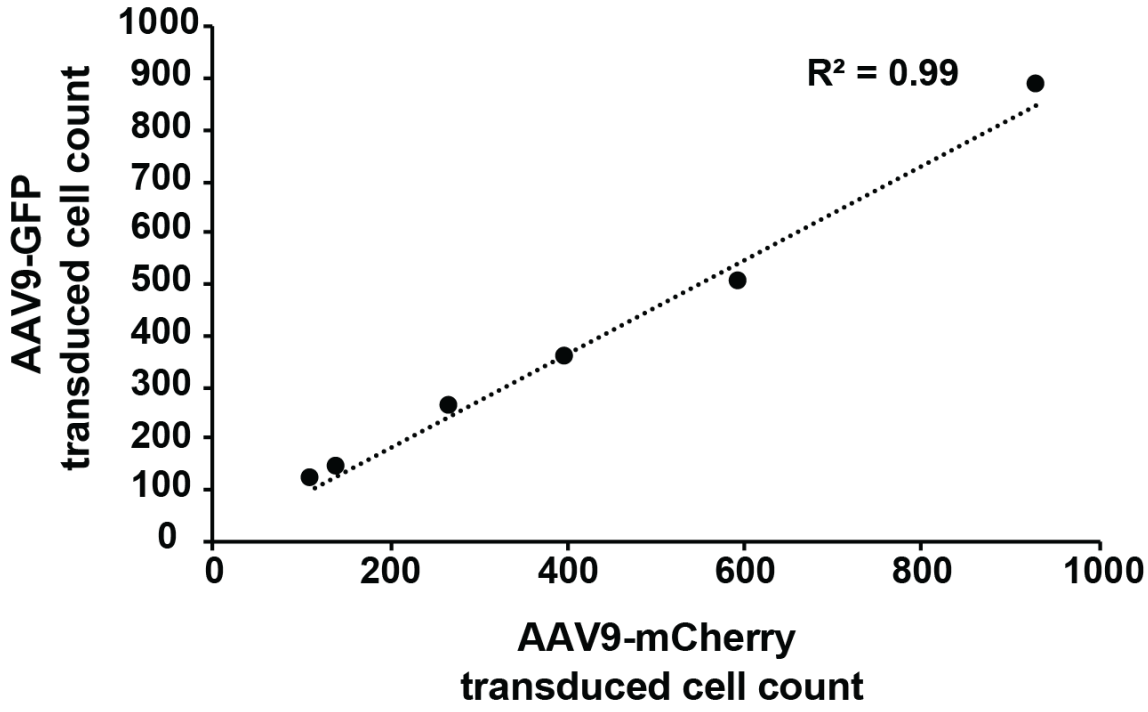

Figure 2-4 AAV9 GFP + AAV9 mCherry fluorescence-based cell counting normalization. Transduced cell counts in the brain comparing AAV9 carrying GFP and mCherry are highly correlated and (Rsq=0.99). The AAVs were administered at 1E10 VGs per gram of body weight to each animal. The mean numbers of transduced cells are not significantly different (fold difference between AAV9-GFP and AAV9- mCherry: 1.07-fold, p=0.081 (ns), paired t-test, 6 sections tested from 2 mice).

Our quantification showed that AAV.FUS.1, 2, 3, and 5 had significantly improved transduction efficiency compared to AAV9 ($p = 0.0274$, 0.0003, 0.0052, 0.0087, respectively, two-way ANOVA with Sidak's multiple comparisons test, $F(4,24) = 59.49$, **Fig. 2-5a, b**) whereas AAV.FUS.4 showed no improvement ($p = 0.2556$). The fold-change in transduction relative to AAV9 was greatest for AAV.FUS.2, and lowest for AAV.FUS.4 (**Fig. 2-6**).

None of the AAV.FUS candidates produced substantial off-target expression within the brain at sites not insonated by FUS, with AAV9 producing $0.29 \pm 0.1\%$ neuronal transduction ($n = 40$ mice), AAV.FUS.3 $0.17 \pm 0.1\%$ ($n = 17$ mice), and other AAV.FUS candidates between $0.24 \pm 0.12\%$ ($n = 6$), $0.37 \pm 0.26\%$ ($n = 5$), $0.2 \pm 0.26\%$ ($n = 6$), $0.026 \pm 0.05\%$ ($n = 6$) for AAV.FUS.1, 2, 4, and 5 respectively (**Fig. 2-5c**).

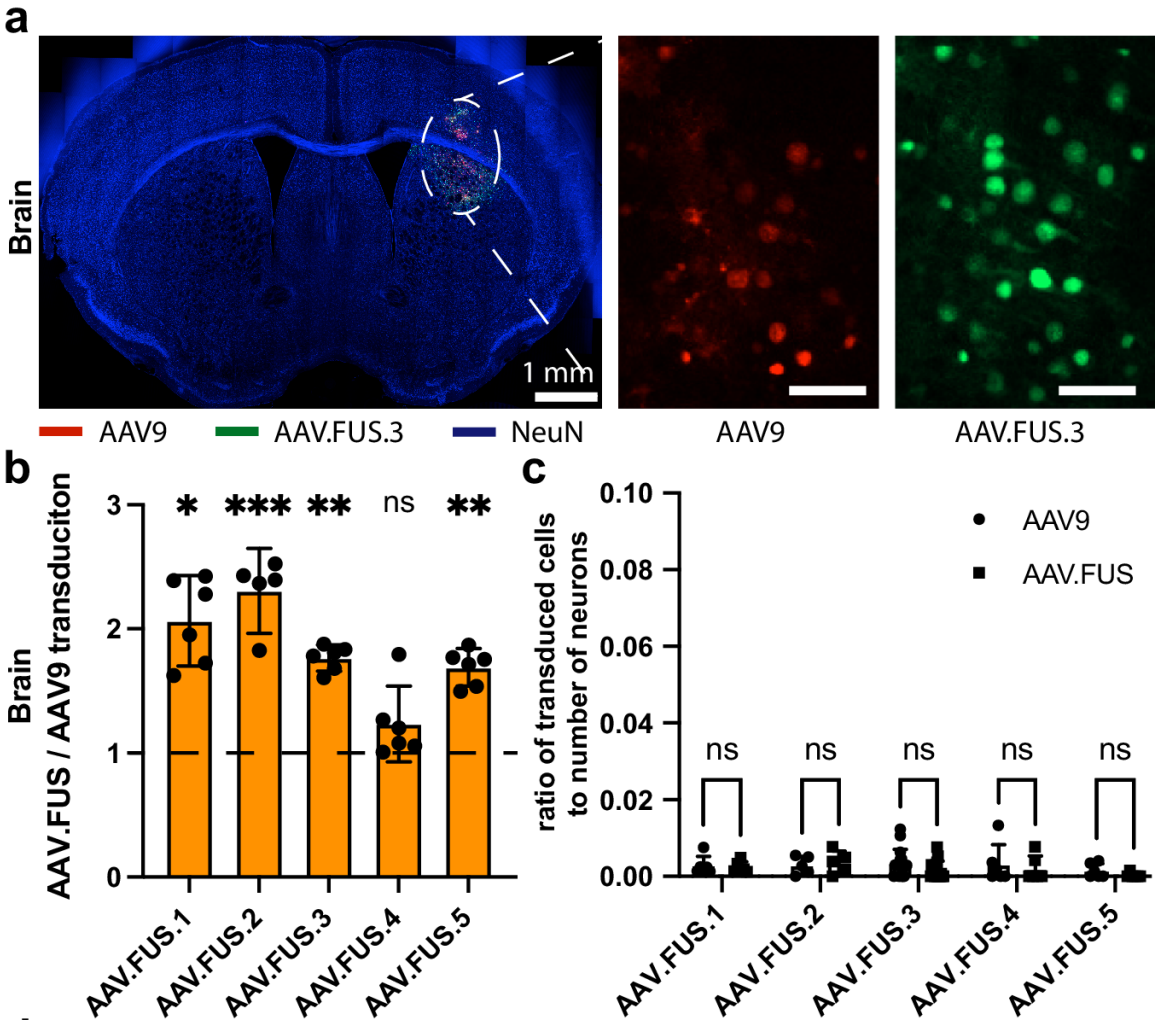

Figure 2-5 AAV.FUS candidates improve efficiency of gene delivery to the brain. (**a**) Representative images were obtained from mice co-injected with AAV9 and a AAV.FUS.3 at 10^{10} viral genomes per gram of body weight each. Sections show brain transduction by AAV9 (red) and AAV.FUS.3 (green), and are counterstained with a neuronal stain (NeuN, blue). (**b**) All but one (AAV.FUS.4) AAV.FUS candidates showed significant improvement over the co-injected AAV9. (p-values for AAV.FUS.1-5, $p = 0.0274$, 0.0003, 0.0052, 0.2556, 0.0087, respectively; Two-way ANOVA with Sidak multiple comparisons test: $F(1, 24) = 59.49$, P value; $P < 0.0001$). Data from 3 male and 3 female mice per serotype. (**c**) We found that few cells were transduced outside of the FUS-targeted site and AAV.FUS.3 and AAV9 were not significantly different. (0.19% vs 0.4%, respectively; $p = 0.072$, two-way ANOVA with Sidak multiple comparisons test; $F(1, 35) = 2.457$, $p = 0.1260$). Similarly, other candidates also showed no differences compared to AAV9 (AAV.FUS.1, $p = 0.99$; AAV.FUS.2, $p = 0.98$; AAV.FUS.4, $p = 0.86$; AAV.FUS.5, $p = 0.83$). Data from 3 male and 3 female mice for all serotypes, except AAV.FUS.2 (2 male, 3 female mice), and AAV.FUS.3 (8 male and 8 female mice). Scale bars are 50 µm. The numbers of animals used in each experiment were: Data from 3 male and 3 female mice per serotype, except AAV.FUS.2 (2 male, 3 female mice). Center for the error bars represents arithmetic mean.

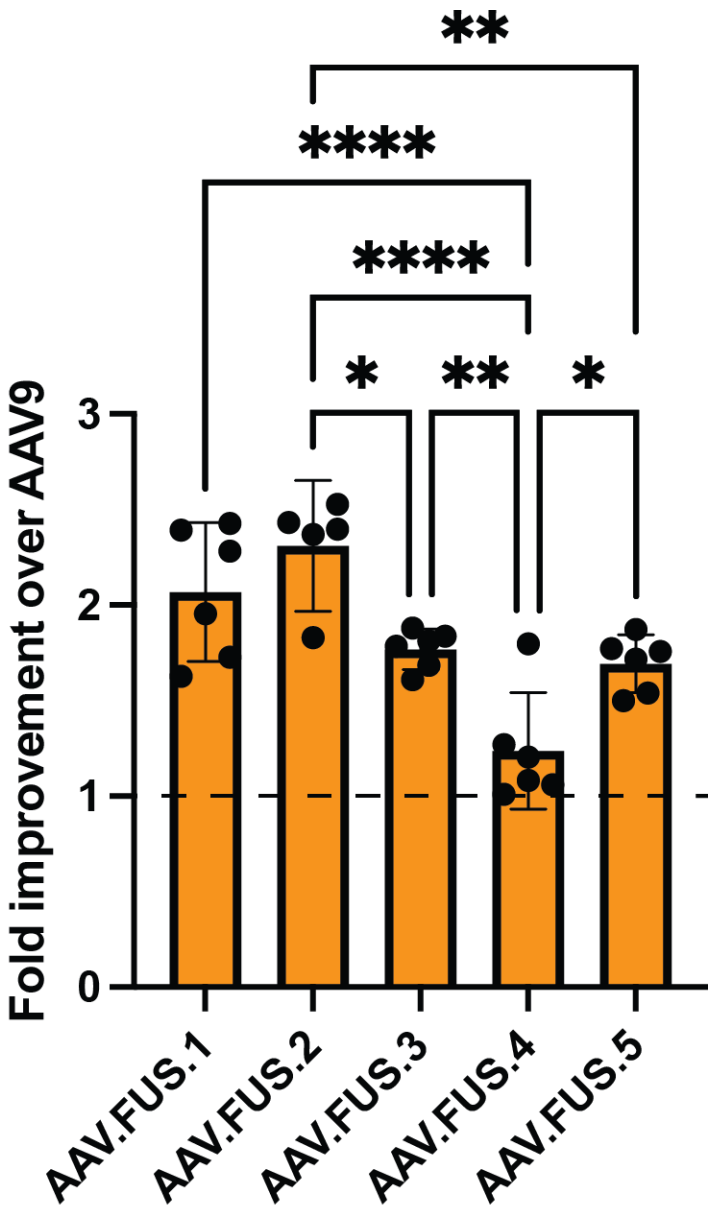

Figure 2-6 Pairwise comparison of AAV.FUS candidates' transduction of the brain. Non-significant comparisons not shown for clarity. (**** = $p < 0.0001$; *** = $p < 0.001$; ** = $p < 0.01$; * = $p < 0.05$; $F(4, 24) = 14.96$, $P < 0.0001$, One-way ANOVA with Tukey HSD post hoc test.). Non-significant pairwise comparisons not shown for clarity. Error bars are 95% CI. All 10 detailed p-values provided in the source data appendix. n = 6 mice used for all serotypes except AAV.FUS.2 which used n=5 mice. IV injection dose, 10^{10} vg/g body weight.

Next, we evaluated the extent to which AAV.FUS candidates transduce off-target peripheral organs. In mice that received intravenous co-injections of AAV9-mCherry and each variant of AAV.FUS-EGFP, we counted transduced cells in the liver, a peripheral organ known to be targeted by AAVs and a potential source of dose-limiting toxicity (Hinderer et al., 2018; and S. Pipe et al., 2019). Two weeks after injection, we imaged liver sections and counted cells expressing each fluorophore (**Fig. 2-7a, b**). We found markedly reduced liver transduction among the AAV.FUS candidates compared to AAV9 (**Fig. 2-7b**). AAV.FUS 3 showed the largest reduction in liver transduction compared to the wild-type serotype (6.8-fold reduction, $p < 0.0001$, one-way ANOVA with Tukey-HSD post hoc test; $F(4, 24) = 93.91$), which was significantly higher reduction compared to the other tested AAV.FUS candidates (**Fig. 2-8**). We did not observe substantial transduction in kidney and lung sections transduced with either viral vector (**Fig. 2-9**, $n = 6$ mice per organ tested), which is consistent with the published data for the parent AAV9 (Kofoed et al., 2022). In kidneys, we observed areas of red autofluorescence, which is consistent with previous reports even in the absence of AAV delivery (Rubin et al., 2019). This autofluorescent signal did not interfere with detection of AAV.FUS.3, which showed no positive signal in these areas (**Fig. 2-9a**).

Our analyses of brain and liver transduction showed that AAV.FUS candidates both decrease the targeting of the liver and increase the transduction efficiency of the targeted brain regions, which leads to a large overall improvement in transduction specificity, expressed as the ratio of the fold-increase in brain transduction and the fold-decrease in liver transduction compared to AAV9. By this metric, AAV.FUS.3 showed a 12.1-fold improvement, significantly greater than the other candidates ($p < 0.0001$ for all pairwise comparisons, one-way ANOVA with Tukey-HSD post hoc test; $F(4, 24) = 70.88$; **Fig. 2-7c**). Representative images can be found in **Fig. 2-10**, and detailed sequence data in **Appendix Information A.**

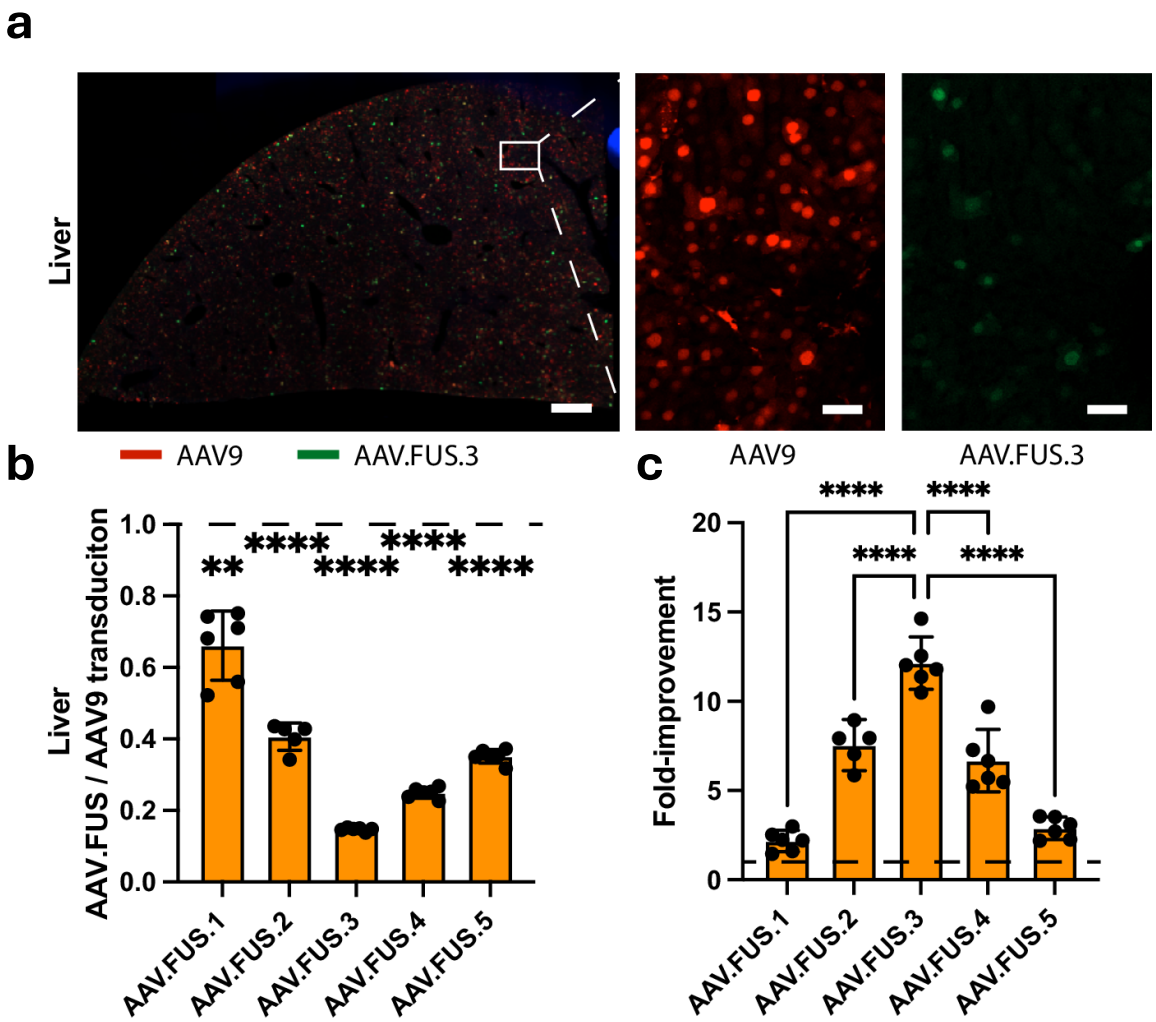

Figure 2-7 AAV.FUS candidates reduce efficiency of gene delivery to the peripheral organs. (**a**) Representative images showing liver transduction by AAV9 (red) and AAV.FUS.3 (green). (**b**) All tested candidates showed reduced liver transduction as compared to the co-injected AAV9 in the same mice for which brain expression was analyzed. (*P*-values for AAV9 vs AAV.FUS.1-5 were $p = 0.0058$ for AAV.FUS.1, and $p < 0.0001$ for other candidates; Two-way ANOVA, $F(1, 24) = 375.9$, $P < 0.0001$. Data from 3 male and 3 female mice for all serotypes, except AAV.FUS.2 (2 male, 3 female mice). (**c**) We defined the fold-improvement in targeting efficiency as the ratio of brain transduction to the liver transduction efficiency using AAV9 as a baseline, which suggested that AAV.FUS.3 is the top candidate for further study. (AAV.FUS.3 compared to AAV.FUS.1,2,4,5, all *p*-values were $p < 0.0001$, one way ANOVA with Tukey HSD post hoc comparison test). Scale bars are 50 µm. The numbers of animals used in each experiment were: Data from 3 male and 3 female mice per serotype, except AAV.FUS.2 (2 male, 3 female mice). Center for the error bars represents arithmetic mean.

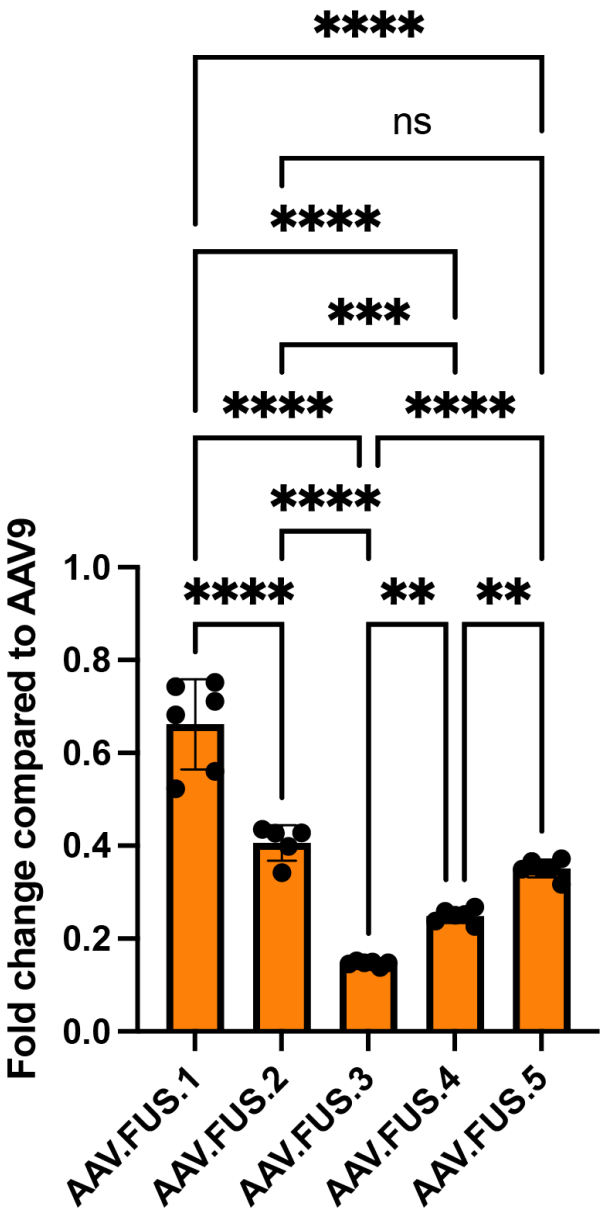

Figure 2-8 Pairwise comparison of AAV.FUS candidates' transduction of the liver. Non-significant comparisons not shown for clarity. AAV.FUS.3 shows significantly reduced liver transduction compared to other AAV.FUS candidates. One-way ANOVA with Tukey HSD post-hoc test. F (4, 24) = 96.69. P<0.0001; All pairwise comparisons are below p<0.0001, except AAV.FUS.2 vs AAV.FUS.4 (p=0.0001), AAV.FUS.2 vs AAV.FUS.5 (p=0.3524), AAV.FUS.3 vs AAV.FUS.4 (p=0.01), and AAV.FUS.4 vs AAV.FUS.5 (p=0.0099)). (**** = p<0.0001; *** = p<0.001; ** = p <0.01; * = p<0.05, ns = non-significant). Error bars are 95% CI. Detailed p-values provided in the source data appendix. n=6 mice used for all serotypes except AAV.FUS.2 which used n=5 mice. IV injection dose, 10^{10} vg/g body weight.

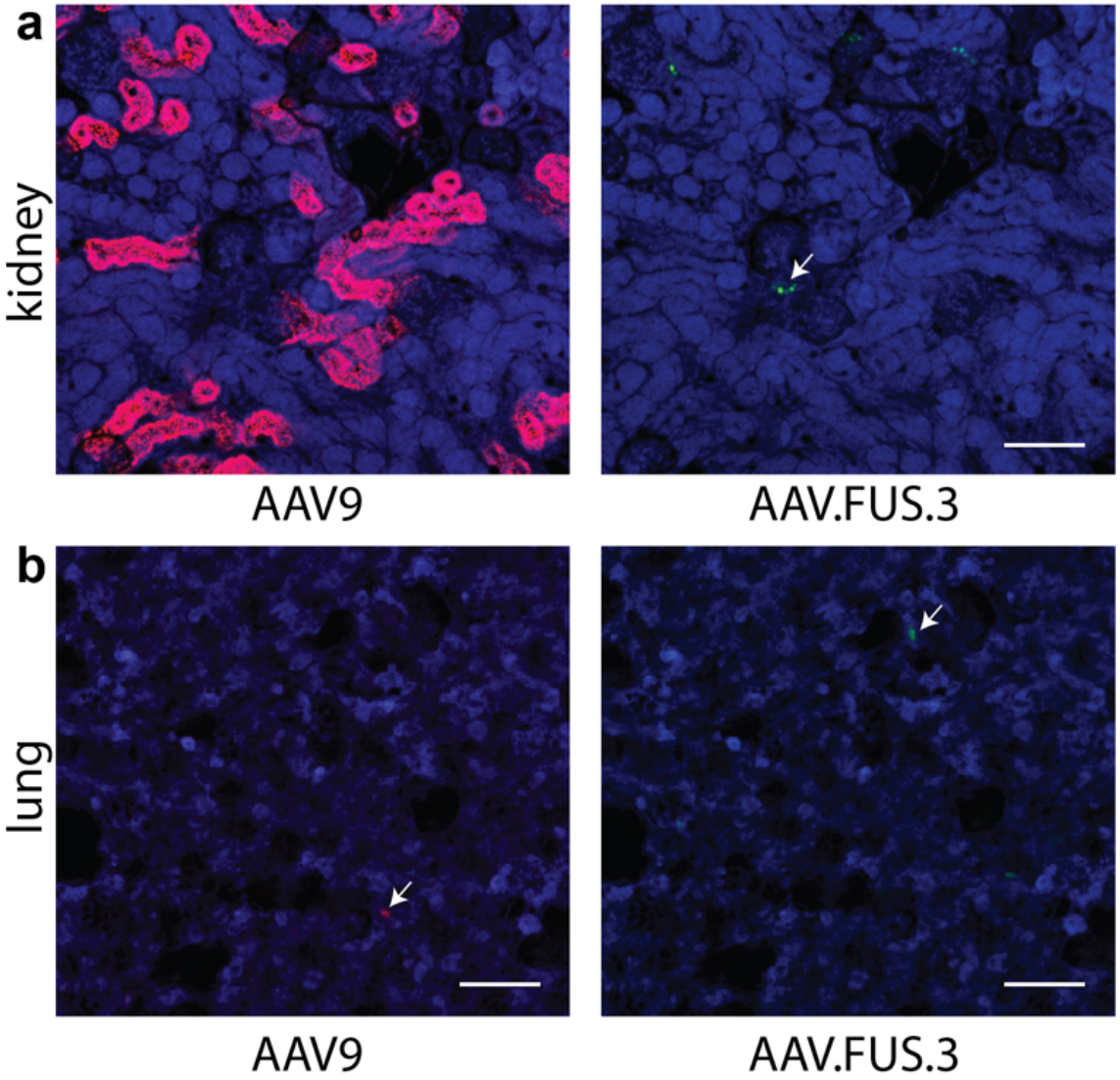

Figure 2-9 Transduction of AAV9 and AAV.FUS.3 in peripheral tissues. Representative images showing liver transduction by AAV9 (red) and AAV.FUS.3 (green). We observed no substantial transduction observed in the (**a**) kidneys and (**b**) lungs, consistent with previous reports21. Representative images were obtained from mice co-injected with AAV9 (red, mCherry) and AAV.FUS.3 (green, GFP). IV injection dose, 10^{10} vg/g body weight. Sections were imaged on a confocal microscope with 10x objective counterstained with a nuclear stain (DAPI, blue). Example positive cells designated with arrows. Scale bars are 100 μm.

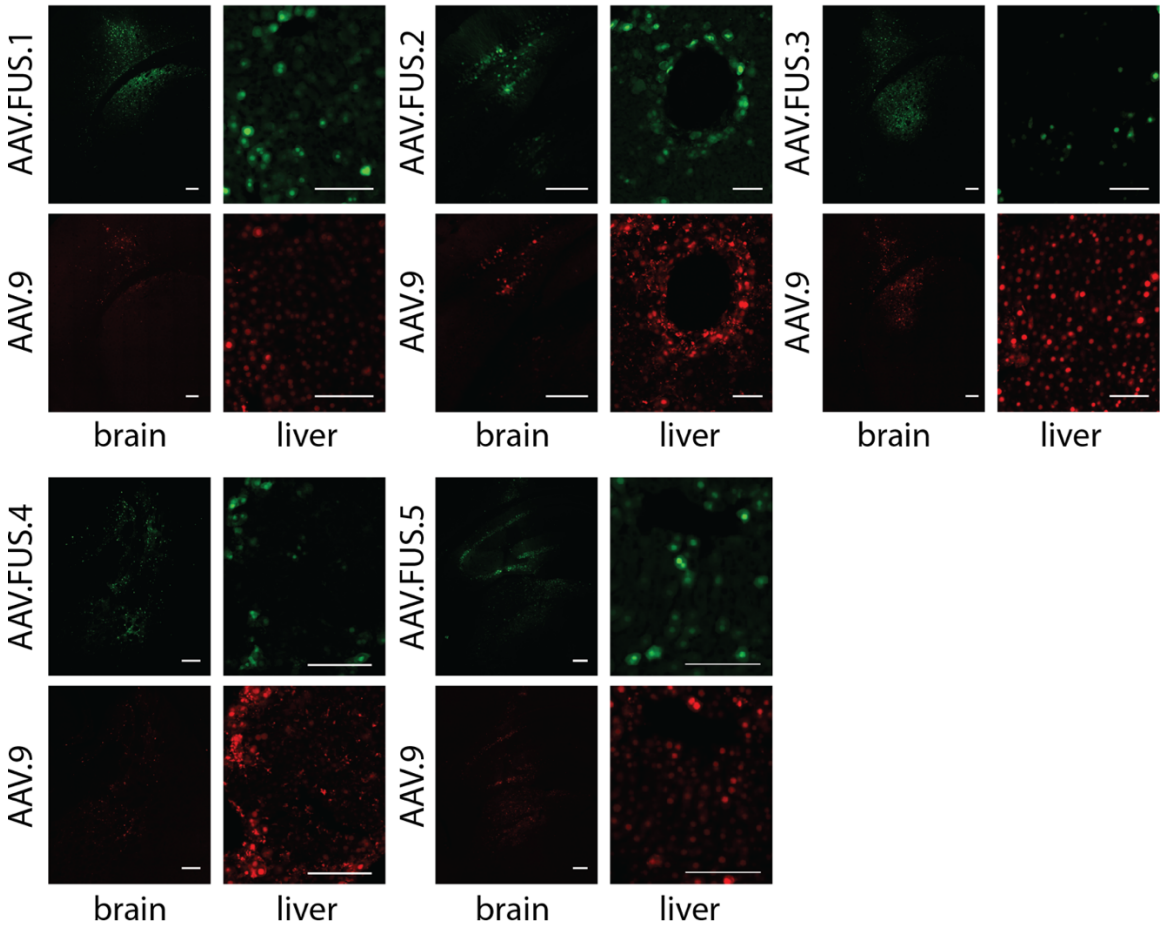

Figure 2-10 Representative images of transduction in brain and liver for all AAV.FUS (green, EGFP) and corresponding co-injected AAV9 control (red, mCherry). IV injection dose, 10^{10} vg/g body weight. Scale bars: 200 microns for the brain, 100 microns for the liver.

A final criterion for successful gene delivery in many applications is the ability to transduce specific cell types at the targeted anatomical location, such as neurons. AAV9 transduces both neuronal and non-neuronal cell types (Alves et al., 2016; Gong et al., 2015; and Lukashchuk et al., 2016). We hypothesized that, since our Cre-dependent screen used mice with the recombinase expressed under a neuronal promoter, our engineered variants could have a higher neuronal tropism relative to their wild-type parent serotype. To test this hypothesis, we immunostained brain sections from mice co-transduced with AAV9-mCherry and each variant of AAV.FUS-EGFP during FUS-BBBO for the neuronal marker NeuN and imaged these sections for GFP, mCherry, and NeuN signal. The fraction of AAV9-transduced (mCherry-positive) cells that were also positive for NeuN was 44.7% (±1.5%, 95% CI; $n = 8$). In contrast, all AAV.FUS candidates had higher neuronal tropism ($p < 0.0001$ for all AAV.FUS candidates, **Fig. 2-11**), with neurons constituting between 64.6% (±1.9%, 95% CI; $n = 6$, AAV.FUS.1) and 69.8% (±3.5%, 95% CI, $n = 6$, AAV.FUS.3) of all transduced cells. AAV9 and AAV.FUS transduced astrocytes to a comparable degree (8% vs 3.4% respectively; $n = 6$ sections analyzed from $n = 3$ mice, $p = 0.0552$, paired t test; $t = 4.076$). However, AAV9 transduced microglia/macrophages significantly more efficiently than AAV.FUS (3.5% and 0.7%, respectively; $n = 6$ sections analyzed from $n = 3$ mice, $p = 0.0174$, paired t test, $t = 7.487$) as well as oligodendrocytes (74.3% and 3.4% respectively; $n = 18$ sections analyzed from $n = 6$ mice, $p < 0.0001$, paired t test; $t = 12.32$). (**Fig. 2-12**). These results show that in addition to improved specificity for targeted regions of the brain, the engineered viral capsids are more selective for neurons over other cephalic cell types.

Based on its leading combination of neuronal tropism and improvement in brain specificity among the engineered variants, we selected AAV.FUS.3 for further evaluation as a FUS-BBBO-specific viral vector.

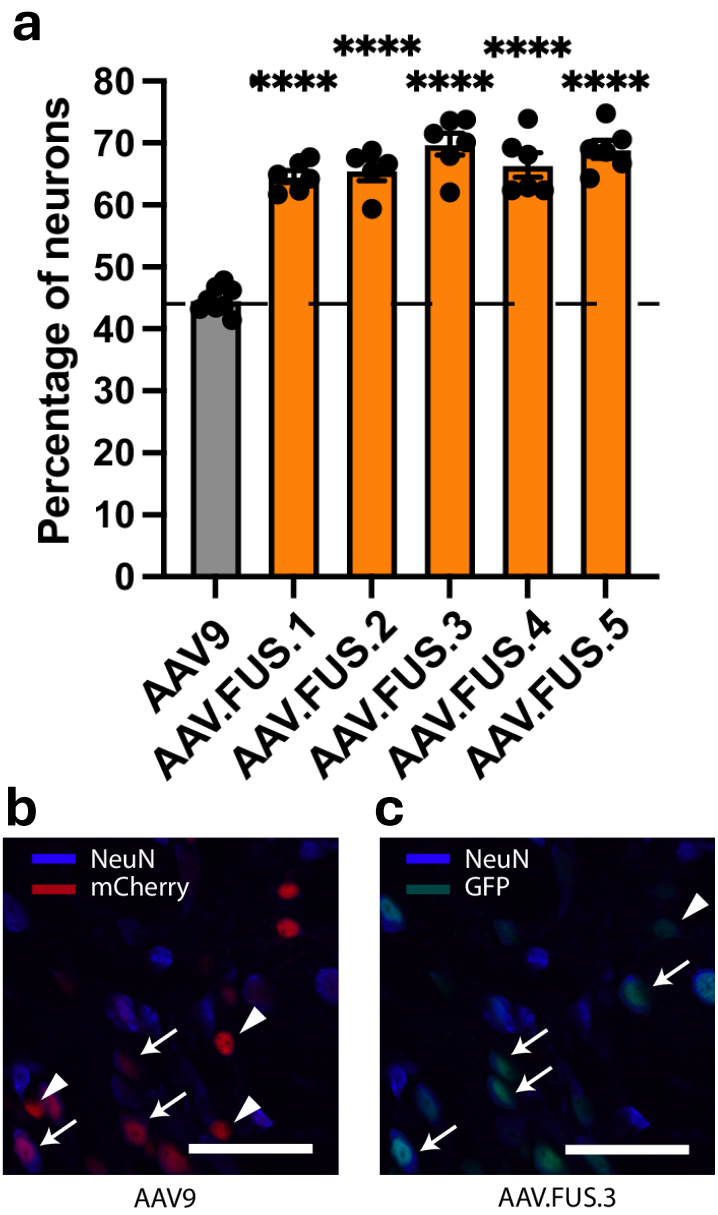

Figure 2-11 AAV.FUS candidates show improved neuronal tropism. (**a**) All AAV.FUS candidates show improved neuronal tropism upon FUS-BBBO gene delivery. AAV.FUS.3 had 56% more likelihood of transducing a neuron than AAV9 (69.8%, vs 44.7% neuronal transduction, respectively; (for all samples $p < 0.0001$, one way ANOVA, $F(5, 31) = 52.60$, $P < 0.0001$; $n = 8$ for AAV9, $n = 6$ for all AAV.FUS.1,3,4,5, n = 5 for AAV.FUS.2, center for the error bars represents arithmetic mean.). (**b**) Representative images showing AAV9 transducing both neurons (blue, NeuN staining, example neurons designated by an arrow) and non-neuronal cells (example non-neuronal cells designated by an arrowhead). (**c**) In comparison, more of the cells transduced with AAV.FUS (green) are neurons (example neurons designated by an arrow), rather than non-neuronal cells (example cell designated by an arrowhead). IV injection dose, 10^{10} vg/g body weight. Scale bars are 50 µm. (****$p < 0.0001$). Error bars are 95% CI.

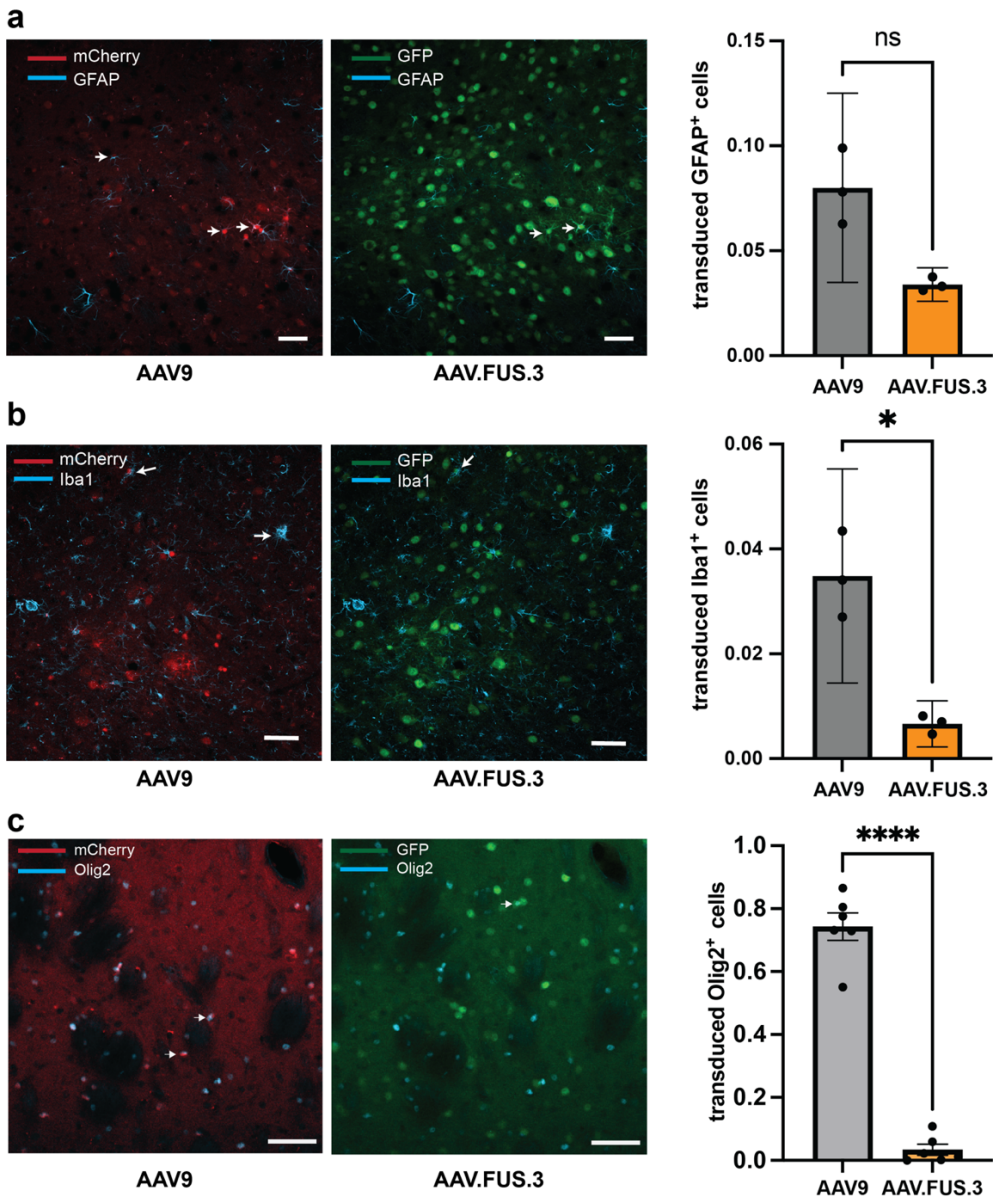

Figure 2-12 Transduction of non-neuronal brain cells by AAV.FUS.3 and AAV9. We observed lower transduction of microglia/macrophages, astrocytes and oligodendrocytes in the brain by either AAV9 or AAV.FUS.3 as compared to neurons. Representative images were obtained from mice co-injected with AAV9 (red, mCherry) and AAV.FUS.3 (green, GFP). (**a**) The transduction of astrocytes (GFAP+) was comparable between the AAV9 and AAV.FUS.3, with 8% and 3.4% average transduction, respectively (n=3 mice, p=0.0552, two-tailed paired t-test; t=4.076). (**b**) Similarly, microglial/macrophagic transduction was also less efficient than neuronal transduction for both serotypes with AAV9 transducing 3.5% and AAV.FUS.3 transducing 0.7% of microglial cell, which was a statistically significant difference (n=3 mice, p=0.0174, two-tailed paired t-test, t=7.487). (**c**) AAV.FUS.3 transduction of oligodendrocytes was significantly reduced relative to AAV9, with average transduction being 3.4% for AAV.FUS.3 and 74.3% for AAV9 (n=6 mice, p<0.0001, two-tailed paired t-test, t=12.32). Sections were imaged on a confocal microscope with 20x objective counterstained for glial cells (GFAP, blue), microglia/macrophages (Iba1, blue) and oligodendrocytes (Olig2, blue). IV injection dose, 10^{10} vg/g body weight. Scale bars are 50 microns.

2.5 AAV.FUS.3 Transduction at a Low Dose Administration

The administration of low doses of adeno-associated virus (AAV) vectors in gene therapy is increasingly recognized as a critical element for both preclinical research and clinical applications. This requirement is driven by several factors, including concerns regarding immunogenicity, vector toxicity, and the need for sustained therapeutic efficacy without adverse side effects.

Research indicates that low-dose AAV administration minimizes the likelihood of immune system activation, which can be detrimental to the success of gene therapy. Increased immunogenic responses are typically associated with high vector exposure, primarily due to the generation of neutralizing antibodies (NAbs) in the patient's bloodstream. Studies underscore how pre-existing NAbs significantly obstruct AAV-mediated gene transfer, leading to diminished therapeutic outcomes in many patients (Kuranda et al., 2018; Au et al., 2022). Thus, utilizing low doses can reduce immune responses, potentially allowing for repeat administrations of the therapy without invoking severe immune reactions (Kuranda et al., 2018; Watano et al., 2020).

Moreover, the structure and delivery method of AAV further compound the importance of maintaining low dosage levels. It has been demonstrated that high doses of AAV can invoke heightened immunogenicity, leading to reduced effectiveness and complications related to toxicity (Arjomandnejad et al., 2023). AAV vectors are often chosen for their low immunogenic characteristics when compared to other viral vectors; however, their effectiveness can be compromised if the dosage is not appropriately calibrated. For example, different serotypes of AAV may exhibit varying biodistribution and transduction efficiencies, which must be carefully considered during therapeutic planning to avoid unnecessary exposure (Mullagulova et al., 2023; Garcia‐Olloqui et al., 2019). Furthermore, it has been reported that using dosages that are excessively high results in an increase in capsid-specific antibodies, negatively impacting subsequent doses and overall therapeutic success (Xu et al., 2024).

In the context of specific diseases like Duchenne muscular dystrophy and spinal muscular atrophy, low-dose AAV administration has been found to achieve significant therapeutic benefits while minimizing adverse effects. The utilization of an AAV delivery system that allowed for enhanced delivery and expression of therapeutic genes led to positive outcomes even at lower doses, showcasing the principle that effective gene therapy does not necessarily equate to high-vector doses (Zhang et al., 2020; Armbruster et al., 2016). Additionally, the application of strategic dose modulation has been advocated as a viable means to refine gene therapy approaches, ensuring that maximal therapeutic efficacy is achieved while concurrently reducing risks associated with high dosage deployment (Chen et al., 2024).

Thus the administration of AAV vectors at low doses is pivotal in mitigating inflammation and immune responses while supporting the long-term expression of therapeutic genes. This approach not only enhances safety profiles but also improves the viability of repeat dosing—a critical aspect when addressing chronic genetic conditions. Future research should continue to refine the thresholds for optimal AAV dosages, balancing efficacy and safety to realize the full potential of gene therapies in clinical settings.

Hence, lowering the dose of AAVs during gene therapy or scientific studies is of high interest due to lower cost and reduced toxicity (Kishimoto & Samulski, 2022). We decided to evaluate whether the improvements in transduction can be retained at lower dose, such as 10^9 vg/g body wight, which has been used in other FUS-BBBO gene delivery studies (Bhardwaj et al., 2025). Our results showed that AAV.FUS can transduce the brain more efficiently than AAV9 at this dose, with a total number of transduced cells being 2.2 ± 0.6-fold higher for AAV.FUS over AAV9 ($n = 6$ mice analyzed, $p = 0.0004$, two-tailed paired t test, $t = 8.182$; **Fig. 2-13a, b**). At the same time, the liver transduction was lower for AAV.FUS compared to AAV9 by 5.2 ± 1.6-fold ($n = 6$ mice analyzed, $p = 0.0004$, two-tailed paired t test; $t = 8.530$; **Fig. 2-13c, d**), reaching the overall brain-to-liver transduction ratio of 11.6 ± 3.7 (95% CI, **Fig. 2-13e**), which was comparable to the brain-to-liver transduction ratio at a higher dose of 1010 vg/g (12.1-fold vs 11.6-fold; $p = 0.798$; two-tailed, heteroscedastic t test, $t = 0.2682$). Finally, we evaluated the overall neuronal transduction

efficiency at this dose and found the average transduction measured across three brain regions (striatum, thalamus, hippocampus) of 12.6% ± 3.7% for AAV9 and 54.4% ± 8.8% for AAV.FUS, for a total of 4.6-fold difference ($p < 0.0001$; two-tailed paired t test; $t = 14.81$; **Fig. 2-13f, g**). Overall, the properties of AAV.FUS.3 for enhanced brain-specific transduction and neuronal tropism over AAV9 were retained at the lower vector dose.

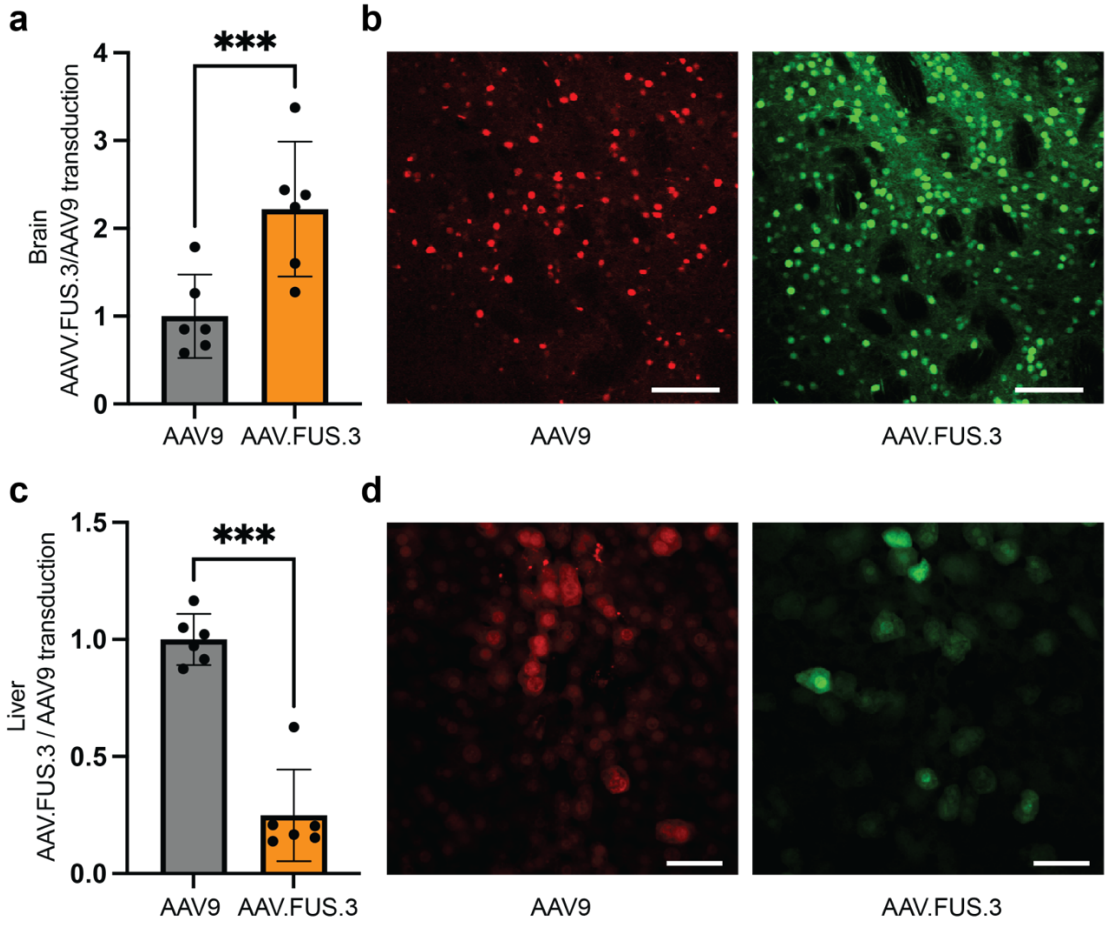

Figure 2-13 AAV.FUS.3 delivered at 1x10^9 vg/g of body weight shows reduced liver transduction and improved neuronal transduction efficiency. (**a**) Representative images were obtained from mice co-injected with AAV9 and AAV.FUS.3 at 1x10^9 viral genomes (vg) per gram of body weight. Sections were imaged on a confocal microscope with 20x objective showing brain transduction by AAV9 (red) and AAV.FUS.3 (green). (n=6 mice, p=0.0004, two-tailed paired t-test; t=8.182). (**b**) All mice showed improvement in transduction and expression over the co-injected AAV9 across various brain regions. (**c**) Representative images from a confocal microscope with a 10x objective showing liver transduction by AAV9 (red) and AAV.FUS.3 (green) at the low dose (n=6 mice, p=0.0004, two-tailed paired t-test; t=8.53. (**d**) The transduction of AAV.FUS.3 relative to AAV9 in the liver decreased significantly as the viral dose is reduced. Scale bars are 100 microns in panel (**b**) and 50 microns in panel (**d**). (Note: **** = p<0.0001, *** = p<0.001; ** = p <0.01; * = p<0.05, ns = not significant).

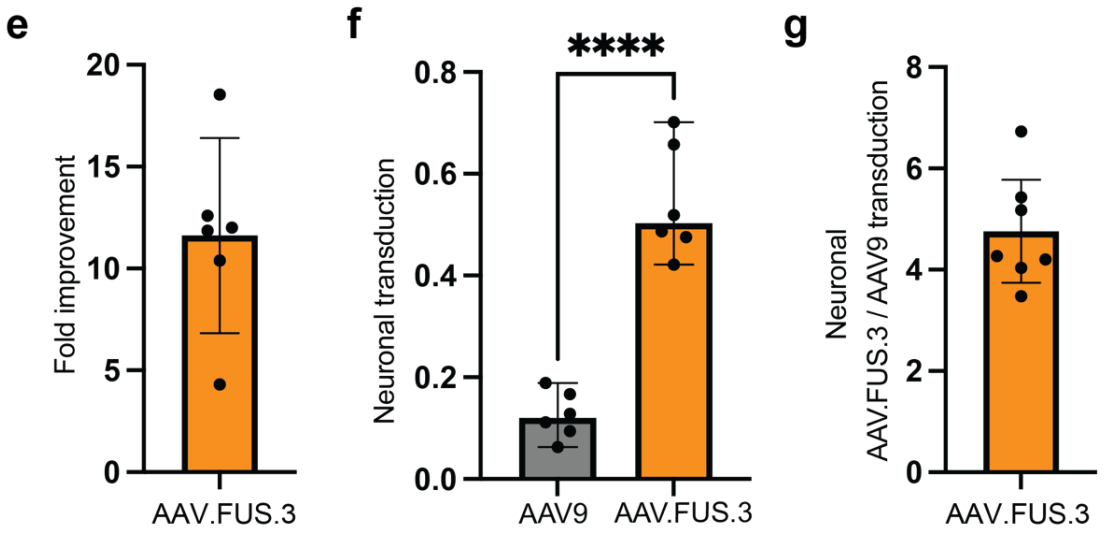

Figure 2-13 *(continued)* AAV.FUS.3 delivered at 1x10^9 vg/g of body weight shows reduced liver transduction and improved neuronal transduction efficiency. (**e**) We defined the fold-improvement in targeting efficiency as the ratio of brain transduction to the liver transduction efficiency using AAV9 as a baseline, showing 11.6-fold improvement in targeting efficiency at the dose of 1x109 vg/g of body weight. (**f**) Neuronal transduction at this tested dose was significantly higher for AAV.FUS.3 over AAV9 (n=6 mice, p<0.0001; two-tailed paired t-test; t=14.81). (**g**) Overall, we observed 4.6-fold higher neuronal transduction by AAV.FUS.3 over AAV9. (Note: **** = p<0.0001, *** = p<0.001; ** = p <0.01; * = p<0.05, ns = not significant).

2.6 Region-specific Transduction Efficiency of AAV.FUS.3

Adeno-associated viruses have emerged as pivotal tools in the fields of gene therapy and neuromodulation, particularly due to their ability to target specific brain regions effectively. The specificity of AAV in targeting various brain regions enhances the therapeutic potential for treating neurodegenerative diseases, as different conditions often affect localized neuronal populations. Research indicates that the manipulation of AAVs can be tailored to enhance their distribution in specific regions of the brain, addressing challenges associated with traditional gene delivery methods.

Recent studies have demonstrated the importance of region-specific gene co-expression networks, suggesting that tailoring gene therapy to specific brain networks can significantly improve therapeutic outcomes. By analyzing gene expression profiles across various brain regions, the study highlights how differences in gene co-expression can inform targeted treatments for specific neuronal populations (Hang et al., 2020). This concept is supported by studies investigating AAV vectors being tested to deliver neuroprotective factors specifically to the striatum for conditions like Parkinson's disease, underscoring the efficacy of localized gene therapy approaches (Raghunathan et al., 2018).

Furthermore, advancements in techniques such as acoustically targeted measurement (REMIS) offer innovative strategies for evaluating the success of gene delivery in specific brain regions, allowing researchers to confirm effective transduction and expression in targeted neuronal populations (Seo et al., 2023). Additionally, significant progress has been made in engineering AAV capsids that offer better tropism and delivery efficiency across different brain regions, as shown with AAV-PHP variants that facilitate enhanced brain vascular association and blood-brain barrier (BBB) penetration (Torregrosa et al., 2021; Leib et al., 2024).

Moreover, as discussed in the Chapter 1, the application of focused ultrasound (FUS) technology presents another approach that, when combined with AAVs, has shown promise in non-invasively delivering therapeutic genes to targeted deep brain structures while improving the efficiency of gene delivery (Kofoed et al., 2024; Noroozian et al., 2019). This

combination enhances local delivery and reduces the risk associated with higher systemic dosages, further supporting the need for regionally targeted therapies.

Furthermore, as gene therapies evolve, the exploration of AAV-mediated strategies continues with the aim of enhancing the targeting and efficacy of treatment for various neurodegenerative conditions. Enhanced selectivity in the delivery of AAVs allows for focused intervention in brain regions affected by specific pathologies, as reiterated in studies addressing both Alzheimer's and Parkinson's diseases (Castle et al., 2020; Tuszynski et al., 2015).

Indeed, the deployment of AAVs for gene therapy in specific brain regions embodies a paradigm shift in how these therapies can be applied to various neurological disorders. By fine-tuning the delivery mechanisms and improving viral vector designs, researchers are paving the way for more effective treatments that harness the unique characteristics of regional brain networks. The future of gene therapy lies in its ability to be personalized to the intricate demands of brain regions, ultimately improving therapeutic outcomes for neurodegenerative diseases.

So, we decided to further characterize AAV.FUS.3's performance relative to AAV9, and we decided to evaluate the efficiency of delivery when these vectors are targeted to different brain regions. To ensure that each region is targeted exclusively, only one brain region was targeted with FUS-BBBO in each tested mouse. To ensure the rigor of this investigation and account for variability in virus titration (Lock et al., 2010), we obtained a new batch of both AAV9 and AAV.FUS.3 and titered them independently. We evaluated the efficiency of transduction when these vectors were targeted by FUS-BBBO to the striatum (caudate putamen), thalamus, hippocampus, and midbrain.

We observed a major improvement in AAV.FUS.3 transduction compared to AAV9 in all targeted regions, with a fold-change ranging from 2.4 ± 0.08 to 4.3 ± 0.08 (95% CI, **Fig. 2-15** and **Fig. 2-16**). Among brain regions, we found that the hippocampus (Hpc) is transduced with a particularly elevated relative efficiency while the cortex (Ctx) showed the lowest with

a 2.4-fold improvement. These results indicate that AAV.FUS.3 can target multiple brain regions with improved efficiency, while suggesting the potential for further engineering AAVs with region-enhanced tropism in FUS-BBBO delivery. Lower magnification images showing transduction in surrounding brain areas can be found in **Fig. 2-14**.

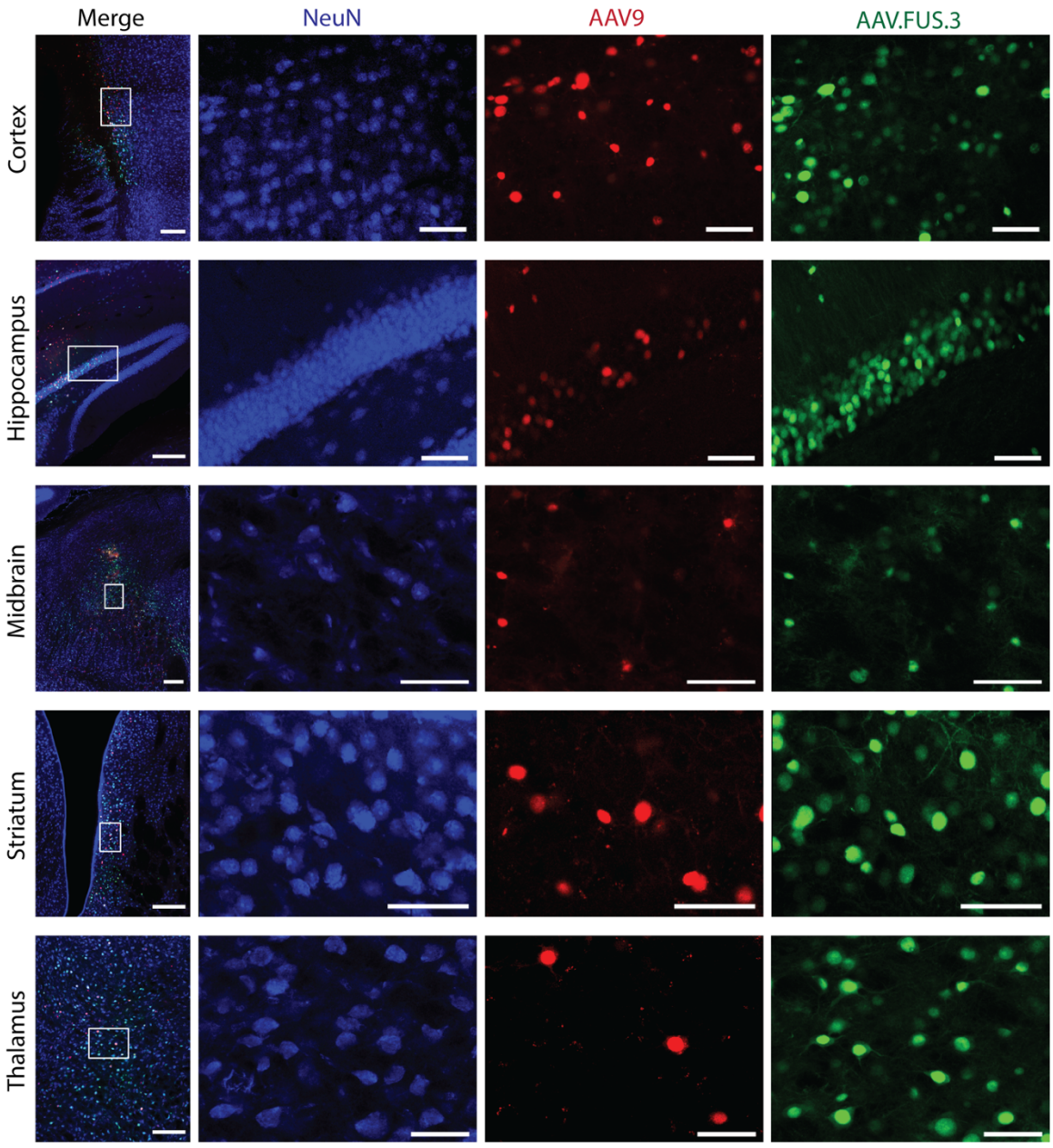

Figure 2-14 Region-specific transduction of AAV9 (red) and AAV.FUS.3 (green) with a neuronal nuclear counterstain (NeuN) in C57BL/6J animals. Images were obtained at 20x magnification (left panels, scale bars 200 µm; 3 rightmost panels, scale bar 50 µm).

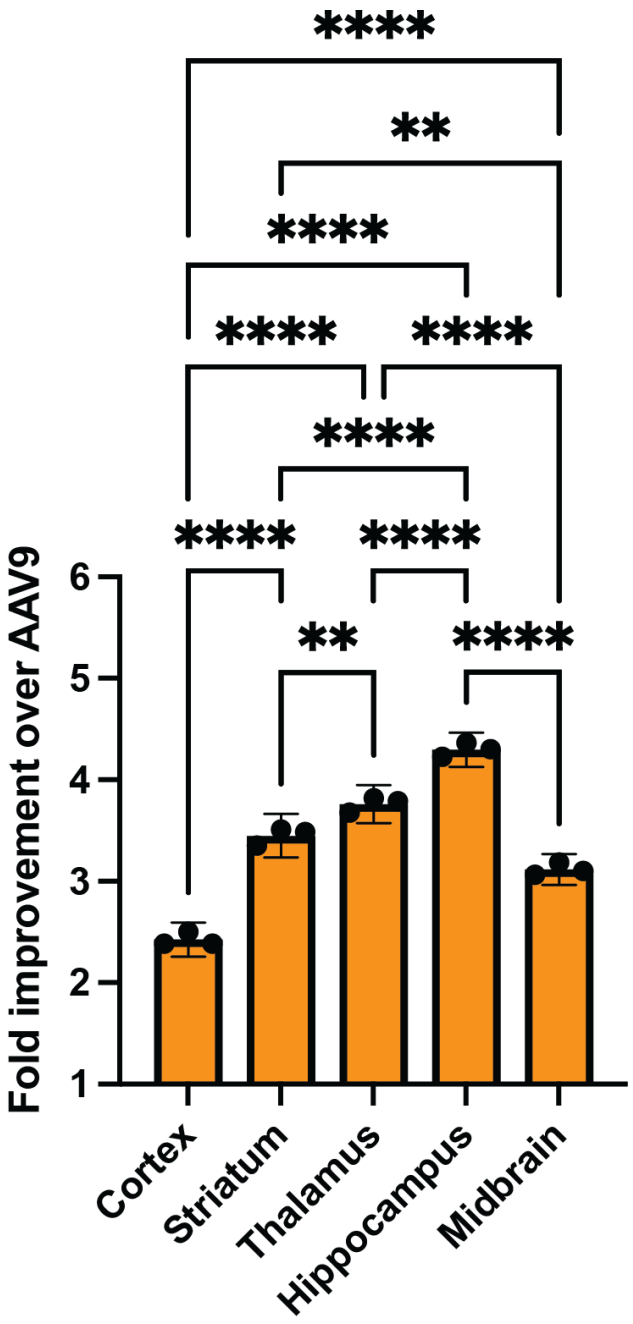

Figure 2-15 Detailed pairwise comparisons for analysis of regional dependence of transduction efficiency for AAV.FUS.3. (**** = p<0.0001; *** = p<0.001; ** = p <0.01; * = p<0.05, ns = not significant; One-way ANOVA with Tukey HSD post-hoc test.). Detailed p-values can be found in the source data appendix. n=3 mice used for all regions. IV injection dose, 10^{10} vg/g body weight.

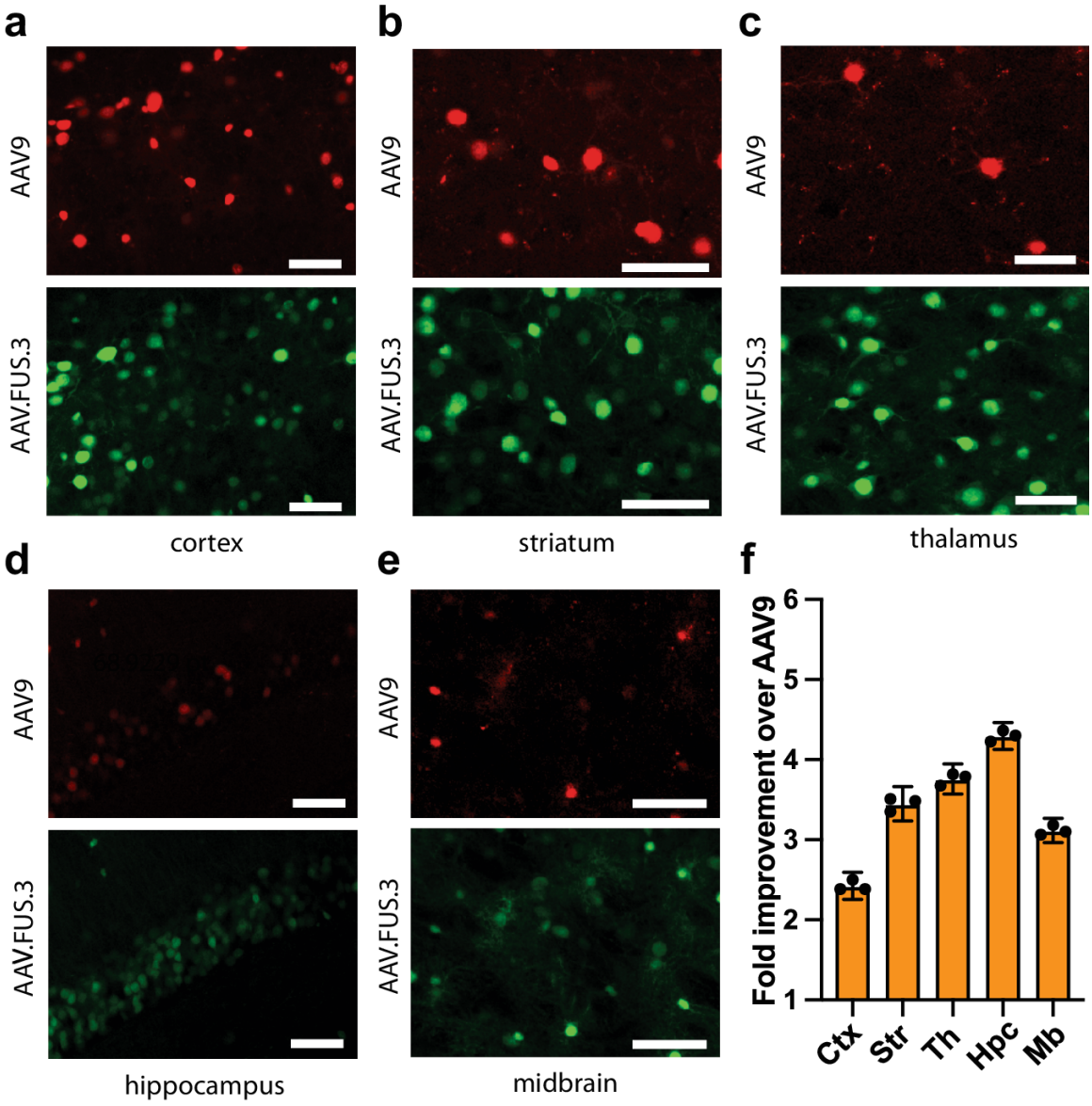

Figure 2-16 AAV.FUS.3 shows regional dependence of transduction efficiency. (**a**) Representative image comparing transduction of the cortex with AAV.FUS.3 (green) and AAV9 (red). (**b**) Representative image comparing transduction of the striatum with AAV.FUS.3 (green) and AAV9 (red). (**c**) Representative image comparing transduction of the thalamus with AAV.FUS.3 (green) and AAV9 (red). (**d**) Representative image comparing transduction of the hippocampus with AAV.FUS.3 (green) and AAV9 (red). (**e**) Representative image comparing transduction of the midbrain with AAV.FUS.3 (green) and AAV9 (red). (**f**) AAV.FUS.3 shows regional differences in transduction efficiency of the tested regions – cortex (Ctx), striatum (Str), thalamus (Th), hippocampus (Hpc), midbrain (Mb). All differences were statistically significant (All pairwise comparison *p*-values < 0.0001, except thalamus vs striatum ($p = 0.0026$) and striatum vs midbrain ($p = 0.0015$), $n = 3$ mice per region, one way ANOVA, $F(4, 10) = 283.4$, $P < 0.0001$; Tukey HSD post-hoc test; center for the error bars represents arithmetic mean.). Scale bars are 50 µm. Error bars are 95% CI.

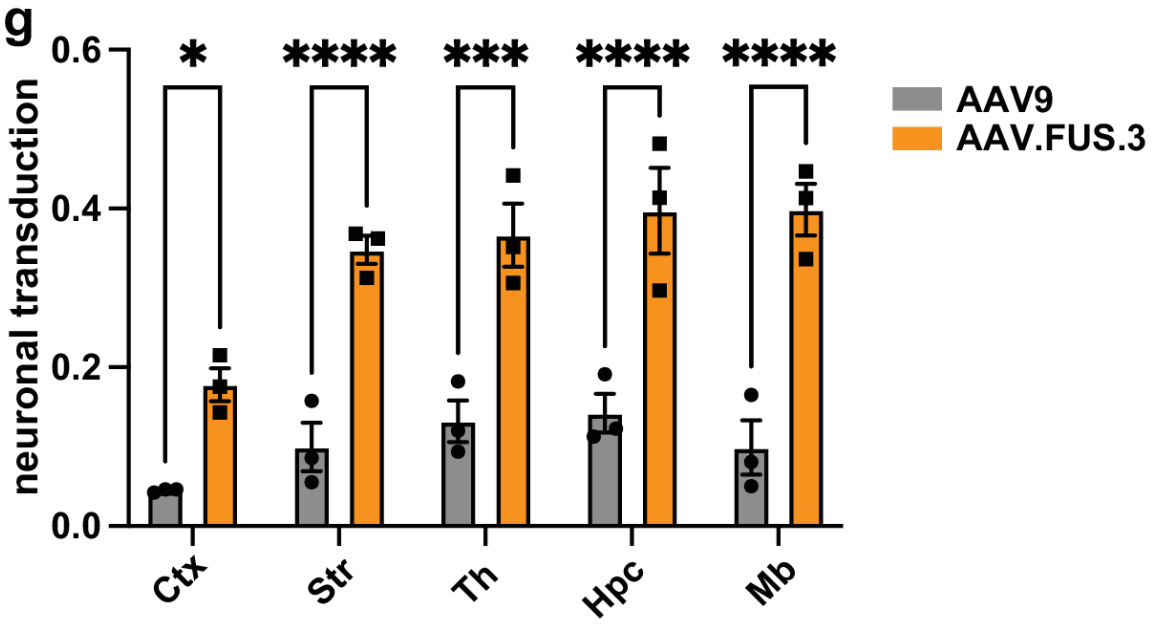

Figure 2-16 ***(continued)*** **AAV.FUS.3 shows regional dependence of transduction efficiency.** (**g**) Neuronal transduction efficiency for AAV9 (gray) and AAV.FUS.3 (orange). AAV.FUS.3 showed significant improvement over AAV9 transduction in all tested regions, $n = 3$ mice per region (two-way ANOVA with Sidak's test; $F(1, 20) = 141.2$; $p = 0.0333$, $p < 0.0001$, $p = 0.0002$, $p < 0.0001$, $p < 0.001$ for Cortex, Striatum, Thalamus, Hippocampus and Midbrain, respectively; center for the error bars represents arithmetic mean.). IV injection dose, 10^{10} VG/g body weight. Scale bars are 50 µm. Error bars are 95% CI.

2.7 AAV.FUS.3 Transduction is Improved Over AAV9 After Direct Intraparenchymal Delivery

The observed enhancement in AAV.FUS.3's transduction efficiency likely stems from a combination of mechanistic factors involving both the physical effects of FUS and the biological properties of the engineered capsid. First, the transient BBB opening induced by FUS may synergize with capsid mutations that promote more efficient extravasation or binding to endothelial receptors, facilitating greater vector entry into the parenchyma. Second, engineered capsids may exhibit improved interactions with cell surface molecules specific to neurons or glial cells, enhancing post-entry processes such as endocytosis, intracellular trafficking, nuclear entry, and uncoating—key rate-limiting steps in successful transduction. Third, FUS itself may alter the perivascular microenvironment, including upregulating cell surface adhesion molecules or temporarily modulating immune surveillance, which could further potentiate vector uptake and reduce clearance. Fourth, capsid modifications may reduce hepatic tropism and off-target sequestration, increasing the effective dose available to the targeted brain regions and improving the brain-to-periphery biodistribution ratio. Finally, local changes in tissue permeability and shear stress induced by acoustic cavitation could influence vector diffusion and cell contact dynamics, which may be better exploited by capsids with altered surface charge or hydrophobicity.

Together, these mechanisms suggest that rationally or evolutionarily engineered AAV capsids are not only better suited for navigating the altered vascular environment induced by FUS-BBBO but may also possess intrinsic features that make them more efficient at transducing neural cells once they enter the brain. Elucidating these synergistic interactions between physical BBB modulation and viral capsid design is essential for optimizing next-generation gene delivery tools for neurological disorders. As such, understanding the basis of these performance enhancements will not only guide future vector development but may also help define the biophysical and cellular constraints governing non-invasive brain-targeted gene therapy.

Given its improved efficiency of neuronal transduction after FUS-BBBO, we hypothesized that AAV.FUS.3 may also show improved efficiency upon intraparenchymal injection. Such improvement in transduction would suggest that at least part of that effect is due to improved transduction efficiency once the AAV.FUS.3 enters the brain, rather than from improve rate of passage across the FUS-opened BBB. Indeed, when injected into the hippocampus, our evolved variant showed 2.29-fold increased transduction efficiency compared to AAV9, which is similar to the 2.56-fold improvement seen with FUS-BBBO (**Fig. 2-17**).

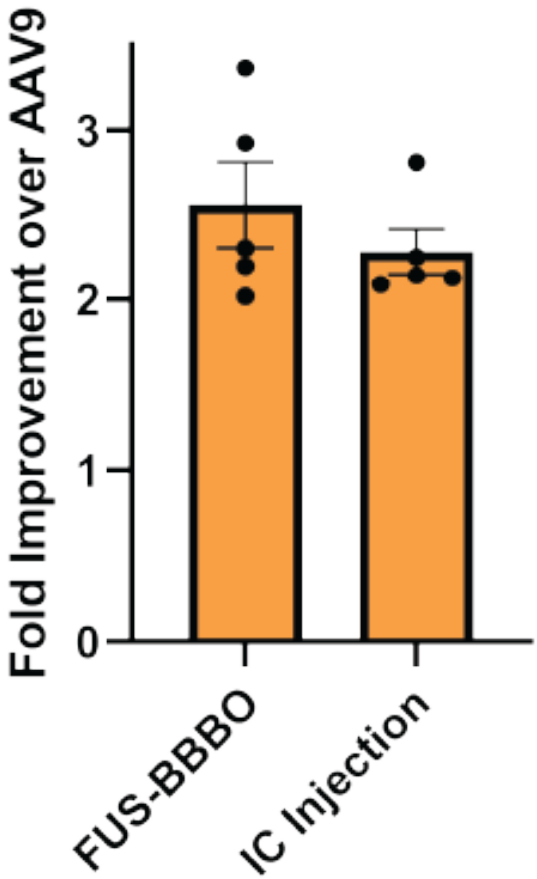

Figure 2-17 Relative efficiency of neuronal transduction for AAV.FUS.3 and AAV9 upon intraparenchymal injection. The intraparenchymal injection dose was $4x10^8$ viral genomes into the CA1 of hippocampus. (n=5 mice per group, p=0.3694, two-tailed unpaired t-test; t=0.9689) while the IV injection dose for FUS-BBBO was 10^{10} vg/g body weight.

2.8 AAV.FUS.3 Transduces the Brain in a Mouse Strain in Which It Was Not Selected

Viral vectors engineered through high-throughput screening and selection can exhibit properties that are limited to the strain of animal in which they were selected (Hordeaux et al., 2018). To evaluate the versatility of AAV.FUS.3, we tested its brain and liver transduction in BALB/cJ mice. Our analysis demonstrated that the enhanced properties of AAV.FUS.3 that we observed in C57BL/6J were also present in the BALB /cJ mice. We found significantly improved brain transduction efficiency (3.9 ± 0.1-fold on average across brain regions) (**Fig. 2-18a**) while showing 4.1 ± 0.3-fold reduction in liver transduction compared to AAV9 in BALB/cJ ($n = 6$ mice tested, **Fig. 2-18b**), for a total brain-to-liver transduction ratio of 16.1 ± 0.9-fold ($n = 6$ mice tested) which was higher than what we found in C57BL/6J mice (16.1-fold and 12.1-fold, respectively, $n = 6$ for each group; $p = 0.000376$, two-tailed heteroscedastic t test, $t = 5.350$). Further analysis showed that AAV.FUS.3 has significantly higher neuronal tropism in BALB/cJ mice as well, with 73% (±2.2%, $n = 6$) total brain cell transduction identified as neurons ($p < 0.0001$, two-tailed paired t test, $t = 21.48$, **Fig. 2-18d**). Overall, in BALB/cJ mice we saw an increase in neuronal transduction across all the tested regions, similar to what was observed in C57BL/6J mice ($n = 4$–6 mice per region; $p < 0.0001$ for all tested comparisons, two-way ANOVA with Sidak's multiple comparison test, $F(1, 44) = 494.1$, **Fig. 2-18e**). Similarly to C57BL/6J, in BALB/cJ mice, we observed the highest improvement in the transduction efficiency of AAV.FUS.3 over AAV9 in the hippocampus (Hpc) (4.3-fold, **Fig. 2-18e**). Lower magnification images showing transduction in surrounding brain areas can be found in **Fig. 2-19**.

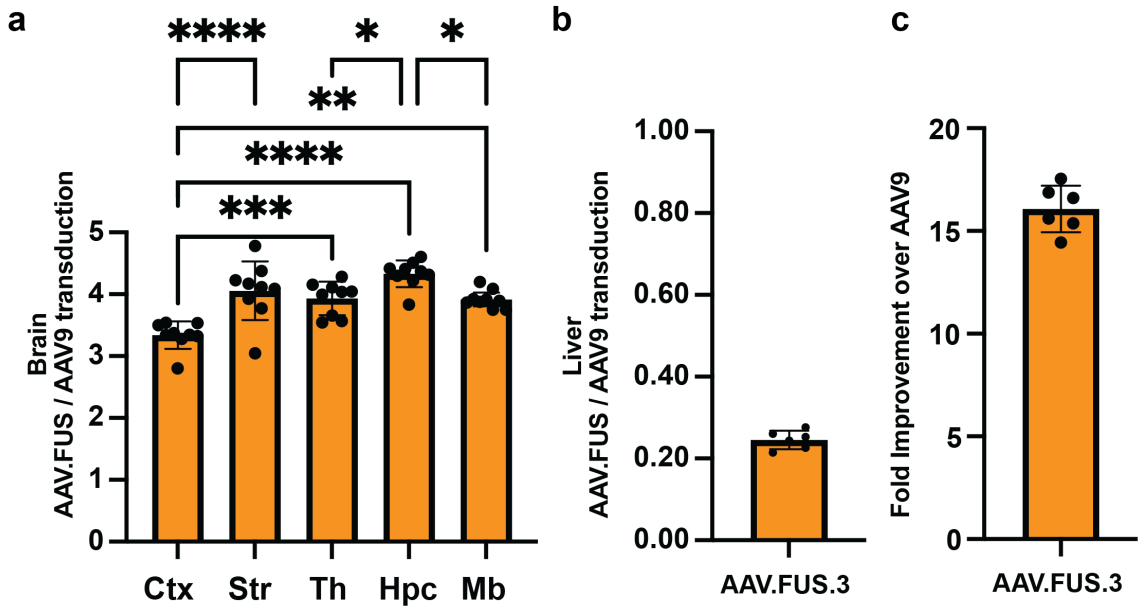

Figure 2-18 AAV.FUS.3 shows similar transduction efficiency in BALB/cJ while maintaining neuronal transduction efficiency. (**a**) Fold-improvement of the total number of transduced cells in the targeted brain areas by AAV.FUS.3 over AAV9 shows hippocampus (Hpc) is mostly highly transduced, and all the other tested regions (cortex (Ctx), Striatum (Str), Thalamus (Th), and Midbrain (Mb)) also showed improved transduction (F (4,40), 14.23, p<0.0001, one-way ANOVA). (**b**) AAV.FUS.3 transduces the livers in BALB/cJ mice less efficiently than AAV9 (4.1±0.3-fold reduction). (**c**) Improvement in brain-to-liver transduction ratio (n=6 mice). Scale bars are 200 microns in panel a and 100 microns in panel c. (**** = p<0.0001, *** = p<0.001; ** = p <0.01; * = p<0.05, ns = not significant). Error bars are 95% CI.

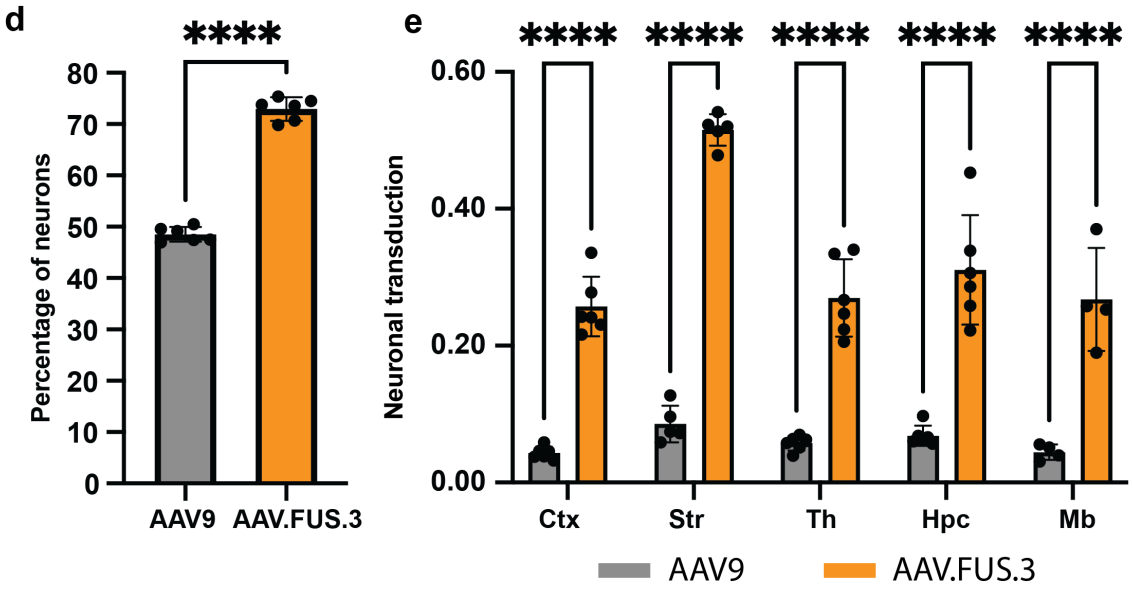

Figure 2-18 *(continued)* AAV.FUS.3 shows similar transduction efficiency in BALB/cJ while maintaining neuronal transduction efficiency. (**d**) Neuronal transduction is improved with AAV.FUS.3 over AAV9 (16.1±0.9-fold improvement, n=6 mice per group, p<0.0001, two-tailed paired t-test; t=21.48).. (**e**) Neuronal transduction efficiency for AAV9 (gray) and AAV.FUS.3 (orange). AAV.FUS.3 showed significant improvement over AAV9 transduction in all tested regions (two-way ANOVA with Sidak's test; F (1, 44) = 494.1; p<0.0001 for all tested regions). Scale bars are 200 microns in panel a and 100 microns in panel c. (**** = p<0.0001, *** = p<0.001; ** = p <0.01; * = p<0.05, ns = not significant). Error bars are 95% CI.

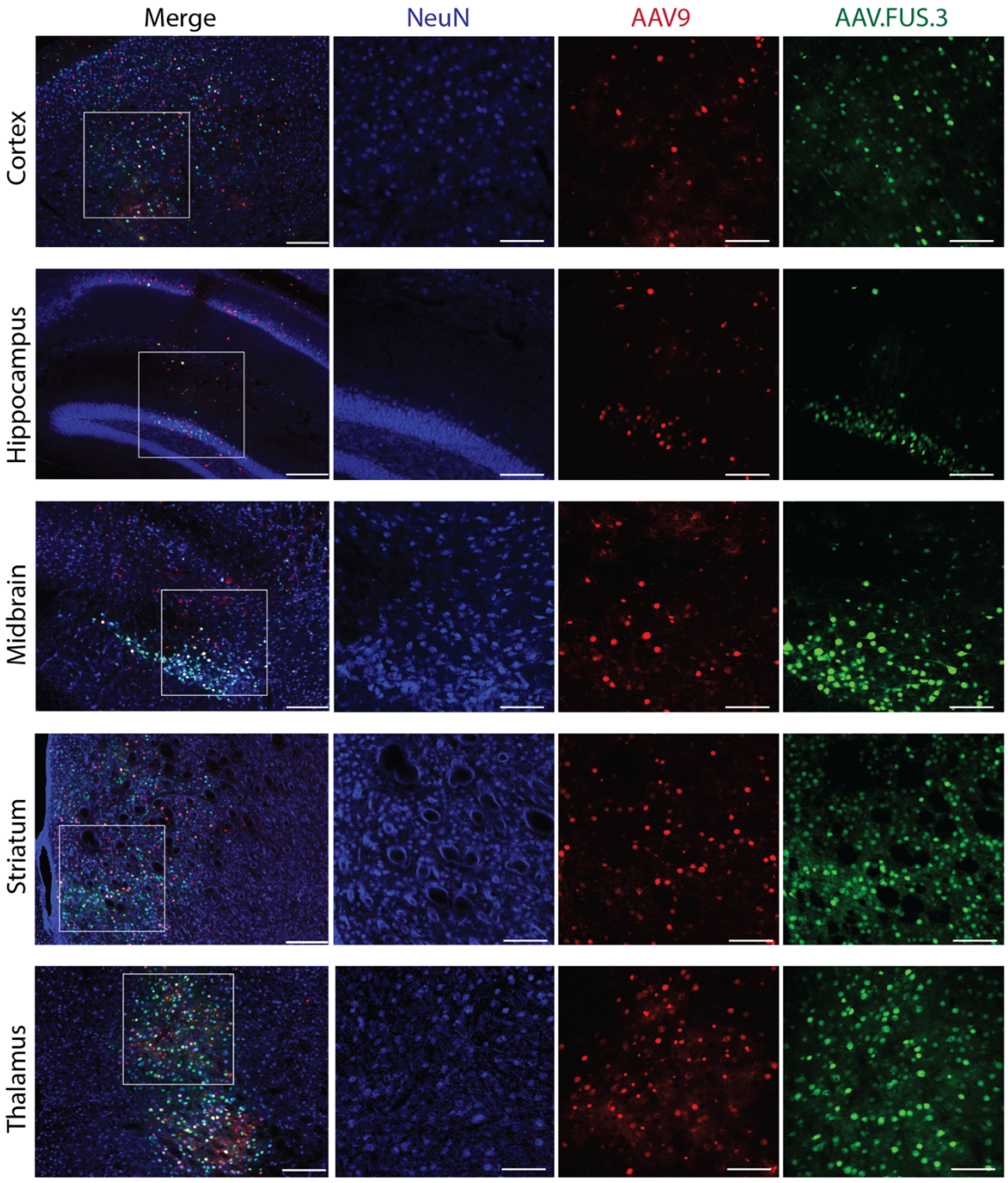

Figure 2-19 Region-specific transduction of AAV9 (red) and AAV.FUS.3 (green) with a neuronal nuclear counterstain (NeuN) in balb/cJ mice. Images were obtained at 20x magnification (left panels, scale bars 200 µm; 3 rightmost panels, scale bar 50 µm).

2.9 Discussion

Our results show that viral vectors can be engineered to improve noninvasive, site-specific gene delivery to the brain using ultrasound-mediated blood-brain barrier opening. Gene therapy is widely used in research and is becoming a clinical reality. However, most of the available methods for gene delivery to the brain either lack regional specificity or are invasive and challenging to apply to large brain regions (Duque et al., 2009; Chan, K. Y. et al., 2017; Deverman, B. E. et al. 2016; Gray, S. J et al. 2013; Eldridge et al., 2015; and Upright & Baxter, 2020). On the other hand, FUS-BBBO has been safely used for gene delivery in a number of studies with naturally-occurring AAVs (Hsu et al., 2013; Kofoed et al., 2022; Szablowski et al., 2018; Thévenot et al., 2012; Wang et al., 2014; and McMahon et al., 2021), including large brain volumes throughout the brain (Felix et al., 2021; and Nouraein et al., 2023). However, the optimization of ultrasound parameters (Chen & Konofagou, 2014; Choi et al., 2010; and Thévenot et al., 2012) and equipment (McDannold et al., 2006; O'Reilly & Hynynen, 2012; White et al., 2005) alone is unlikely to affect the peripheral transduction. Thus, improving efficiency and tissue specificity of gene delivery with newly engineered vectors could lower the cost of the virus production and reduce immune responses to the vectors (Mingozzi & High, 2013), but also reduce non-specific transduction (Rubin et al., 2019; Weitzman & Linden, 2011; and Yue et al., 2008) of peripheral tissues and associated toxicity (High et al., 2018; Hinderer et al., 2018; and Sun et al., 2013). These improvements can facilitate the widespread use of FUS-BBBO and provide a strategy to generate other improved AAVs for FUS-BBBO delivery.

In this study, we approached the problem of improving FUS-BBBO gene delivery by engineering the viral vectors themselves. The resulting improvements include an increase in brain transduction per viral vector injected, a reduction in peripheral expression, and an increase in neuronal tropism. Among the selected five AAV.FUS candidates, four transduced target brain sites more efficiently than AAV9 while also lowering transgene expression in the liver in the same mice. Our top candidate, which we call AAV.FUS.3, demonstrated improved transduction in five different brain regions and an overall efficiency of targeting the brain, defined as the ratio of brain to liver (peripheral) transduction, improved 12.1-fold

compared to AAV9. This improvement in tissue specificity is particularly important because peripheral transduction can lead to toxicity. For example, AAV-based gene therapy has been shown to induce dose-dependent liver toxicity in clinical trials (Kishimoto & Samulski, 2022; and S. W. Pipe et al., 2023). Our results show that AAV.FUS3 maintains its improved targeted brain transduction and reduced liver transduction relative to AAV9 at a lower dose of virus. The absolute transduction level observed at 10^9 vg/g suggests that this relatively low dose may be sufficient for brain transduction. Furthermore, the relative similarity in transduction levels between 10^9 and 10^{10} vg/g suggests that higher systemic doses of AAVs may result in diminishing returns, consistent with previous work (Burr et al., 2022). Larger-scale studies will be needed to evaluate peripheral transduction and toxicity in all peripheral organs and peripheral nervous system such as dorsal root ganglia (DRG) (Buss et al., 2022; and Hinderer et al., 2018) in large animal species before potential translation of AAV.FUS.3.

Our results suggest the need to investigate the mechanisms by which AAVs enter the brain after FUS-BBBO and what accounts for the differences in efficiency among serotypes. The prevailing understanding of FUS-BBBO mechanisms suggests that FUS loosens tight junctions in the vasculature, allowing molecules and nanoparticles such as AAVs to pass from the blood into the brain (Poon et al., 2016). Within this framework, reductions in peripheral uptake (leaving more AAV to circulate) and reduced binding to extracellular matrix (Dalkara et al., 2013) could help certain serotypes enter through physically generated openings and reach neurons more efficiently. We also found that direct intraparenchymal co-injection of AAV.FUS.3 and AAV9 showed improved transduction of the former, suggesting that AAV.FUS.3 transduces brain cells more efficiently after reaching the brain parenchyma. A final potential contributing factor is any molecular change that FUS-BBBO could cause to the vascular endothelium, leading to more complex interaction changes between viral vectors and their target. Understanding these factors would enable additional future engineering and optimization of FUS-BBBO-based gene delivery.

With further studies, AAVs engineered for FUS-BBBO-based gene delivery may provide clinical benefits over existing serotypes. Naturally occurring AAV serotypes, such as AAV9, have been successfully used in clinically approved therapies (Day et al., 2021; Gaudet et al., 2012; Maguire et al., 2019; and S. W. Pipe et al., 2023), including AAV9 intravenous delivery at doses higher than presented in this study (Day et al., 2021). Recently, a groundbreaking study has also shown that delivery of AAV9 into the brain can be achieved in non-human primates using FUS-BBBO (Blesa et al., 2023), further bolstering the translational potential of this procedure. The current limitations of gene therapies include commonality of pre-existing neutralizing antibodies in a large fraction of the population (Weber, 2021); high liver transduction leading to toxicity (Kishimoto & Samulski, 2022) and potential carcinogenicity (Sabatino et al., 2022); AAV-induced toxicity in DRGs in primates (Buss et al., 2022; Hinderer et al., 2018); and high cost of the therapy (Harrison & Friedmann, 2023). At least some of these problems could be addressed with viral vector engineering for improved brain transduction after FUS-BBBO. We expect viral capsids engineered under our paradigm can be instrumental in facilitating both pre-clinical and clinical studies. To make such engineered AAVs translatable, the major future challenge remains to identify which of these engineered vectors will be efficacious in humans.

Overall, this study shows that the molecular engineering of AAV capsids can lead to improved ultrasound-mediated gene delivery to the brain. Our screen yielded AAV.FUS.3, the first, to the best of our knowledge, viral vector expressly engineered to work in conjunction with a specific physical delivery method.

2.10 Materials and Methods

Animals

Animals. 10–14 week-old C57BL/6J, BALB/cJ, and Syn-1-Cre mice were obtained from Jackson Lab. Both male and female mice were used in the study, as described in the source data file. Animals were housed in a 12 h light/dark cycle and were provided with water and food ad libitum. All experiments were conducted under a protocol approved by the Institutional Animal Care and Use Committee (IACUC) of the California Institute of Technology and Rice University.

Focused ultrasound equipment and BBB opening procedures

FUS-BBBO. Syn1-Cre, C57BL/6J, and BALB/cJ mice (10–14 weeks old) were anesthetized with 2% isoflurane in air, the hair on their head removed with Nair depilation cream and then cannulated in the tail vein using a 30-gauge needle connected to PE10 tubing. The cannula was then flushed with 10 units (U)/ml of heparin in sterile saline (0.9% NaCl) and attached to the mouse tail using tissue glue (Gluture). Subsequently, the mice were placed in the custom-made plastic head mount and imaged in a 7 T MRI (Bruker Biospec). A fast low-angle shot sequence (echo time TE = 3.9 ms, repetition time TR = 15 ms, flip angle 20°) was used to record the position of the ultrasound transducer in relation to the mouse brain. Subsequently, the mice were injected via tail vein with AAVs. Within two minutes after viral injection, the mice were also injected with 1.5×10^6 DEFINITY microbubbles (Lantheus) and 0.125 μmol of ProHance (Bracco Imaging) dissolved in sterile saline, per g of body weight. The dose of DEFINITY was identical as used in our previous studies (Russell, S. et al. 2017). The dose of ProHance was chosen based on the manufacturer's recommendations. Within 30 s, the mice were insonated using an eight-channel FUS system (Image Guided Therapy) driving an eight-element annular array transducer with a diameter of 25 mm and a natural focal point of 20 mm, coupled to the head via Aquasonic ultrasound gel. The gel was placed on the top and both sides of the animal's head to minimize reverberations from tissue/air interfaces. The focal distance was adjusted electronically. The ultrasound

parameters used were 1.5 MHz, 1% duty cycle, and 1 Hz pulse repetition frequency for 120 pulses and were derived from a published protocol. The pressure was calibrated using a fiber optic hydrophone (Precision Acoustics), with 21 measurements and uncertainty of ±3.8% (SEM). The pressure for FUS-BBBO was chosen to maximize the safety of delivery and was chosen on the basis of our previous studies1 and preliminary data in our laboratory. The ultrasound parameters were 1.5 MHz, 0.33 MPa pressure accounting for skull attenuation (18%) (Choi et al., 2006), 1% duty cycle, and 1 Hz pulse repetition frequency for 120 pulses. For each FUS site, DEFINITY and Prohance were re-injected before the additional insonation. Each animal underwent four insonations located in one hemisphere, starting from the midbrain and going forward. The time between each insonation was approximately 3 min and included 120 s of insonation and 1 min for readjustment of positioning on the stereotaxic frame. The center focus of beams was separated by 1.35–1.5 mm (depending on mouse weight 25–35 g) in the anterior / posterior direction.

Alternative Focused ultrasound equipment and BBB opening procedures

For the low-dose AAV.FUS.3 evaluation, we used different equipment since the original setup became unavailable. For this study, we used the RK50 (FUS Instruments) with the same center frequency (1.5 MHz) and f = 0.7. We used the same pulse length, frequency, and number of pulses as before. Since the pressure calibration shows high variation (±20% for fiber optic hydrophone used in this study; Precision Acoustics, Dorchester, UK) we adjusted the voltage on the transducer empirically to match the previous experiment and provide BBB opening without tissue damage (input peak-to-peak voltage of 14.2 V, corresponding to the peak negative pressure of 0.52 MPa when calibrated against the original transducer using a needle hydrophone (Onda)). Instead of MRI guidance, we used bregma-lambda targeting. Briefly, the mouse was mounted on a stereotactic platform using ear bars, bite bar and nose cone. A midline scalp incision was vertically made to expose the skull after disinfecting the site using three alternating scrubs of chlorhexidine scrub and chlorhexidine solution. Bregma-lambda locations were then registered in the RK50 software using a guide pointer, and FUS-BBBO was carried out as described above.

Plasmids and DNA library generation

The plasmids used were either obtained from Addgene, Caltech's vector core, or modified from these plasmids. The AAV library genome used for selection (acceptor plasmid, rAAV9Rx/a-delta-CAP) was obtained from Caltech's vector core facility, as were other plasmids (REP2-CAP9Stop-DeltaX/A, pUC18). The Rep-Cap plasmid for packaging AAV.FUS candidates were modified from Addgene plasmid #103005 by introducing mutations selected from the screen. For testing the transduction, we used a plasmid obtained from Addgene (pAAV-CaG-NLS-EGFP - #104061) and a plasmid modified in-house with exchanged EGFP for mCherry protein (pAAV-CaG-NLS-mCherry).

Primers and procedures for DNA library generation

Mutations were introduced into the acceptor plasmid using a PCR with degenerated primers (7MNN) with a sequence

5' - GTATTCCTTGGTTTTGAACCCAACCGGTCTGCGCCTGTGCNMNNMN
NMNNMNNMNNMNNTTGGGCACTCTGGTGGTTTGTG - 3',

targeted as a 7-aminoacid insertion between residues 587 and 588. The amplified insert was then introduced into the capsid plasmid through restriction cloning using XbaI and AgeI enzymes. DNA from the treated brain was recovered by PCR using two pairs of plasmids – the first step of amplification was done using

5' - CAGGTCTTCACGGACTCAGACTATCAG - 3'

and

5' - CAAGTAAAACCTCTACAAATGTGGTAAAATCG - 3'

primers which selected for the DNA that has been modified by Cre enzyme. The second stage, intended to amplify the DNA was performed using a pair of primers:

5’ - ACTCATCGACCAATACTTGTACTATCTCTCTAGAAC - 3’

and

5’ - GGAAGTATTCCTTGGTTTTGAACCCAA - 3’

Virus production and purification

AAV library was purified as previously published (Deverman, B. E. et al., 2016). In short, we transfected the DNA carrying a genome containing capsid which has been modified by the 7-mer insertion (10 ng per 100 mm diameter dish), the helper DNA containing REP protein (10 μg per 100 mm diameter dish, and 9.99 μg of empty pUC19 carrier plasmid), and an AdV helper plasmid (20 μg per 100 mm diameter dish) using PEI. Media was changed 16 h after transfection, and then collected 48 h post-transfection and stored in 4 C. 60 h after the transfection, we scraped the cells into San digestion buffer (Tris pH 8.5 with 500 mM NaCl and 40 mM MgCl2 with Salt Active Nuclease). Virus in the media was precipitated using 1/5 volume of 5X PEG8000+NaCl (40% PEG-8000 and 2.5 M NaCl), incubated on ice for 2 h, and spun at 3000g for 30 min at 4 C. The media and cell-scraped stocks were then combined and precipitated using iodixanol gradient precipitation (virus appears on the 40–60% iodixanol interface), diluted into 15 ml PBS with 0.001% Pluronic-F68, and sterile-filtered through a 0.2-μm PES filter. Finally, the buffer was dialyzed using Amicon 100 KDa cut-off centrifuge filters at least 3 times to remove residual iodixanol, after which the virus was tittered using a standard qPCR protocol (Deverman, B. E. et al., 2016) (Vigene Biosciences, Rockville Maryland). All batches of the AAV were purchased from the same company and the same production batch was used for co-administration of AAVs. AAV.FUS candidates were packaged and titered using a commercial service (Vigene biosciences) to ensure reproducibility for external investigators, as the titers can show variability between

different labs (Lock, M. et al., 2010). We have re-titered the AAV.FUS.3 and AAV9 from another batch again in our lab, to make sure that the improvement of AAV.FUS over AAV9 is consistent between investigators.

In vivo selection and gene delivery

To enable in vivo selection of AAV.FUS we delivered the AAV library to one hemisphere through FUS-BBBO. We targeted four sites corresponding to the striatum, dorsal hippocampus, ventral hippocampus, and midbrain using MRI guidance. We used 0.33 MPa pressure and other parameters as described in the Focused ultrasound equipment and BBB opening procedures section. The parameters used were identical during the in vivo selection and testing of the AAV.FUS candidates. The AAVs were delivered intravenously. For the first round of selection, the dose delivered was 6.7E9 viral genomes per gram of body weight. The library for the first round of evolution contained 1.3E9 sequences, yielding approximately 5 genomes of each clone per gram of body weight. For the second round, where the library contained 2098 candidates, 1.3E9 viral genomes per gram of body weight were delivered, yielding 6.2E5 viral genomes for each clone per gram of body weight. Following the selection of a single candidate (AAV.FUS.3) for further analysis, we repeated the above procedure using a dose of 1E9 viral genomes per gram of body weight. Following FUS-BBBO or intraparenchymal injections, mice were returned to the home cages for 14 days, after which they were euthanized by CO_2 overdose.

Intraparenchymal injections

Using a stereotaxic frame (Kopf), intraparenchymal co-injections of AAV9 and AAV.FUS.3 were also performed using a microliter syringe equipped with a 34-gauge beveled needle (Hamilton) that is installed to a motorized pump (World Precision Instruments). Each AAV was injected unilaterally at a dose of 4E8 viral genomes per gram of body weight to the CA1

in the hippocampus (AP –1.94 mm, ML + 1.0 mm, DV –1.3 mm) infused at a rate of 200 nL/min, and the needle was kept in place for 5 min before removing it from the injection site.

Tissue preparation for DNA extraction

The brains of mice euthanized with CO_2 overdose were extracted, and the targeted hemisphere was separated from the control hemisphere with a clean blade. Each hemisphere was then frozen at −20C prior to DNA extraction. The brains were then homogenized in Trizol using a BeadBug tissue homogenization device with dedicated pre-filled 2.0 ml tubes with beads (Zirconium coated, 1.5 mm, Benchmark Scientific, Sayreville, New Jersey) for 1–3 min until tissue solution was homogenous. The DNA was then extracted with Trizol and amplified first with CRE-independent, and then CRE-dependent PCR, first through 15–25 cycles, and then 15 cycles of PCR (Deverman, B. E. et al., 2016) with Q5 Hot-Start DNA polymerase using the manufacturer's protocols (NEB, Ipswich, MA).

For the first step of PCR amplification we used

5' - CAGGTCTTCACGGACTCAGACTATCAG - 3'

as a forward primer, and

5' - CAAGTAAAACCTCTACAAATGTGGTAAAATCG - 3'

as a reverse primer. For the second step, we used

5' - ACTCATCGACCAATACTTGTACTATCTCTCTAGAAC - 3'

as a forward primer, and

5' - GGAAGTATTCCTTGGTTTTGAACCCAA - 3'

as a reverse primer.

Next generation sequencing data analysis

The variable region of all detected capsid sequences was extracted from raw fastq files using the awk tool in Unix terminal. This process filtered out sequences not containing the constant 19 bp region flanking each side of the variable region. Sequences were then sorted, checked for length, and ordered from highest to lowest copy number in the sequencing experiment. During the first screen, the top 3000 were chosen. Among these 3000, any sequence that was only a point mutation away from a sequence and 30x less abundant was removed and assumed to be a potential sequencing readout error. This led to our final library of 2098 sequences, which were synthesized by Twist Biosciences (San Francisco, CA) for use in the second round of screening. This second AAV library also included a set of 2098 "codon-optimized" capsid variants that were encoded for the same protein as the original sequences but using a different DNA sequence chosen by the IDT codon optimization tool. To process the second batch of sequencing data, we first normalized the copy numbers of the sequences in each experiment to one to ensure the comparability of different samples. Then, we filtered out sequences that were not contained within the input library. Finally, we evaluated the normalized frequency of reads for each sequence, defined as the normalized copy number of each sequence averaged among original and codon-optimized variants for each capsid. Top sequences for further analysis were selected to be the most abundant sequences that appeared at least 100x more frequently in the targeted brain hemisphere than the non-targeted hemisphere in all tested mice, and from these sequences, the top 5 were chosen as AAV.FUS candidates.

Histology, immunostaining, and image processing

After cardiac perfusion and extraction brains were post-fixed for 24 h in neutral buffered formalin (NBF). Brains were then sectioned coronally at 50-μm on Compresstome VF-300

(Precisionary Instruments, Natick, MA). Sections were immunostained with anti-NeuN Alexa Fluor 405-conjugated antibody (1:500 dilution, RBFOX3/NeuN Antibody by Novus Biological, stock number: NBP1-92693AF405), anti-GFAP Alexa Fluor 405-conjugated antibody (1:500 dilution, GFAP Antibody by Novus Biological, stock number: NBP1-05197AF405), and anti-Iba1 Alexa Fluor 405-conjugated antibody (1:500 dilution, Iba1 Antibody by Novus Biological, stock number: NBP1-75760AF405). For oligodendrocyte staining, sections were immunostained with rabbit anti-Olig2 antibody (1:200 dilution, Abcam, stock number: 109186) and Alexa Fluor 647-conjugated goat anti-rabbit IgG antibody (1:200 dilution, Invitrogen, stock number: A21244). Sections were imaged on a Zeiss LSM-800 microscope using a 20x objective. Channels' laser intensities normalized to the brightness of mCherry and GFP proteins, the fluorescence of which was used to evaluate transduction. Images were then randomized, and anonymized. The experimenter was blinded in terms of fluorophore color, tested AAV strain, or the mouse identification (H.L., M.H). One data set (**Fig. 2-12**) was not anonymized due to the error in file-sharing setting. Three 50-μm coronal sections of the brain were analyzed for each mouse, for each strain of the AAV including the section at the center of the FUS-target and the sections 500 and 1000 μm anterior to that section.

The FUS-BBBO-targeted regions for evaluation of transduction efficiency and the total transduced cells were selected by setting the regions of interest (ROI) to be the area bound by gene expression at the FUS-targeted site due to AAV transduction such that less than 1% of all transduced cells are outside the bounds of the ROI.

The data was then independently validated by an experimenter blinded to the goals of the study (J.T). The inter-experimenter variability was 12.5% (1.9-fold (RL, primary scorer) vs 2.1-fold difference (JT, secondary scorer), $n = 15$ randomly selected images, a total of 11,230 cells counted) and the difference between the scores was not statistically significant ($p = 0.071$, two-tailed, paired t test). To evaluate the BBB permeability of the AAV in the absence of FUS-BBBO (off-target transduction), a randomly chosen untargeted region at least 2 mm from the center of the targeted region (4 times the distance of distance half-width

half maximum of pressure, resulting in ~16-fold pressure reduction) was used within the same sections that were used to evaluate transduction efficiency at FUS focus.

Statistical analysis

A two tailed t-test, without assuming equal variance, was used when comparing the means of two data sets. For the comparison of more than two data sets, one-way ANOVA was used, with Tukey's HSD post-hoc test to determine the significance of pairwise comparisons. When more than one variable was compared across multiple samples, two-way ANOVA was used, followed by Sidak's multiple comparisons test with F statistic provided with regards to differences between AAV9 and AAV.FUS candidates. Pairing was used if the compared data was obtained from the same specimen (e.g. histological analysis after co-injection of two viral vectors into a single mouse), and not used if the data were analyzed from different unrelated specimens. Specific p-values are provided in a source data appendix, due to the large numbers of pairwise comparisons in this study. Software (Prism 9) was used for statistical analysis, and the minimum p-value calculated by the software was $p < 0.0001$.

2.11 Other Information

Supplementary Note 1: An open reading frame encoding the CAP protein of AAV.FUS.3 Highlighted region (yellow) indicates the site of insertion.

5′–

ATGGCTGCCGATGGTTATCTTCCAGATTGGCTCGAGGACAACCTTAGTGAAGGAATTCG
CGAGTGGTGGGCTTTGAAACCTGGAGCCCCTCAACCCAAGGCAAATCAACAACATCAAG
ACAACGCTCGAGGTCTTGTGCTTCCGGGTTACAAATACCTTGGACCCGGCAACGGACTC
GACAAGGGGGAGCCGGTCAACGCAGCAGACGCGGCGGCCCTCGAGCACGACAAGGCCTA
CGACCAGCAGCTCAAGGCCGGAGACAACCCGTACCTCAAGTACAACCACGCCGACGCCG
AGTTCCAGGAGCGGCTCAAAGAAGATACGTCTTTTGGGGGCAACCTCGGGCGAGCAGTC
TTCCAGGCCAAAAAGAGGCTTCTTGAACCTCTTGGTCTGGTTGAGGAAGCGGCTAAGAC
GGCTCCTGGAAAGAAGAGGCCTGTAGAGCAGTCTCCTCAGGAACCGGACTCCTCCGCGG
GTATTGGCAAATCGGGTGCACAGCCCGCTAAAAAGAGACTCAATTTCGGTCAGACTGGC
GACACAGAGTCAGTCCCAGACCCTCAACCAATCGGAGAACCTCCCGCAGCCCCCTCAGG
TGTGGGATCTCTTACAATGGCTTCAGGTGGTGGCGCACCAGTGGCAGACAATAACGAAG
GTGCCGATGGAGTGGGTAGTTCCTCGGGAAATTGGCATTGCGATTCCCAATGGCTGGGG
GACAGAGTCATCACCACCAGCACCCGAACCTGGGCCCTGCCCACCTACAACAATCACCT
CTACAAGCAAATCTCCAACAGCACATCTGGAGGATCTTCAAATGACAACGCCTACTTCG
GCTACAGCACCCCCTGGGGGTATTTTGACTTCAACAGATTCCACTGCCACTTCTCACCA
CGTGACTGGCAGCGACTCATCAACAACAACTGGGGATTCCGGCCTAAGCGACTCAACTT
CAAGCTCTTCAACATTCAGGTCAAAGAGGTTACGGACAACAATGGAGTCAAGACCATCG
CCAATAACCTTACCAGCACGGTCCAGGTCTTCACGGACTCAGACTATCAGCTCCCGTAC
GTGCTCGGGTCGGCTCACGAGGGCTGCCTCCCGCCGTTCCCAGCGGACGTTTTCATGAT
TCCTCAGTACGGGTATCTGACGCTTAATGATGGAAGCCAGGCCGTGGGTCGTTCGTCCT
TTTACTGCCTGGAATATTTCCCGTCGCAAATGCTAAGAACGGGTAACAACTTCCAGTTC
AGCTACGAGTTTGAGAACGTACCTTTCCATAGCAGCTACGCTCACAGCCAAAGCCTGGA
CCGACTAATGAATCCACTCATCGACCAATACTTGTACTATCTCTCTAGAACTATTAACG
GTTCTGGACAGAATCAACAAACGCTAAAATTCAGTGTGGCCGGACCCAGCAACATGGCT
GTCCAGGGAAGAAACTACATACCTGGACCCAGCTACCGACAACAACGTGTCTCAACCAC
TGTGACTCAAAACAACAACAGCGAATTTGCTTGGCCTGGAGCTTCTTCTTGGGCTCTCA
ATGGACGTAATAGCTTGATGAATCCTGGACCTGCTATGGCCAGCCACAAAGAAGGAGAG
GACCGTTTCTTTCCTTTGTCTGGATCTTTAATTTTTGGCAAACAAGGAACTGGAAGAGA
CAACGTGGATGCGGACAAAGTCATGATAACCAACGAAGAAGAAATTAAAACTACTAACC
CGGTAGCAACGGAGTCCTATGGACAAGTGGCCACAAACCACCAGAGTGCCCAATGGAGC
GAGGGCGGCCAGCCCGCACAGGCGCAGACCGGTTGGGTTCAAAACCAAGGAATACTTCC
GGGTATGGTTTGGCAGGACAGAGATGTGTACCTGCAAGGACCCATTTGGGCCAAAATTC
CTCACACGGACGGCAACTTTCACCCTTCTCCGCTGATGGGAGGGTTTGGAATGAAGCAC

CCGCCTCCTCAGATCCTCATCAAAAACACACCTGTACCTGCGGATCCTCCAACGGCCTT
CAACAAGGACAAGCTGAACTCTTTCATCACCCAGTATTCTACTGGCCAAGTCAGCGTGG
AGATCGAGTGGGAGCTGCAGAAGGAAAACAGCAAGCGCTGGAACCCGGAGATCCAGTAC
ACTTCCAACTATTACAAGTCTAATAATGTTGAATTTGCTGTTAATACTGAAGGTGTATA
TAGTGAACCCCGCCCCATTGGCACCAGATACCTGACTCGTAATCTGTAA-3’

Supplementary Note 2: Alternative insertions for the other AAV.FUS candidates:

FUS.1 insert after 1764th nucleotide, 588th residue

GCGGGGAATACTAGTGATCGG

FUS.2 insert after 1764th nucleotide, 588th residue

GCCACCGACGCCTACAACAAG

FUS.3 insert after 1764th nucleotide, 588th residue

TGGAGCGAGGGCGGCCAGCCC

FUS.4 insert after 1764th nucleotide, 588th residue

AGCGTGGGCAGCGCCGACCCC

FUS.5 insert after 1764th nucleotide, 588th residue

GTGCGGATGGAGGGTGAGGTG

Data availability

The authors declare that all data supporting the results in this study are available within the paper, its Supplementary Information and its Source Data file. Microscopy images and raw sequencing data are available from the corresponding author upon reasonable request owing to their large size and numbers. The NGS data generated through this study have been deposite in the Sequence Read Archive (SRA) database under accession code: PRJNA1112439.

Acknowledgements

We thank Drs. Benjamin Deverman, Nicholas Flytzanis, Nicholas Goeden, and Viviana Gradinaru, and the CLOVER center at Caltech for helpful discussions and the Biological Imaging Facility of the Beckman Institute. This research was supported by the National Institutes of Health (grant UG3MH120102 to M.G.S.), the Jacobs Institute for Molecular Engineering in Medicine, the Sontag Foundation, the Merkin Institute for Translational Research, and 2019 NARSAD Young Investigator Grant from the Brain and Behavior Research Foundation (grant 27737 to J.O.S.). Related work in the Shapiro Lab is supported by the David and Lucille Packard Foundation and the Heritage Medical Research Institute and in Szablowski lab by The G. Harold and Leila Y. Mathers Charitable Foundation. M.G.S. is an Investigator of the Howard Hughes Medical Institute. JEH acknowledges support from Rose Hills foundation and Barry Goldwater Scholarship and from the NSF GRFP. MH acknowledges support from NSF GRFP.

Contributions

H.L. (Hongyi R. Li), J.O.S. (Jerzy O. Szablowski), and M.G.S. (Mikhail G. Shapiro) conceived and planned the research. H.L., M.H. (Manwal Harb), and J.O.S. performed the in vivo experiments with additional input from J.E.H. (John E. Heath), J.O.S., H.L., and J.E.H. performed the in vitro experiments. J.E.H. and J.O.S. processed the next-generation sequencing data. H.L., M.H., and J.S.T. (James S. Trippett) processed and analyzed histological image data. J.O.S. and M.G.S. wrote the manuscript with input from all other authors. M.G.S. and J.O.S. supervised the research.

Chapter 3

SIC PARVIS MAGNA: ENGINEERING VIRAL VECTORS FOR ACOUSTICALLY TARGETED GENE DELIVERY TO THE NON-HUMAN PRIMATE

3.1 Abstract

Spatially targeted gene delivery to the brain has the potential to treat prevalent neurological and psychiatric diseases such as Parkinson's disease, refractory epilepsy and obsessive-compulsive disorder. However, the site-specific delivery of gene delivery vectors such as adeno-associated viruses (AAVs) is typically performed via invasive injections, limiting their scope of clinical applications. Over the last couple decades, focused ultrasound blood-brain-barrier opening (FUS-BBBO) has emerged as a noninvasive procedure that enables the site-specific entry of biomolecules, nanoparticles and small viral vectors such as AAV into the brain from systemic circulation. However, when used in conjunction with natural AAV serotypes, this approach has limited transduction efficiency, and results in undesirable transduction of peripheral organs. In this project, we used high throughput *in vivo* selection in non-human primates (NHPs) to engineer new AAV vectors specifically designed for local neuronal transduction at the site of FUS-BBBO. In previous work, we have demonstrated that this strategy works well in mice, resulting in vectors with substantially enhanced ultrasound-targeted gene delivery and neuronal tropism and reduced peripheral transduction. Now, we move this technology toward clinical translation by completing a similar screen in NHPs, thereby validating this approach in a large-animal model, identifying specific viruses with greater translatability into humans, and paving the way for larger-scale disease model studies and human clinical translation. The project carries significant translational relevance. It aims to enable targeted treatments for neural circuit diseases. Potential applications of noninvasive spatially targeted gene therapy include epilepsy, Parkinson's disease, chronic

depression, obsessive compulsive disorder (OCD), and any other condition that is currently being treated with local ablation or DBS. Potential genetic payloads to treat such conditions include growth factors, prime editors, neurotransmitter synthesis enzymes and chemogenetic receptors, among others. This work is a critical step toward clinical translation of ultrasound-targeted AAV therapy. By developing viral serotypes that more efficiently enter the brain at the site of FUS-BBBO, reducing the transduction of off-target organs, and reducing the required systemic dose, this work will greatly improve the safety profile and reduce the manufacturing cost of this class of therapies, making it more likely that they will benefit patients. By validating our technology in NHPs, we will take the critical next step toward clinical translation. The successful completion of this project substantially derisk this technology and allow us to seek large-scale support from potential biotech partners, venture capital investors or non-profit/government agencies to take this technology into clinical development.

3.2 Introduction

Gene therapy is one of the most promising emerging approaches to treating human disease. Recently, a number of gene therapies were approved for clinical use, including blindness (Russell, S. et al., 2017), muscular dystrophy (Mendell, J.R. et al., 2017), and metabolic disorders (Gaudet, D. et al., 2013). Many of these therapies use adeno-associated viral vectors (AAVs) to deliver genes to various organs, but few target the brain. Although several neurological and psychiatric diseases could benefit from gene therapies targeting specific neural circuits, a key challenge limiting the development of such treatments is the need for invasive intracranial injections of the viral vectors. While recent advances are enabling brain-wide gene delivery from systemic (Duque, S. et al., 2009; Chan, K.Y. et al., 2017; and Deverman, B.E. et al., 2016) or cerebrospinal fluid circulation (Gray, S.J. et al., 2013) – relevant for a number of conditions – these approaches do not provide the spatial targeting needed to address regionally defined neural circuits.

Regional targeting is important in diseases with local circuit dysregulation or cell degeneration such as epilepsy, Parkinson's disease, OCD and chronic depression. Some of these diseases are currently being addressed with deep-brain stimulation (DBS) therapies, which require invasive neurosurgery and lack cell type specificity in their brain circuit effects.

Focused ultrasound blood-brain barrier opening (FUS-BBBO) is a technique developed over the past ~20 years with the potential to overcome these limitations by providing a route to noninvasive, site-specific gene delivery to the brain (Thévenot, E. et al. 2012; Wang, S. et al. 2017; Szablowski, J.O. et al. 2018; and Alonso, A. et al. 2013). In FUS-BBBO, ultrasound is focused through an intact human skull (Rezai, A.R. et al. 2020; and Lipsman, N. et al. 2018) to transiently loosen tight junctions in the BBB and allow for the passage of molecules from the blood into the targeted brain site. FUS-BBBO can target intravenously administered nanoparticles such as AAVs to millimeter-sized brain sites or cover large regions of the brain without tissue damage. These capabilities place FUS-BBBO in contrast with intracerebral injections, which are invasive and deliver genes to a single 2-3 millimeter-sized region per

injection (Upright, N.A. & Baxter et al. 2020; and Eldridge, M.A.G. et al. 2016), consequently requiring a large number of brain penetrations to cover major regions (e.g. an epileptogenic focus). At the same time, the spatial targeting capability of FUS-BBBO differentiates it from the use of spontaneously brain-penetrating engineered AAV serotypes, which lack spatial specificity (Chan, K.Y. et al. 2017). FUS-BBBO has been successfully used to open the BBB in human patients (Rezai, A.R. et al. 2020; and Lipsman, N. et al. 2018) and is moving toward FDA approval for indications focused on cross-BBB delivery of small molecules and biologics.

In proof-of-concept studies, FUS-BBBO has been used in rodents to introduce AAVs encoding reporter genes such as GFP (Thévenot, E. et al., 2012 and Wang et al., 2015), growth factors (Karakatsani et al., 2019) and optogenetic receptors. In our work, the delivery of chemogenetic receptors to the hippocampus provided the ability to modulate memory formation (Szablowski et al., 2018). Despite its promise, three critical drawbacks currently limit the potential of FUS-BBBO in research and therapy applications. First, while the BBB effectively prevents non-FUS-targeted regions of the brain from transduction by systemically administered AAV, peripheral organs allow AAV entry and consequently receive a high dose of the virus, which can lead to toxicity (Nature Biotechnology, 2020). Second, the relative inefficiency of AAV entry at the site of FUS-BBBO leads to the requirement of high doses of systemic AAVs, on the order of $\sim 10^{10}$ viral particles per gram of body weight. While this magnitude has been used in recent clinical trials, it drives higher peripheral transduction and adds to the cost of potential therapies. Third, efficient delivery of AAV typically requires acoustic parameters below, but close to (Wang et al., 2015 and Sun et al., 2015), the threshold for brain tissue damage, reducing the margin for error in interventional planning.

These limitations arise from the fact that wild-type serotypes of AAV did not evolve to cross physically loosened biophysical barriers and are therefore not optimal for this purpose. In this project, we will address these limitations by developing new AAV serotypes specifically optimized for FUS-BBBO delivery. Capsid engineering techniques (Li & Samulski, 2020) in which mutations are introduced into viral capsid proteins have been used to enhance gene

delivery properties such as tissue specificity (Chan et al., 2017, Gray et al., 2013, Tervo et al., 2016, and Li et al., 2024), immune evasion (Maheshri et al., 2006), or axonal tracing (Tervo et al., 2016). However, they have not yet been used to optimize viral vectors to work in conjunction with physical delivery mechanisms.

Previously, we performed *in vivo* selection of mutagenized AAVs in mice in conjunction with FUS-BBBO (see ***Chapter 2***) by adapting a Cre-recombinase-based screening methodology. We identified 5 viral capsid mutants with enhanced transduction at the site of FUS-BBBO but not in the untargeted brain regions (**Fig. 2-3b**). We then performed detailed validation experiments comparing each of these mutants to the parent wild-type AAV9, revealing a significant increase in on-target transduction efficiency, increased neuronal tropism, and a marked decrease in off-target transduction in peripheral organs, resulting in an overall performance improvement of more than 10-fold (**Fig. 2-7c**). These results demonstrated the evolvability of AAVs for specific physical delivery methods (Li et al., 2024).

Having demonstrated the possibility of engineering AAVs for enhanced targeted delivery to the brain in mice, our next step toward clinical translation is to execute this strategy in non-human primates (NHPs), the established model for developing viral gene delivery vehicles for clinical use in humans. In particular, NHPs such as rhesus macaques and baboons, which have a high protein homology with humans (compared to mice), meet FDA requirements for testing gene and cell therapy products (Research, 2024).

3.3 An Optimized Protocol of FUS-BBBO Mediated in vivo Screening for AAVs in the Brain of Non-Human Primate

While our previous work (see ***Chapter 2***) has demonstrated the feasibility of combining focused ultrasound–mediated blood–brain barrier opening (FUS-BBBO) with *in vivo* AAV capsid screening in mouse model, translating these advances to non-human primates (NHPs) requires substantial re-optimization of the FUS-BBBO protocol tailored to the anatomical and physiological characteristics of the primate brain. Mouse models have proven invaluable for high-throughput vector evolution and for validating key physiological principles underlying ultrasound-mediated delivery. However, the primate brain differs remarkably from the rodent brain in terms of size, vascular architecture, skull anatomy, acoustic properties, and immune responsiveness—all of which critically influence the spatial precision, safety, and efficiency of FUS-BBBO. Additionally, the distribution of viral receptors and cellular tropism in the primate brain may differ from that in mice, meaning that AAV capsids optimized for murine FUS-BBBO conditions may not perform similarly in NHPs unless the delivery parameters are carefully adapted. Therefore, even as we begin developing primate-specific AAVs intended for use with FUS-BBBO, it is essential to establish and optimize an NHP-specific sonication protocol that ensures reproducible, safe, and localized BBB opening. Such a protocol will be foundational not only for screening capsid libraries in primates but also for validating therapeutic efficacy and delivery efficiency in a system that more closely models the human brain, thereby enabling more accurate translational insights.

Building on our prior experience performing effective and safe FUS-BBBO in mice, we established and refined a standardized set of animal preparation procedures and ultrasound parameters that consistently enabled successful delivery of viral vectors to the brain mediated by FUS-BBBO in NHPs.

During the parameter development and optimization, each animal was prepared with four small craniotomies, two in each hemisphere above the primary visual cortices (V1). FUS-BBBO was performed using a 1 MHz single element transducer coupled to the brain via a

coupling cone and sterilized ultrasound gel. This is the frequency brings in favorable trade-offs between transcranial efficiency and focal zone size. As our initial parameters based on previous FUS-BBBO work in NHPs (Upright & Baxter, 2020) and our study in mice (Li et al., 2024), we started with Definity microbubbles injected intravenously at $1.2x10^8$ bubbles/kg and apply 10 ms sonications repeated at 2 Hz for 120 seconds. Using the four brain regions of two animals, we tested pressures ranging from 100 kPa to 350 kPa (MI between 0.12 - 0.43), which have been shown to be safe for FUS-BBBO in NHPs (Blesa et al., 2023; and Hinderer et al., 2018). Passive cavitation detection (PCD) was used to monitor the inertial cavitation of bubbles, which we subsequently correlated with tissue damage. The BBB opening was evaluated using T1-weighted MRI (with injection of Prohance as in **Fig. 2-3a**) and any gross damage visualized using T2* imaging. All conditions was replicated in two independent settings. Once we find a pressure that results in a safe BBB opening – with T1 enhancement, but without hypointense spots on T2* – we performed a systemic injection of 10^{13} VG/kg AAV9 encoding a chemogenetic receptor. For our initial test of expression and function we used the inhibitory DREADD hM4Di-mCherry under the CamKII promoter. Simultaneously, we co-injected the same dose of 1^{13} VG/kg AAV9 encoding nuclear-localized GFP under the synapsin-1 pan-neuronal promoter, which would help us quantify transfection efficiency by counting nuclei (putting a nuclear-localized fluorophore in the same vectors results in a construct too large for efficient packaging). We allowed at least 6 weeks for gene expression before assessment. AAV-delivered expression is expected to last for several years.

The iterative optimization finally yielded the following parameters that produced most effective and reproducible FUS-BBBO in NHPs, which led to robust AAV transductions in the region of impact (ROI) in the NHP brains:

1MHz ultrasound transducer; Peak negative pressure (PNP) of 420 kPa; 10 ms pulse duration; 2Hz pulse repetition frequency; 120 sec stimulation duration; intravenous injectables: Prohance 0.2 ml/kg (body weight) and Definity 20ug/kg (body weight).

Using the NHP-optimized focused ultrasound parameters above results in reproducible FUS-BBBO that lasts for over one hour (**Fig 3-1**).

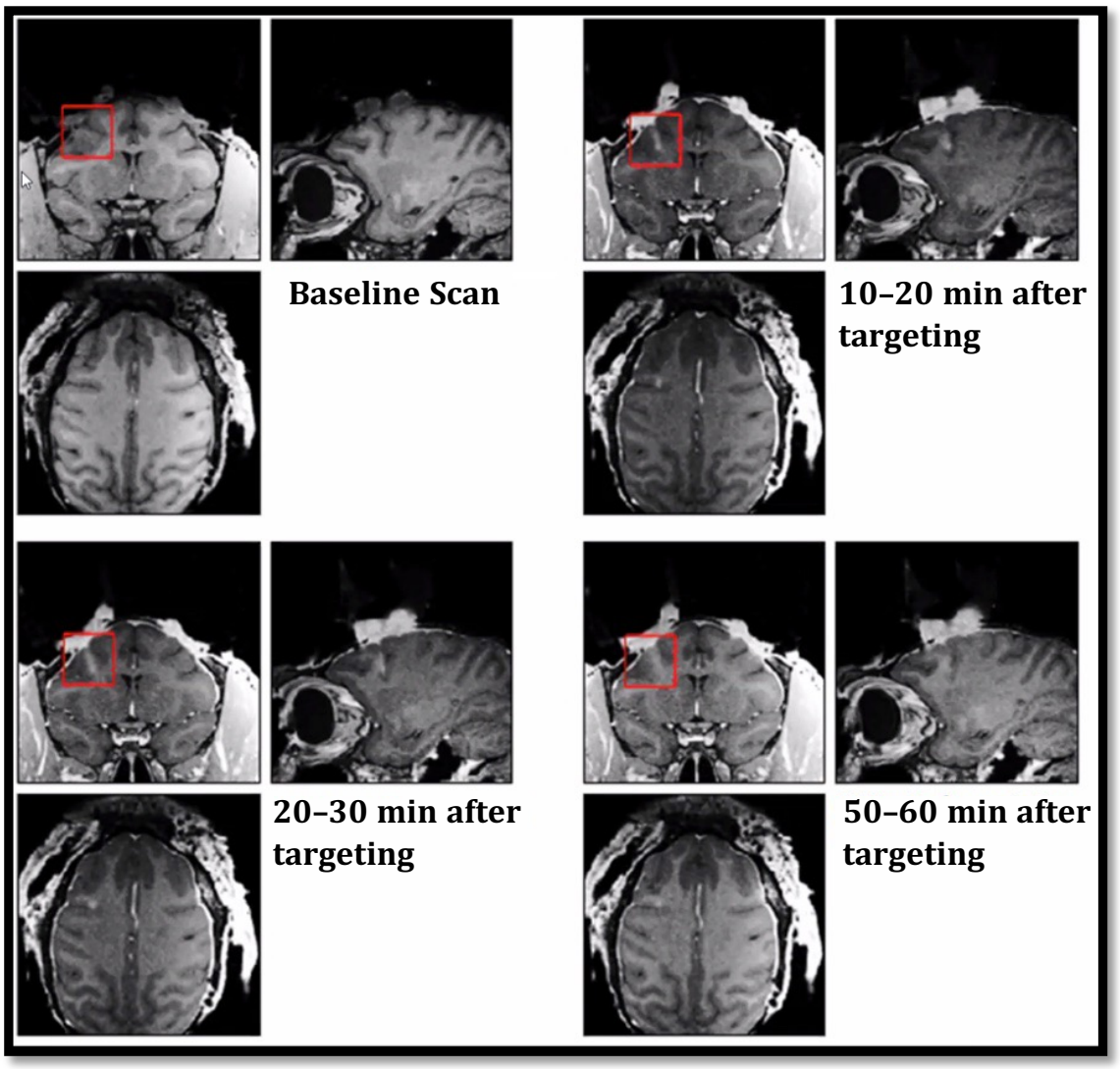

Figure 3-1 Effective blood–brain barrier opening in the non-human primate brain using optimized FUS parameters and delivery protocol. Safe and noninvasive opening of the BBB with FUS in V1 region of NHP which was used to deliver viral vectors carrying DNA with a cell specific promoter and a chemogenetic receptor. Highlighted in the red squares, the BBB opening is visualized by extravasation of gadolinium contrast agent in a T1-weighted MRI, showing bright contrast.

Having established the set of robust and reproducible FUS-BBBO protocol in the non-human primate (NHP) brain, we next sought to leverage this platform as the foundation for a targeted AAV screening pipeline. While previous studies have demonstrated the feasibility of AAV evolution and selection in the context of FUS-BBBO in mice, the translation of such screening strategies to NHPs requires a dedicated methodology that accounts for the unique anatomical, immunological, and physiological features of the primate brain. Our optimized FUS-BBBO protocol enables spatially precise and transient opening of the BBB, providing a critical delivery window for systemically administered AAV capsid libraries. By integrating this protocol with high-throughput vector barcoding and next-generation sequencing, we are now expanding its application into a full-scale in vivo screening platform aimed at identifying and evolving AAV variants specifically tailored for efficient, cell-type–specific transduction of the NHP brain via FUS-mediated delivery. This approach not only bridges a major translational gap between rodent and primate models but also lays the groundwork for engineering vectors with clinical potential for non-invasive, targeted gene therapy in humans. Hence, we developed the following standard of operating procedure (SOP) for experiments of *in vivo* screening of engineered AAV capsids specializing in FUS-mediated delivery to the NHP brain.

An Optimized Standard of Operating procedure (SOP) of FUS-BBBO Mediated *in vivo* Screening for AAVs in the Brain of Non-Human Primate (NHPs)

1. Purpose

This SOP provides the timeline of the procedures for Cre-dependent selection of AAVs expressing reporter proteins delivered to in rhesus macaques by ultrasound-mediated opening of the blood brain barrier.

2. Scientific Rationale

a. The scientific rationale of intravenous injection of AAV in conjunction with ultrasound-mediated opening of the blood brain barrier (BBBO) can be referred to ***Chapter 2*** of this thesis.

b. Gradinaru's group at Caltech developed a capsid selection method, called Cre-recombination-based AAV targeted evolution (CREATE), which can generate AAV variants that efficiently and widely transduce the adult mouse central nervous system (CNS) after intravenous injection.

c. We would like to use CREATE Gradinaru developed for AAV evolution in rhesus macaques. Because of the lack of Cre expression macaque, we will adopt a dual-vector approach of CREATE, requiring US-mediated delivery of AAV library (with AAV expressing Cre recombinase) and IC injection of AAV expressing Cre recombinase.

d. This procedure involves many well adopted and widely applied sub-procedures, including craniotomy, ultrasound-mediated delivery of AAVs, head post implantation, and multiple IC injection of viruses in non-human primates, which will be done during the surgery. The reasons of combining these procedures in one surgery are:

   i. The ultrasound transducer will have much better access to the brain through craniotomies without chamber and acrylic. The chamber and acrylic may block

the transducer and result in poor BBBO. Therefore, we would like to do ultrasound BBBO immediately after craniotomies and before the chamber implantation. Importantly, we encountered this problem in Pippin, which led to significant mis-targeting. We are confident that this will not happen if we perform the sonication before implanting the chamber.

ii. We need to inject the Cre intracranially to the sonicated regions. It will be easier to do it in the same surgery with ultrasound BBBO because we can accurately move the Hamiliton syringes to the sonicated region and reduce the risk of missing the target. Furthermore, we will be able to directly see the needle puncturing the dura and entering the brain and hence will be much more likely to inject at the correct depth.

iii. Importantly, IV injection of AAVs in the BBBO procedure will cause immune responses of the animal, prohibiting any further AAV injections (e.g., IC injection of AAV with Cre). Therefore, we will do all the AAV IV and IC injections on the same day, which is safer for the animal.

e. Since the animal will be used for this viral evolution experiment and will not perform any behavior experiments, we are less concerned about the sonication and IC Cre injection sites, meaning we may perform sonication and IC Cre injection to any brain regions.

f. The animal will be euthanized for histology after the expression of virus, which we expect to be around 4-8 weeks. we added an option to keep the animal for up to 8 weeks before the euthanasia if we chair train the animal and the animal can be chaired reliably. Otherwise, we will only keep the animal for 4 weeks.

g. The rationale is described below: Ample expression of single serotype of AAV in NHP will take about 4 weeks. In our Cre-dependent selection experiment, successful recovery of enriched viral genome of rAAV library variants requires sufficient expression of Cre from AAV9 (Ravindra et al. 2020), which will take longer time because of the dual vector delivery, which we expect to be as long as 8 weeks.

h. Since this will be a terminal experiment, we do not plan to train the animal if we only keep it for 4 weeks and it does not need to perform any task. We would like to clean

chambers and margins of the animal once a week, by ketamine (or ketamine and dexdomitor) sedation each time.

3. Welfare Concerns Associated with this Procedure

a. There is risk of toxicity with AAV9 injection when this is done at high doses. Hinderer et al. (2018) reported that 2×10^{14} genome copies per kilogram of AAV9 led to transaminase elevations in 3 NHPs and liver failure leading to euthanasia in one animal. In another study, Hordeaux et al. (2018) found that at 2×10^{13} VG/kg of AAV9 and PHP.B (a different serotype developed by the Gradinaru lab), two NHPs showed good tolerance, but at a slightly higher dose, (7.5×10^{13} VG/kg), an animal injected with PHP.B vector developed severe clinical symptoms. Furthermore, in November 2014 our lab injected an animal that had previously undergone AAV injections as well as extensive injections of MION contrast agent with 5×10^{13} vector genomes of each virus AAV9:CAG-tdTomato and AAV-PHP.B:CAG-GFP delivered together intravenously. This animal developed severe clinical symptoms (ataxia and hepatic failure). Thus there is some concern about toxicity of AAV-9 injection at very high titers, especially in NHPs that have previously undergone AAV injections or have decreased liver function.

b. The administration of AAV may result in a systemic immune response, and possibly organ specific toxicity. If the immune response or toxic effect is significant, it could result in clinical illness, with symptoms ranging from a mild fever and lethargy to severe anaphylaxis. The animal should be monitored closely by the laboratory staff for signs of a reaction after the injection (at least hourly for the first 6 hours and then twice daily for the first week), and the veterinary staff should provide treatment as warranted.

c. The tier of Cre recombinase intracranially injected to the brain is low since we will only inject up to 6 ul of virus (for 6 injections), of titer up to $1x10^{13}$ VG/kg.

d. For all animals that undergo intravenous and intracranial virus injection, we will screen its blood for neutralizing antibodies to the parent AAV used for library generation, since such antibodies sometimes exist in individual macaques.

e. It is worth noting that this is an exploratory protocol and we are testing viral injection protocols that are fundamentally novel and carry risks (e.g., we will be injecting libraries of mutated AAV's, something that has not been done before in NHPs). Above, we have explained how we will mitigate the risks. As already stated, a key long-term goal of this research is to evolve viruses that can cross the blood brain barrier much more efficiently at the site of ultrasound treatment, while reducing transduction in other brain regions and other organs and lowering the overall viral titer needed, making the approach safer not only for NHP experiments but potentially for human gene therapeutic approaches.

4. Personal Protective Equipment (PPE) Requirements

a. PPE (N95 face mask, gloves, and eye protection) should be worn both during preparation of the viral vector and delivery of the vector.

b. After the procedure and before moving the animal to the housing area: Dispose of gloves, in the red bag biohazard waste container in the lab. Change to a new set of gloves.

c. During the one-week period the animal is considered ABSL-2: Prior to entering the NHP animal housing wear a disposable lab coat, N95 face mask, gloves, and eye protection. This PPE is removed before leaving the animal facility.

5. Overall Procedure

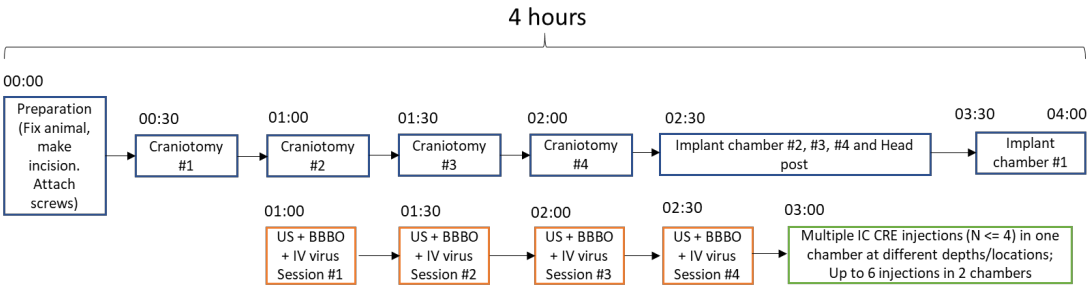

The estimated timeline of the entire procedures is shown above, which is expected to be less than 4 hours. Procedures in the blue boxes and orange boxes will be performed in parallel by different personnel. Thus the sonication and virus delivery will not take up any extra time.

5.1 Craniotomies and chamber implantation

The animal will be anesthetized and transferred to procedure room for surgery. The animal will be anesthetized during the whole procedure. In the surgery, up to four craniotomies will be implemented, with no more than three craniotomies on each hemisphere. The size of each craniotomy may be as large as ~3.14 cm^2 (2 cm in diameter), though smaller craniotomies are preferred (~1.3 cm in diameter, 1.3cm^2 in area). The chamber will be slightly larger than the craniotomy to cover it. To avoid being blocked by adjacent chambers, we may also just use one (~8 cm x ~8 cm) or two large chambers (~5 cm x 5 cm) to cover all or multiple craniotomies. The craniotomies will be performed before ultrasound BBBO procedure. During intravenous injection of virus (less than 1 min) and microbubbles (less than 1 min) and sonication (~2 min for each sonication, up to 2 sonications for one craniotomy), the surgery of the new craniotomy may pause and then resume after the BBBO procedure is done.

5.2 Ultrasound-Mediated Delivery of AAVs

5.2.1 Preparing the animal before viral vector work begins:

a. NHP leg is shaved.

b. The night prior to virus injection, fast the animal.

c. The animal is fasted and water restricted the morning of the procedure.

d. Prior to the administration of AAV, a baseline blood draw for a CBC/Chem panel can be collected, which may not be needed if a recent CBC/Chem panel has been completed during semi-annual physical exams.

5.2.2 Pre-Injection Procedure (Place catheter and prep contrast/microbubble agent)

1. Place saphenous vein catheter:

I. Poke a hole in the middle of a medium absorbent pad and place around the leg of the NHP. Carefully covering the chair and other part of the animal.

II. Wipe leg area with alcohol pad and inset catheter into saphenous vein. Remove guide and discard into sharps container.

III. Fixe a 3-way luer stopcock to catheter.

1. Prep contrast/microbubble agent:

I. Rub all rubber stoppers with alcohol pad.

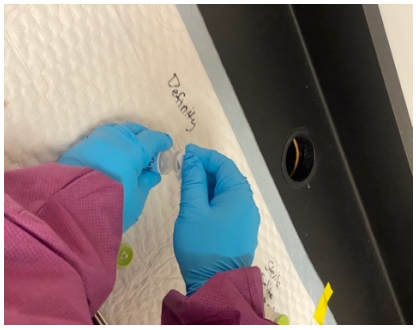

II. Draw out Definity bubbles with a syringe with a G21 needle from original vial and insert thru the rubber stopper into a sterile saline vial.

IV. Check 3-way luer stopcock OFF for catheter

2. Place sterile square of gaze under the 3-way luer stopcock.
3. Inject 5 ml of saline to test catheter placement

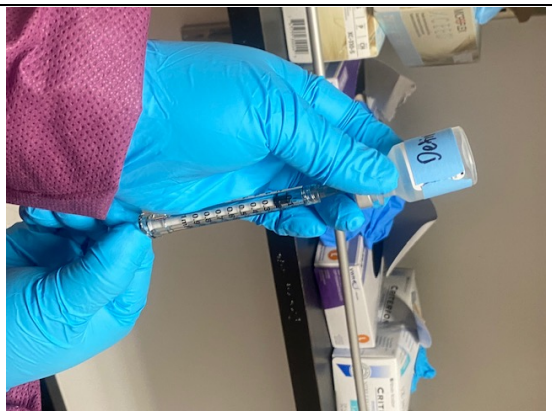

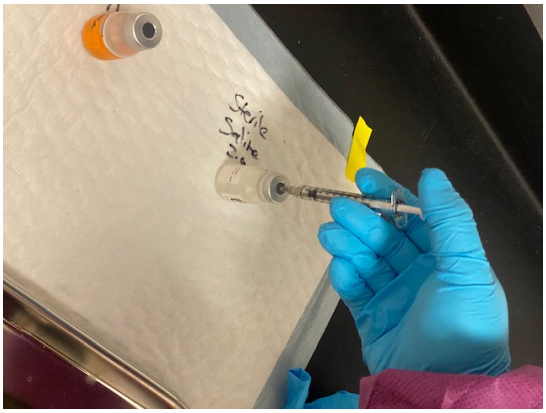

III. Draw out Gadolinium contrast agent (Prohance, 0.2ml/kg) with a new syringe and insert thru the rubber stopper into the same sterile saline vial.

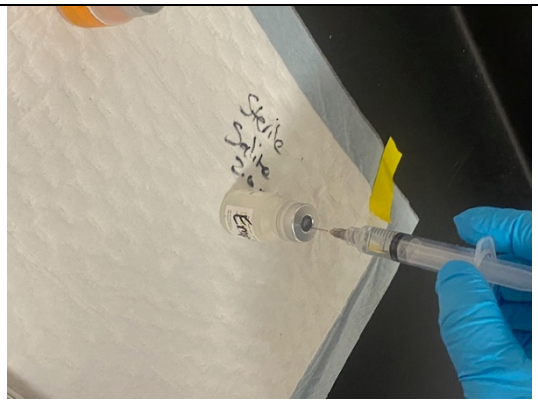

IV. Mix the bubbles and Gadolinium by shaking the tube by hand for 15 seconds.

V. Draw out the contents into a new syringe, carefully recap using the one-hand technique.

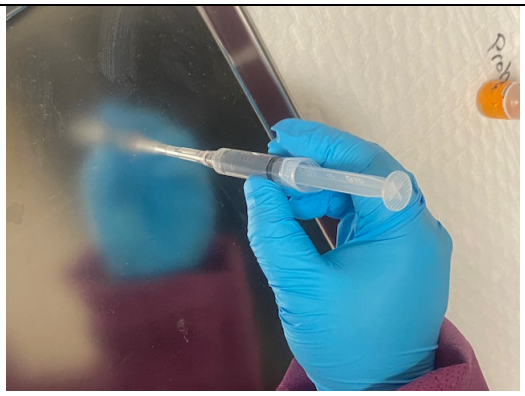

2. Place syringe in a clean tray.

5.2.3 Intravenous Injection and Sonication Procedure

Up to four successful sonications in up to four craniotomies is performed. We may re-do the sonication if it is failed due to 1) poor coupling between transducer and the dura 2) poor quality of the microbubbles 3) desynchronized sonication and microbubble injection. AAVs may be IV administrated in one injection before all sonications or administrated in several injections among sonications, where the total tier is still below 1×10^{13} VG. Microbubbles will be injected IV at the start of each sonication. We will wait for 10 min between two consecutive sonications.

5.2.3.1 Intravenous Injection and Sonication Procedure

Loading the viral vector

a. Throughout the procedure described here, all participants will wear proper PPE (disposable lab coat, N95 face mask, gloves, and eye protection).

b. Work is performed inside the biosafety cabinet (BSC).
   I. Spray all surface of BSC with 10% bleach and wipe; or wipe with Rescue wipes.
   II. Take AAV vial out of transport container.
   III. Wipe rubber stopper of vial with alcohol pad.
   IV. Draw 5 ml of the AAV solution into a syringe.
   V. Very carefully remove needle from vial and recap shut using one-hand technique.
   VI. Set syringe in stainless steel syringe tray lined with paper towel and a wet Rescue wipe.
   VII. Place empty AAV vial in ziplock bag. Spray with 10% bleach or wipe with Rescue wipe.
   VIII. Discarded empty AAV vial into small biohazardous bag – bring this to the main biohazardous waste container when done.
   IX. Close needle tray, wipe with Rescue wipe and set on counter top bench outside of BSC.
   X. Remove outer gloves.
   XI. Spray all surface of BSC with 10% bleach and wipe; or wipe with Rescue wipes.
   XII. Put on 2nd pair of gloves.

AAV Injection Procedure

a. Screw saline syringe onto the 3-way luer stopcock

b. Unscrew AAV needle from syringe, discard into sharps container

c. Screw AAV syringe onto the 3-way luer stopcock

d. Check 3-way luer stopcock ON for AAV injection

e. Inject AAV - Up to 5 ml of the virus mixture with a dose of up to $1x10^{13}$ particles/kg of each virus will be injected. To ensure steady viral syringe handling, another lab member will assist with stabilizing the catheter and leg and remove the catheter screw cap prior to picking up the viral syringe.

f. Check 3-way luer stopcock ON for flush injection.

g. Inject saline.

h. Check 3-way luer stopcock OFF for catheter.

i. Unscrew both syringes and discard in sharps container.

I. If the sterile gaze underneath the 3-way luer stopcock become visibly contaminated with viral prep, discard and replace with a new one.

5.2.3.2 Injection of microbubbles (at the start of each insonation)

a. Injection of microbubble agent (at the start of each insonation)

i. Remove needle part of all syringes and discard into sharps container.

ii. Screw contrast syringe onto the 3-way luer stopcock

iii. Screw saline syringe onto the 3-way luer stopcock

iv. Check 3-way luer stopcock ON for contrast injection

v. Inject microbubbles

vi. Check 3-way luer stopcock ON for flush injection

vii. Inject saline

viii. Check 3-way luer stopcock OFF for catheter

ix. Unscrew both syringes and discard in sharps container.

1. If the sterile gaze underneath the 3-way luer stopcock become visibly contaminated with contrast agent, discard and replace with a new one.

b. Ultrasound treatment

i. The animal is head-fixed on the surgery table and is anesthetized.

ii. Bring the ultrasound machine to the surgery room and make sure it is properly configured. Ultrasound will be applied through craniotomy. The transducer will be coupled to the dura with sterile ultrasound gel.

iii. Position Ultrasound probe (no direct contact with NHP) to the craniotomy.

iv. Injection of microbubble as described in (**a).**

v. Apply ultrasound by turning on the electronic sequence for stimulation.

    1. Ultrasound parameters: *1MHz ultrasound transducer; Peak negative pressure (PNP) of 420 kPa; 10 ms pulse duration; 2Hz pulse repetition frequency; 120 sec stimulation duration; intravenous injectables: Prohance 0.2 ml/kg (body weight) and Definity 20ug/kg (body weight).*

vi. Remove transducer and disinfect with wiping with Rescue wipes.

vii. Wipe ultrasound gel with sterile gaze

viii. Repeat "b. Ultrasound treatment" to iterate all the craniotomies (up to four).

c. Waiting for 3 minutes, remove the IV catheter:

i. One person cut the holding tapes and handles the catheter

ii. One other person holds a sterile gaze and is ready to put pressure on the injection site.

iii. As the first person remove the catheter/3-way luer stopcock in one block, the second person applies pressure on the injection site.

iv. Catheter/3 way luer stopcock is discarded in biohazardous waste can. And gloves are changes immediately, put new gloves on.

v. Once pressure has been applied for 3 min, remove gaze, discard in biohazardous waste, change gloves.

vi. Wipe injection site with alcohol pad, if blood is visible.

vii. All personnel must changes their outer gloves at this stage (remove outer gloves, put new ones on).

5.3 Preparation of AAVs expressing Cre recombinase

a. Retrieve virus from -80 freezer.

b. Put the virus into an ice box and carry it into the preparation room.

c. Under the biosafety hood, the virus solution will be drawn by pipetteman, and then the virus tube will be closed and returned to the ice box. Gloves will be changed, and the ice box will be returned to the freezer.
d. In a biosafety cabinet: Virus solution will be released from the pipette onto a sterile petri plate. We will use fresh parafilm, and the side that is sealed is sterile. The vial will be transferred to the preparation room in a metal container, where a Hamilton syringe will be used to draw up the virus. All reusable equipment (e.g., Hamilton syringe, stereotax) and work surfaces will be treated by bleach at the end of the experiments. Hamilton syringe cannulas and guide tubes will be disinfected with glutaraldehyde.

5.4 Intracranial (IC) injection of AAVs expressing Cre recombinase

a. The injections will take place while the animal is anesthetized during the surgery in preparation room.
b. For each injection, we will inject 1ul of virus, of titer up to $1x10^{13}$ VG/ml into the brain. Up to six injections may be performed in up to two craniotomies. We may perform multiple IC injections at different depths or locations (up to four) for each craniotomy.
c. The Hamilton syringe will be transferred to the monkey in a metal container, and then the cannula/glass pipette will be lowered through a grid hole in a grid to the site of interest. The Hamilton syringe, cannula/glass pipette will be mounted to the stereotaxic manipulator arm with a custom-made adaptor.
d. Note that the glass pipette and metal cannula are two different means of injecting viruses. For superficial injections, we will use a glass pipette, because it is thinner (causing less damage), and one can see the virus being injected. For deep injections, we will use the metal cannula.
e. Virus will be injected by hand pressure from the hamilton syringe or by an automated pump into the brain. The injection needle itself will be attached to a microdrive to allow for precise targeting of the injection. We will use either metal cannulas or glass pipettes; glass pipettes will be thrown in sharps; metal cannulas

may be reused following disinfection with glutaraldehyde. Outer gloves will be changed immediately following injection.

f. The date and time of injection of the viral vector will be recorded in the animal's medical records.

3.4 Iterations of *in vivo* Directed Evolution Yields AAVs with Efficient FUS-BBBO Transduction in the Non-Human Primate

In parallel with testing the viral vectors identified from selection in transgenic mice, we performed viral screening directly in non-human primtes (NHPs), or Rhesus Macaque. This is needed because viral serotype properties are imperfectly transferrable between species, and significant room for improvement is therefore likely to remain even for the best mouse AAV.FUS (see ***Chapter 2***). Screening in NHPs was planned to be performed using a small number of animals (n=4). AAV evolution in this species will require adapting CREATE to non-transgenic animals (**Fig. 3-2**). In this strategy, the AAV library containing the floxed element used for PCR recovery (see screening strategy in ***Chapter 2***) is combined with a second AAV vector expressing Cre recombinase under the Synapsin promoter (AAV-Cre), allowing recombination to take place in neurons containing both vectors. To implement this two-vector strategy in macaques, we packaged Synaprin-Cre in the wildtype AAV9 serotype and introduce it into the brain at high dose with FUS-BBBO and intracranial injection at the site of FUS-BBBO. At the same time, we will intravenously introduce a competent AAV mutant library. Cells that receive both vector types will recombine, allowing sequence recovery for downstream next-generation sequencing (NGS). This strategy allows us to perform CREATE screening in wild-type macaques. In addition, we are able to perform Cre-independent PCR in the same extracted brain tissues, providing a backup screening strategy in case of poor Cre expression.

Before injecting a particular animal, we screened its blood for neutralizing antibodies to the parent wildtype AAV9 used for library generation, since such antibodies sometimes exist in individual macaques. Animals will then undergo FUS-BBBO with IV injection of AAV9-Cre (10^{13} VG/kg body weight) and a library of AAVs at 10^{13} VG/kg of body weight. This library includes the "competent" variants and 3 winners identified in the mouse screening in mice model screening (see ***Chapter 2***), as well as some non-preselected variants. FUS-BBBO will be performed through craniotomies as in ***Chapter 3.3***, targeting 4 sites unilaterally within the cortex. After 14 days we euthanized the animals and recover the DNA at FUS-BBBO sites and at untreated control sites. The recovered DNA was amplified through PCR and

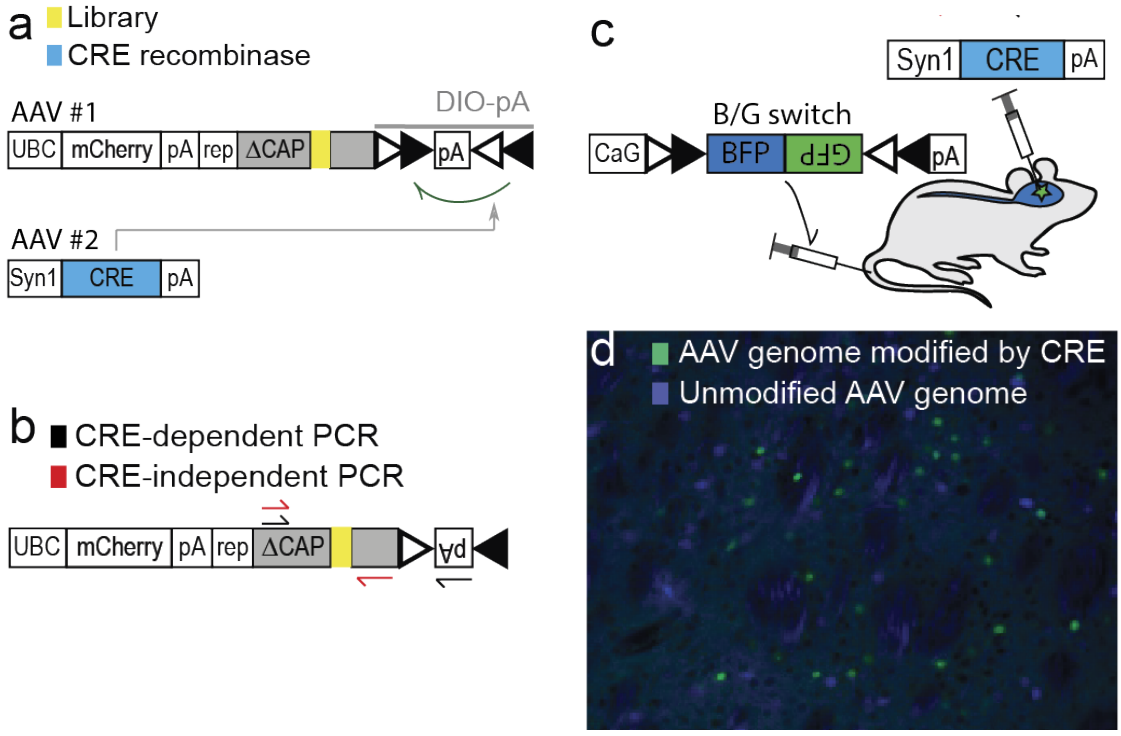

Figure 3-2 Two-vector approach to viral screening. (**a**) Design of the two-vector system for CREATE viral engineering in wild-type animals. (**b**) Either Cre-dependent or independent PCR can be done to recover samples, allowing us to obtain DNA from cells where CRE- negative cells, if needed. (**c**) Preliminary data for two virus approach to permeable AAV.PHP.eB was injected systemically to transduce pressed under Syn1 promoter CREATE in wild-type mice. BBB CNS with floxed invertible element that changes fluorescence from blue to green when modified by Cre. (**d**) Local delivery of Cre ex- caused recombination in ~50% of cells transfected with B/G switch.

sequenced. Sequences specific to FUS-BBBO sites would be re-synthesized and used in packaging a library for a second round of evolution.

The first viral vector screen in macaque was performed on July 28, 2021. After low-yield first attempt for large scale (for NHP level intravenous dose) AAV library packaging, the second attempt at AAV library packaging was a success. Titer for recombinant AAV library was 3 x 10^{13} viral genomes (VG.) total in 1.5 mL, and the re-titered result for previously prepared AAV9 hSyn-Cre-P2A-tdTomato virus is 1.2 x 10^{14} vg total in 3 mL. Both titers for library and AAV9-Cre are more than required amount for first round viral screen (5 x 10^{12} - 1 x 10^{13} viral genomes for efficient screening).

On July 28, the experiment began with implementing 4 craniotomies (2 on each hemisphere). Then, the 6 kg macaque monkey was intravenously injected with AAV library and AAV9-Cre at combined-1 x 10^{13} vg/kg concentration. Then, we intravenously injected activated microbubble (Definitity^{TM}) of 20uL/kg for 4 times, before focused ultrasound sonication at each craniotomy site at recorded angle of attack on stereotaxis (**Fig. 3-3a**). Then, to ensure sufficient expression of Cre, in the posterior craniotomy site on left hemisphere, we intracranially administered AAV9-Cre at 2 depths with 1.0uL dosage each (**Fig. 3-3b**). At the end of the experiment, all 4 craniotomies were protected with a 3D-printed chamber sealed on top of skull. After 4 weeks of viral expression, the macaque was euthanized and tissue samples were extracted from all 4 FUS-targeted craniotomy sites, along with peripheral organs (heart, liver, and kidney). We successfully recovered viral library genomes from extracted brain tissues based on a Cre-dependent protocol, which was sequenced with next-generation sequencing (NGS). To ensure reasonable allocation of resources, we Sanger sequenced recovered DNA samples prior to analyze with more costly NGS procedures. Results from Sanger sequencing were served as quality control prior to the NGS: we were able to observe variation region of 21-bp insertion from recovered DNA, indicating successful transduction of rAAV library items and recovery (**Fig 3-3c**). The NGS results eventually provided us with information for synthesizing the second round of viral

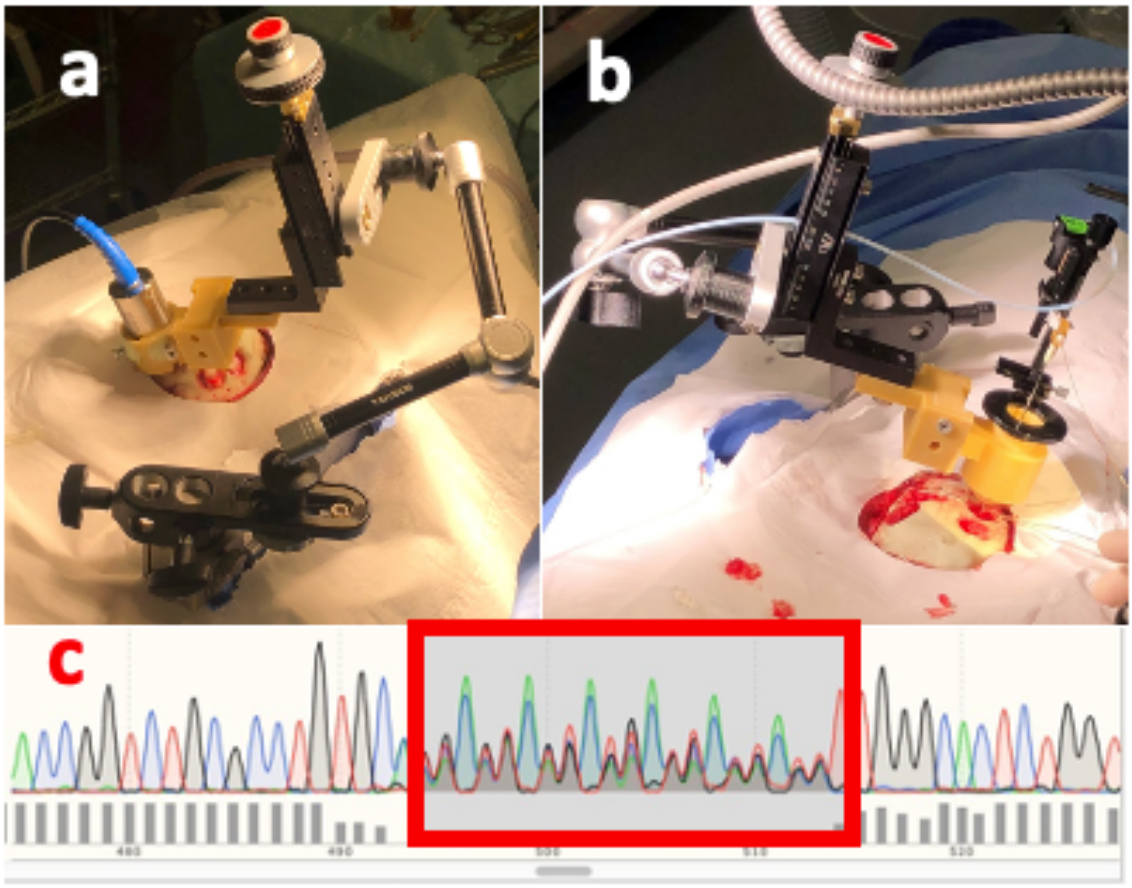

Figure 3-3 First round two-vector approach to viral screening in the non-human primate (NHP). (**a**) Single element 1MHz ultrasound transducer held by swappable adapter system, targeting one craniotomy site (**b**) Intracranial injection system mounted on same swappable adapter system of penal a, injecting AAV9-Cre into one of craniotomy sites (**c**) Trace Chromat data of Sanger sequenced recovered viral library DNA via Cre-dependent procedure. The 21-base variation regions represents our modification of VP3 capsid design (7-mer amino acid insertion) in vector library.

vector screen that renders statically analyzable data for selecting final candidates for FUS targeting optimized AAV vectors.

After four weeks of *in vivo* viral expression, the first-round viral vector screen in our NHP subject concluded with euthanasia on August 25, 2021. Immediately after euthanasia, post-mortem tissue recovery was performed to extract brain tissue at FUS-targeted sites in each craniotomy, as well as from heart, kidney, and liver. The brain tissue samples were then subjected to TRIzol extraction procedures to recover rAAV library genome from transduced cells. We used the purified rAAV library genome as template to implement Cre-dependent and Cre-independent PCR amplification to generate ample amount of DNA for NGS sequencing. We analyzed our NGS results by read counts for library variants. Encouragingly, we were able to obtain Cre-recombined library sequences from all of our craniotomies.

Based on our sequencing analysis, we selected 8900 7-mer amino acid insert candidates to be re-screened to quantify enhancement and FUS-target specificity of FUS-BBBO-mediated transduction in second round. To these variants, we added the top 100 from our mouse screen (see ***Chapter 2***). We synthesized 18000 (duplicate of 9000 7-mer amino acid sequences for codon redundancy to ensure quality and quantity of AAV library packaging) candidates which were then packaged into NHP second round rAAV library. Based on a comparative analysis of our fist round NGS data from the craniotomy that received IC injection of AAV9-Cre against the other three craniotomies that only experienced IV injection of virus in addition to FUS-BBBO, we found that IC injection led to significant increase in read counts from Cre-dependent recovery (**Fig. 3-4a**). Based on this observation, we decided to implement two craniotomies in our NHP for second round selection, out of which one was subject to only IV viral injection and FUS-BBBO while the other one also received IC injection of AAV9-Cre to achieve better yield of read count in NGS.

The second viral vector screen in macaque was performed on January 10, 2022. We followed same protocol and parameters as applied in first round screen. Comparing T1-weighted MRI scans at the beginning and the end of experiment, gadolinium (Gadoteridol) contrast agent extravasation revealed that the focused ultrasound was able to introduce BBBO at both sites

of targeting (**Fig. 3-4b**). Euthanasia and tissue extraction for second viral screening was planned four weeks after.

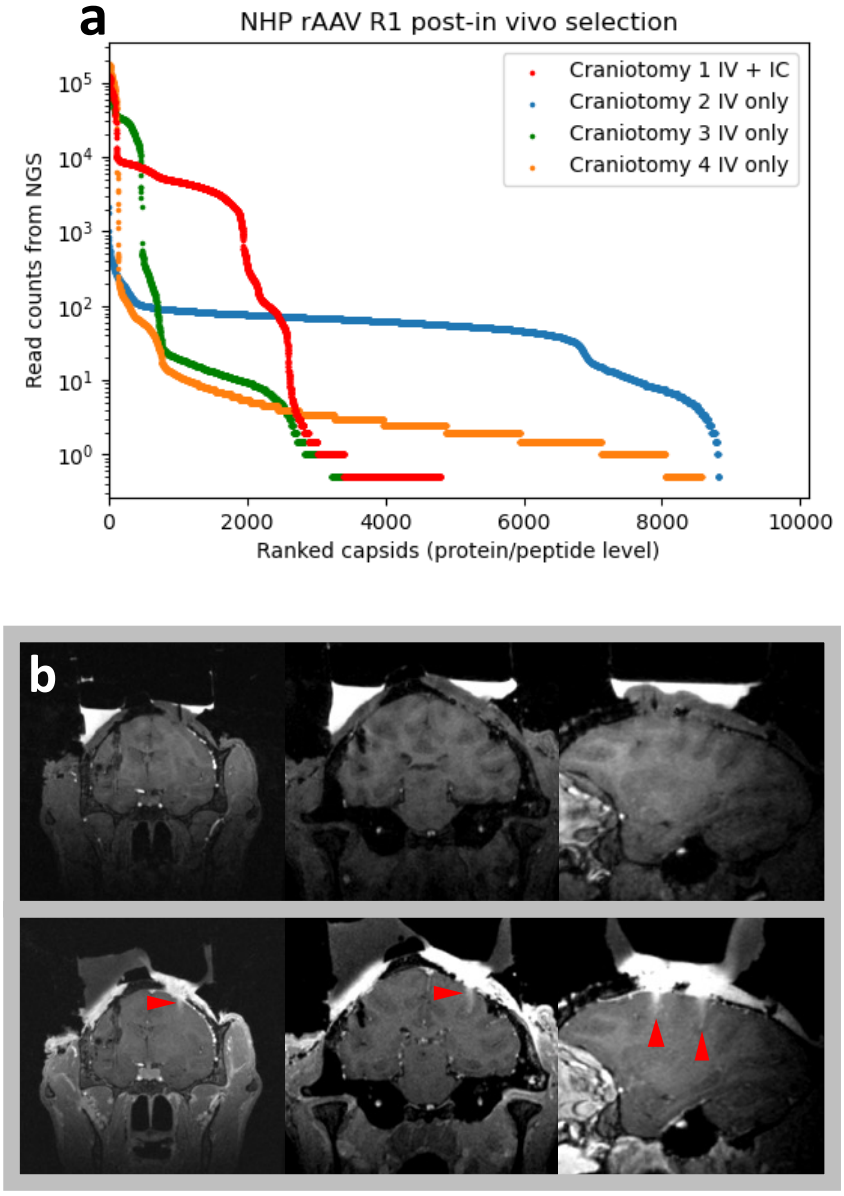

Figure 3-4 First round viral screening candidates ranking and second round screening's FUS-BBBO validation. (**a**) The distributions of AAV capsid read counts for libraries recovered by NGS from brain tissue across different craniotomies post first round screening. (**b**) In the second round of viral screening, MRI images showing NHP brain with 2 sites before (top panel) and after(bottom panel) opened with FUS-BBBO in one hemisphere. The bright areas (arrowheads) indicate successful BBB opening and extravasation of the MRI contrast agent Prohance (Gadoteridol) into the brain. This BBB opening was used for delivery of the AAV library.

The second round of viral vector screen in macaque was performed on January 10, 2022. We followed same ultrasound protocol and parameters as applied in the first-round screen. Euthanasia and tissue extraction for second viral screening was performed on 7th of February. Brain tissue was extracted from both FUS targeted sites as well as an untargeted site as part of a negative control. Peripheral organs that are typically transduced by wildtype AAV9, such as heart, liver, and kidneys have also been preserved for viral DNA recovery. The brain tissue and peripheral organ samples were then subjected to TRIzol extraction procedures to recover AAV library genomes from transduced cells. We used the purified AAV library genome from tissue as template for Cre-dependent and Cre-independent PCR amplification to generate sufficient DNA for NGS sequencing. Comparing to the first-round selection, the smaller size of second-round selection library enables sufficient coverage for NGS to provide statistically meaningful count numbers for variants. Therefore, we used NGS results of read counts to analyze the enrichment scores of our variants. For each variant recovered depending on Cre driven by (co-injected) AAV9 with neuron-specific promoter in NHP brain, calculation of an enrichment score for each variant can correct for biases in viral production prior to selection, making it possible to compare the relative ability of the variants to transduce neurons in brain regions subjected or not subjected to FUS-BBBO.

The enrichment scores of variants across different libraries were calculated from the read counts (RCs) according to the following formula:

$$\text{Enrichment score} = \text{Log}_{10} \frac{[(\text{variant 1 RC in tissue library1} / \text{total number of reads in library1})]}{[(\text{variant 1 RC in virus library} / \text{total number of reads in virus library})]}$$

The enrichment scores for individual variants in brain tissue obtained from sites with (x-axis) and without (y-axis) FUS-BBBO targeting are plotted in **Fig. 3-5**. Each dot represents a unique capsid protein sequence, and the red dot represents wildtype AAV9. Markers on the

right side of the vertical dotted line represent sequences that are transducing neurons with higher efficiency than WT AAV9 in FUS-BBBO treated regions. Markers at or below the horizontal dotted line represent sequences that retain or reduce the relatively low permeability of AAV9 into BBB-intact brain. Thus, using AAV9 as a standard, we can identify variants that appear to provide enhanced efficiency for FUS-BBBO mediated transduction while maintaining or improving specificity versus background transduction of untargeted brain tissues. Further analyzing of the second-round viral selection NGS results and cross-comparing them with data gained from murine model selection shows that there are total of 76 of top performing 100 mouse have shown in the best performing NHP variants in second round; out of which, 24 shared viral variants are presenting extraordinary spatial specificities, where they are much more highly enriched in the focused ultrasound targeted brain regions yet being rare to find in the brain tissue that did not experience FUS-BBBO (**Fig. 3-5**).

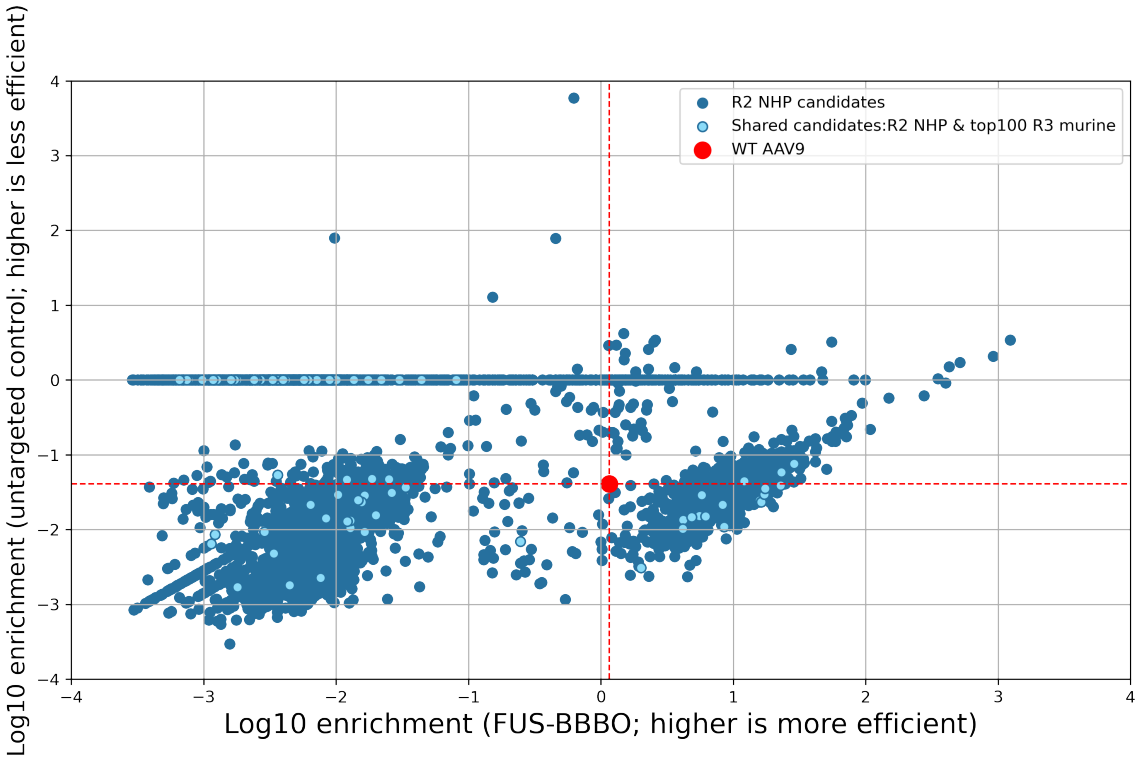

Figure 3-5 Enrichment scores for viral variants recovered from the second round of screening in NHPs. Each dot represents a unique capsid sequence, and the red dot represents wildtype AAV9. Light blue dots represent engineered viral variants that are both present in top 100 mouse candidates and second round selection in NHPs.

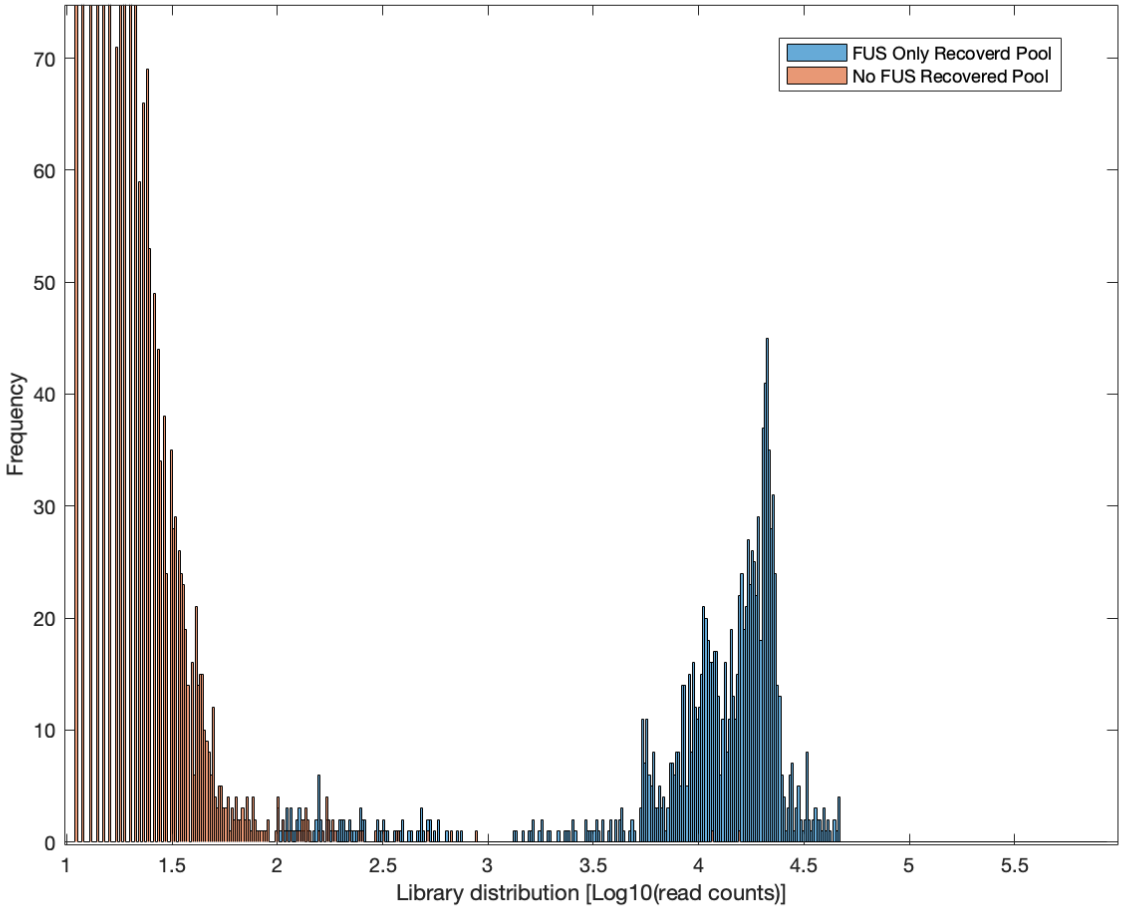

Figure 3-6 Read count distribution for viral variants recovered from the second round of screening in NHPs. The read count distribution from brain tissue samples experienced different FUS condition recovered from the second round of screening in NHPs reveals that FUS-BBBO did exert selection pressure for small cohort of viral variants that exceling in transduction of brain tissue at high frequency, or efficiency.

3.5 Future Perspectives and Discussion

As discussed in the previous section ***Chapter 3.4***, in our two previous screens in macaques, we tested a library of 7-mer inserts in the VP1 loop (between amino acid 588 and 589) of AAV9. For the first round, we packaged a library of $1.3x10^9$ variants with a Cre-dependent insert, following the CREATE strategy, and assisted by the CLOVER center at Caltech. To enable Cre recombination, we co-administered this library with AAV9 encoding Cre under a neuron-specific synapsin promoter (administering a high enough dose of AAV9 to enter the brain at the BBBO site). We performed FUS-BBBO in 2 locations in the brain, and after 4 weeks collected brain tissues and analyzed them by next-generation sequencing (NGS). This allowed us to identify sequences that showed successful FUS-BBBO crossing and synthesize a second library of 2098 variants (which included the top variants from our mouse study) that we administered to a second animal. In the second round, we were looking for variants that enter the brain with increased efficiency relative to AAV9 in the FUS-treated brain region but not in an untreated control region (because we want variants that we can spatially target). From this second-round screen (**Fig. 3-5**), we have identified 486 sequences that are well-represented in sequencing depth and fulfill our criteria. Intriguingly, 2 of the top 5 viral vector variants we identified as the top performers in our mouse study showed up among the top sequences for NHPs, suggesting that the mechanisms underlying performance improvement may be transferable between species.

To select 5 lead candidates for validation as FUS-BBBO-optimized AAVs in NHPs, we will perform one additional library screen. We will use data from our previous two rounds of NHP selection to design and synthesize a third-round AAV capsid library, which will allow us to down-select the lead candidates. We will administer this library to a macaque, collect its brain and peripheral organs (liver, heart, kidney, spleen, muscle), and perform DNA extraction for sequencing-based analysis. Although in mice we typically use a larger number of animals in each screen, given the scarcity, cost and, humanitarian considerations associated with macaques, it is appropriate to perform this step in a single animal. Our success in two previous rounds of single-animal screening supports the sufficiency of this approach.

To confidently down-select from our second-round winners to a handful of top variants, we will perform an additional third-round screen. For this experiment, we will synthesize a library of ~100 capsid sequences (representing the top performers from our 486 second-round sequences, while being a small enough library to have high statistical sampling of each variant) using DNA ordered from Twist Biosciences, clone it into viral backbones and package it with the help of the commercial partners. In the third-round screen, we will also incorporate spatial single-cell analysis tools to acquire dataset from NHP brain tissue that enables spatially and cell-type accurate distribution of viral variants in the regions of impact for FUS-BBBO and that of lacking it.

We will perform FUS-BBBO transcranially using a custom 128-element ultrasound array developed for us by collaborators at Vanderbilt University, specifically for use in NHPs. This device enables reliable non-invasive BBB opening under MRI guidance, as confirmed by the uptake of a gadolinium contrast agent, which is otherwise unable to cross the intact BBB (**Fig. 3-7**). We will use MRI to target FUS-BBBO to 3 different locations in one hemisphere (cortex, hippocampus, basal ganglia) in conjunction with intravenous microbubbles, applying ultrasound with a frequency of 1 MHz, target focal pressure of 400 kPa, 1% duty cycle, 1 Hz pulse repetition frequency and a total of 120 pulses per site. We will quickly administer a gadolinium contrast agent (ProHance) and acquire an MRI image to confirm BBBO opening at the desired locations. After confirming BBB opening, we will administer $1x10^{13}$ viral genomes of the library per kg body weight, together with $1x10^{10}$ VG/kg of AAV9-Syn-Cre. During this procedure, the animals will be anesthetized and monitored by dedicated veterinary staff. 4 weeks after this procedure, we will euthanize the animal and extract its brain and peripheral organs and collect samples for DNA extraction.

Subsequently, we will perform Cre recombination-dependent and -independent PCR amplification of the AAV constructs in samples extracted from the targeted brain hemisphere and untargeted brain hemisphere, as well as the peripheral organs. We will sequence the recovered library using the NGS facility. We will analyze the sequencing results to identify 5-10 variants meeting the following criteria: (1) at least 100-fold enhanced Cre-independent

transduction at FUS-targeted brain region compared to non-targeted control, (2) increased Cre-dependent transduction at FUS-targeted brain region compared to AAV9, as seen in all three FUS-BBBO locations in the brain, (3) reduced Cre-independent transduction of peripheral organs compared to AAV9. From the vectors that meet these criteria, we will select 5 that maximize brain transduction specificity as defined by the ratio of brain to liver transduction, as in our mouse study (Li et al. 2024).

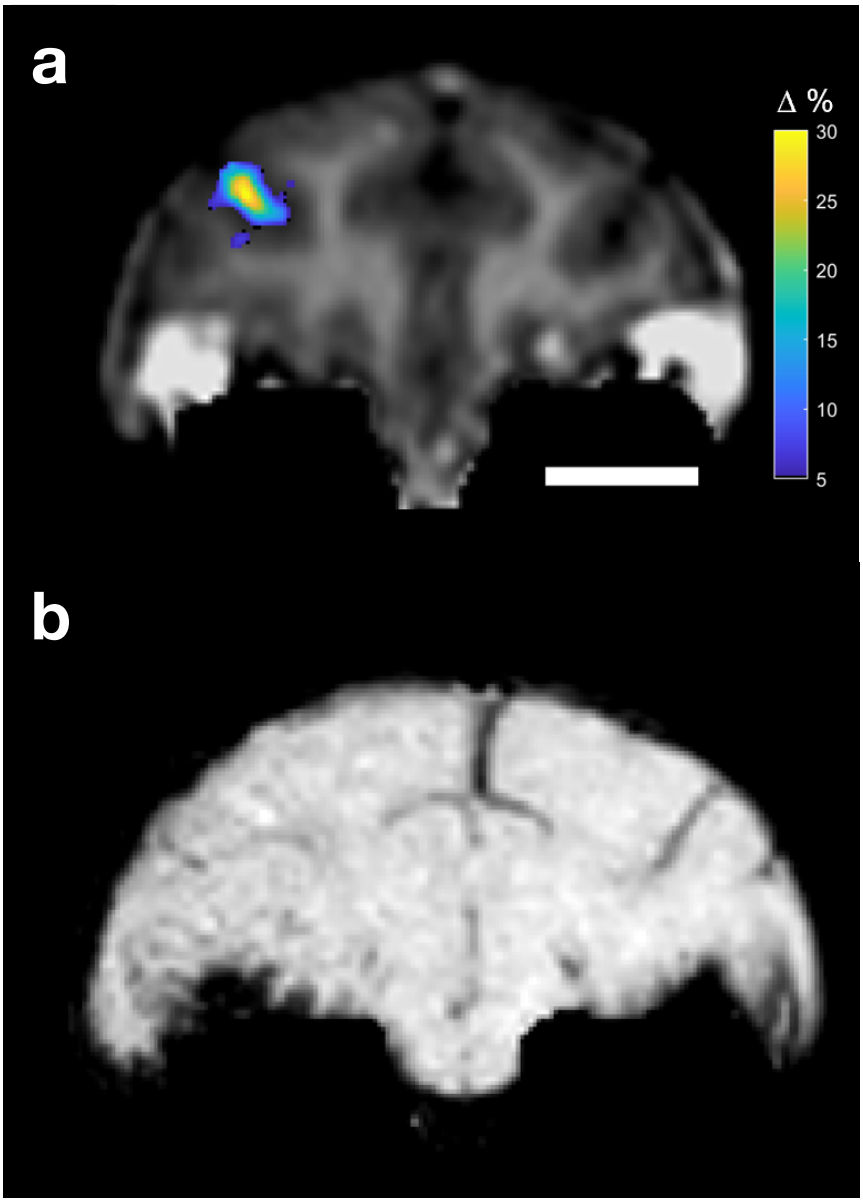

Figure 3-7 Representative BBB opening achieved with our custom FUS array in macaque. (**a**) Percent change in T1-weighted contrast following BBBO therapy overlaid on t1-weighted image of the brain. The targeted site shows strong contrast. (**b**) Susceptibility-weighted images used to check for hemorrhage following therapy. No darkening is seen that would indicate hemorrhage around the region where opening occurred. Scale bar is 1 cm.

After identifying 5 lead candidates from our third-round screen, we will validate them in two additional macaques. This validation will allow us to directly compare the performance of these variants in the brain and other tissues by counting the numbers of transduced cells and characterizing the cell-type tropism of each vector. For this experiment, we will prepare each serotype, and AAV9, with a cargo virus genome encoding differently-colored fluorescent proteins (e.g., EBFP2, YFP, mCherry, iRFP670), and labeled with distinguishable immunostaining tags, driven by a under a well-tolerated universal promoter EF1a promoter. As an independent validation of transduction efficiency, we will also extract viral DNA from half of the targeted FUS sites and perform quantitative PCR (qPCR) to measure the number of genomes of each lead candidate as compared to AAV9, as in previous studies. We will co-administer this set of vectors to new NHPs at a total dose of $1x10^{10}$ VG/kg body weight, during a FUS-BBBO procedure (performed as described in ***Chapter 3.4***). The FUS will target unilateral structures in the cortex, hippocampus, and basal ganglia. After 4 weeks of expression, we will euthanize the animals and collect their brains and peripheral organs for immunofluorescent imaging. The virus preparation will be contracted to commercial vendors, and the tissue sectioning and imaging will be done at Caltech.

We will quantify the transduction levels of each viral serotype in each targeted brain region, contralateral control, and other areas of the brain (to assess off-target transduction). We will co-stain with markers of cell types (key types of neurons, astrocytes, microglia, oligodendrocytes, endothelial cells) and quantify the relative tropism of each viral variant. To avoid spectral overlap, we will perform stains separately on adjacent slices. In addition, we will section and image tissues from peripheral organs and again quantify relative transduction. These validation experiments will provide us with strong evidence concerning which of our variants shows the highest efficiency at targeted transduction, lowest off-target transduction and highest tropism for specific cell types and brain areas. In addition, this data will allow us to conclude whether our screening approach is effective in NHPs.

Upon successfully reaching this point, we will be in a strong position to obtain the larger commercial, venture or grant resources needed to pursue further validation in a larger animal

cohort, apply it to specific disease models, and bring this technology toward clinical applications.

Chapter 4

AD MENTEM PER SONUM: INTERFACING INTACT BRAIN WITH ACOUSTICALLY TARGETED GENE DELIVERY FOR NON-INVASIVE NEUROENGINEERING

4.1 Abstract

The ability to interface with the brain at a molecular level presents a transformative opportunity for both fundamental neuroscience and the development of precision neurotherapies. A central challenge in realizing this potential lies in the delivery of genetic and molecular tools across the blood-brain barrier (BBB) with cell-type specificity, spatial precision, and minimal invasiveness. Recent advances in focused ultrasound-mediated blood-brain barrier opening (FUS-BBBO), when paired with systemically delivered engineered viral capsids such as AAV.FUS (see ***Chapter 2*** and ***Chapter 3***), have introduced a powerful modality known as acoustically targeted gene delivery. This method enables the non-invasive, region-specific transduction of brain tissue with genetic constructs, offering a path toward selective modulation and monitoring of neural circuits without the need for surgical intervention.

Acoustically targeted gene delivery represents a convergence of neuroengineering, molecular genetics, and acoustic physics, offering unique advantages for brain interfacing. Unlike conventional techniques that rely on direct injection or broadly distributed systemic delivery, acoustically targeted gene delivery leverages focused ultrasound in conjunction with intravenously administered microbubbles to transiently and reversibly disrupt the blood-brain barrier at targeted loci. Simultaneous intravenous infusion of AAVs allows the localized entry of genetic cargo into neural tissue, enabling spatially resolved expression of synthetic receptors, ion channels, or reporter genes. Crucially, this technique retains

compatibility with a wide range of engineered payloads, expanding its versatility for both therapeutic and diagnostic applications.

In this Chapter, we will explore the potential of acoustically targeted gene delivery as a foundational platform for bidirectional molecular interfacing with the brain. In the input direction, acoustically targeted gene delivery facilitates precise delivery of genetic constructs encoding chemogenetic actuators—engineered receptors that confer neuromodulatory control in response to exogenous ligands. By using acoustically targeted gene delivery to introduce such receptors selectively into targeted brain regions, it becomes possible to modulate pathological neural activity with high specificity and minimal systemic effects. This approach opens avenues for developing novel treatments for neurological conditions. For instance, in later sections of this Chapter, we will present a modular strategy for molecular input, wherein acoustically targeted gene delivery is used to deliver chemogenetic receptors (such as DREADDs or KORDs) to discrete brain regions and cell types. This approach will be applied toward two translational goals: developing a targeted therapy for epilepsy that modulates hyperexcitable neural networks, and a therapeutic strategy for opioid addiction that engages limbic stress circuitry to suppress maladaptive behaviors.

Complementing this input capability, acoustically targeted gene delivery also enables output interfacing via the expression of acoustic reporter genes (ARGs), such as genetically encoded gas vesicles. These nanostructures provide contrast for ultrasound imaging and allow real-time, noninvasive monitoring of gene expression and cellular dynamics within the intact brain. When targeted appropriately, ARGs serve as molecular reporters for biological processes, enabling the visualization of cellular responses to therapy, disease progression, or neural activity patterns. Together, these input and output strategies establish a closed-loop framework for molecularly precise, noninvasive interrogation and modulation of neural circuits.

Overall, the work presented in this Chapter positions acoustically targeted gene delivery not merely as a delivery method, but as a transformative interface for accessing, controlling, and imaging the brain with molecular precision. Through the development and application of this

platform, we aim to illuminate new strategies for treating neurological disorders, advancing systems-level understanding of brain function, and eventually achieve non-invasive brain molecular interface, pun intended.

4.2 Acoustically Targeted Chemogenetics for Epilepsy Control and Memory Deficit Rescue

4.2.1 Introduction

Epilepsy is a severe neurological disorder that affects approximately 1% of the population.(Ngugi AK et al., 2010) Nearly 30% of patients exhibit poor seizure control with medications, necessitating surgery, such as resective surgery or neuromodulation (i.e., deep brain stimulation, responsive neurostimulation, vagus nerve stimulation). While seizures can often be treated with medications and/or surgery, patients frequently still suffer from cognitive deficits including memory impairment. Furthermore, antiepileptic drugs themselves can cause and/or exacerbate cognitive deficits. Treating cognitive deficits in epilepsy represents a significant unmet need (Ponds RW et al., 2006).

Deep brain stimulation (DBS) is a form of neuromodulation that applies electrical stimulation to specific regions of the brain via implanted electrodes. It has traditionally been used to treat movement disorders, such as Parkinson's disease, essential tremor, and dystonia. More recently, DBS of the anterior thalamic nucleus and centromedian nucleus have shown promising results in reducing the seizure burden in epileptic patients (Ponds RW et al., 2006; and Salanova V et al., 2015). Although DBS for seizure control is typically performed in the gamma frequency range (130-180 Hz), more recent work suggests that theta frequency stimulation could be helpful for memory encoding and retrieval (Vertes RP et al., 2005). Specifically, it has been demonstrated that theta stimulation, but not gamma stimulation, of the medial septal nucleus (MSN), the primary generator of hippocampal theta oscillations, can restore hippocampal theta oscillations and spatial working memory in disease processes with abnormal hippocampal theta oscillations (traumatic brain injury, schizophrenia and

epilepsy) (Lee DJ et al, 2015; Lee DJ et al, 2017; Zepeda NC et al., 2022; and Izadi A et al., 2019). Furthermore, it has been demonstrated that MSN theta frequency DBS increases seizure threshold, (Lee DJ et al, 2017; and Izadi A et al., 2019) with long-term antiepileptic effects beyond the stimulation period (Izadi A et al., 2021). Given this, we hypothesize that enhancing theta oscillations, as opposed to gamma oscillations, will improve both seizure susceptibility and memory.

In support of this hypothesis, our collaborator, Darrin Lee's Lab at USC demonstrated that hippocampal theta power is diminished in the MSN and hippocampus following pilocarpine-induced status epilepticus (SE) and is associated with deficits in spatial learning ((Lee DJ et al, 2017; and Chauviere L et al., 2009)). Furthermore, they have demonstrated that stimulation of the MSN in the theta frequency range increased hippocampal oscillations and restored cognitive function in pilocarpine-induced SE rodents. Memory benefits gained from MSN stimulation were also found to be specific to theta frequency stimulation in a rodent model of traumatic brain injury (Lee DJ et al, 2017). However, the chemogenetic neuromodulatory effects of MSN neurons in SE animals have never been explored. In this study, we propose to test the hypothesis that chemogenetic stimulation of the glutaminergic neurons situated at MSN in the septohippocampal circuit in a pilocarpine model of epilepsy will restore cognitive deficits and reduce seizure susceptibility.

Developing technologies that can target, and control specific neural circuits is a key driver of neuroscience progress. Neural control technologies should ideally provide a combination of spatial, temporal, and cell-type specificity and be minimally-invasive to facilitate their translation across animal models and, ultimately, human patients. While DBS has been shown to be effective at modulating neural circuits with reasonable spatial specificity, it is invasive and lacks the ability to target specific cell-types. Here, we propose, for the first time, an approach to modulate neural circuits with spatial, temporal, and cell-type specificity. In our approach, we employ minimally-invasive Acoustically Targeted Chemogenetics (ATAC) (see ***Chapter 1***), a cutting-edge technology that uses transient ultrasonic stimulation to open the blood brain barrier (BBB), to transduce neurons at specific locations in the brain

with virally-encoded engineered chemogenetic receptors. Because of their selective tropism, these virally encoded receptors can be designed to selectively transfect specific cell populations. Developing this technology will allow us, for the first time, to administer designer compounds systemically to selectively activate or inhibit the activity of specific neuronal cell types. In our previous work, we have implemented this concept in mice by using ATAC to minimally-invasively deliver AAV9 viral vectors encoding chemogenetic DREADDs to excitatory neurons in the hippocampus and show that this enables pharmacological inhibition of memory formation (Szablowski JO et al., 2018). Our study showed that this effective neuromodulation can be achieved completely non-surgically with minimal damage to brain tissue.

The unique expertise brought together by this multi-disciplinary consortium will allow us to develop a novel minimally-invasive neuromodulation approach that can deliver spatial, temporal, and cell-type specific control.

Spatial specificity is mediated through ATAC which employs focused ultrasound BBB opening (FUS-BBBO). FUS is an advanced biomedical technology that takes advantage of ultrasound's ability to specifically activate focal areas in deep tissues such as the brain with millimeter spatial precision (Carpentier A et al., 2016; Elias WJ et al., 2016; and Dobrakowski PP et al., 2014). FUS-BBBO combines transcranial ultrasound in the low-intensity regime with systemically administered microbubbles, whose stable cavitation in blood vessels at the ultrasound focus results in localized, temporary and reversible opening of the BBB (Hynynen K et al., 2001; and Tung YS et al., 2011). This allows small molecules, proteins, nanoparticles or viral capsids (Hynynen K et al., 2001; Samiotaki G et al., 2015; and Hsu PH et al., 2013) to enter the brain at the site of applied ultrasound. FUS-BBBO has been demonstrated to work safely and effectively in larger species (McDannold N et al., 2012; Downs ME et al., 2015; and Tung Y-S et al., 2011), and can be used to "paint" brain regions of arbitrary size and shape. Temporal and cell-type specificity are mediated by chemogenetic constructs, DREADDs, that are activated by exdogenous drugs. In this study, the cell-selective viral construct (targeting glutamate neurons) will be delivered to the MSN

via acoustically targeted gene delivery. The cell-selective MSN neurons can then be activated at specific time points with an intraperitoneal injection of the designer drug to drive neuronal activity.

In pairing FUS-BBBO, a brief, non-invasive procedure with systemic injection of viral DREADDs, we will be able to selectively modulate a specific brain region (MSN) using systemically bioavailable compounds.

In all, in this study, we propose to drive hippocampal theta oscillations through cell-type specific stimulation of the MSN, thereby, modulating the septohippocampal circuit and concomitantly decreasing seizure susceptibility and improving cognition.

4.2.2 Results

We have gathered compelling preliminary data to support our hypothesis that electrically stimulating the MSN can drive hippocampal theta oscillations, increase seizure threshold, and improve spatial memory. Later, using a chemogenetic direct viral injection approach, we have demonstrated that cell-type specific glutamate activation of the MSN drives hippocampal theta oscillations and can increase seizure threshold. Further, we have demonstrated that it is possible to target the MSN with the ATAC technique, providing exciting pre-clinical evidence for the use of ATAC to treat seizures and cognitive dysfunction in epilepsy.

Hippocampal oscillations can be modulated using MSN stimulation: We have demonstrated the ability to effectively implant MSN bipolar stimulating electrodes and hippocampal recording electrodes in rats and mice and subsequently obtain high quality recordings in freely moving animals (**Fig. 4-1a**). When stimulating the MSN with theta oscillations, we increase theta power within the hippocampus (**Fig. 4-1b**). Further, we have demonstrated that MSN theta stimulation increases seizure threshold both acutely after stimulation (Izadi A et al., 2019) and up to 40 days after cessation of stimulation (Izadi A et al., 2021). Taken

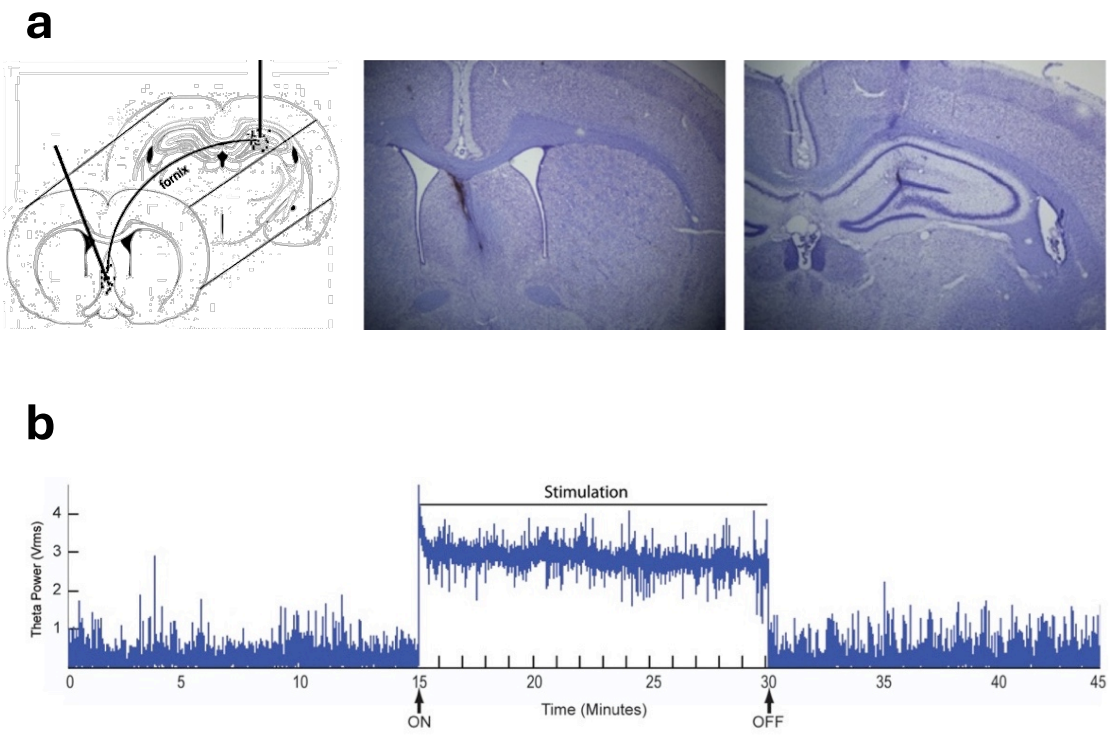

Figure 4-1 Deep brain electric simulation in MSN increases hippocampal theta oscillations acutely. (**a**) Schematic of MSN and hippocampal depth electrodes (Left) and representative cresyl violet stains demonstrating the electrode tracts in the MSN (Center) and hippocampus (Right). (**b**) Representative image demonstrating that MSN theta (7.7 Hz) stimulation increases hippocampal theta oscillations acutely (power analysis).

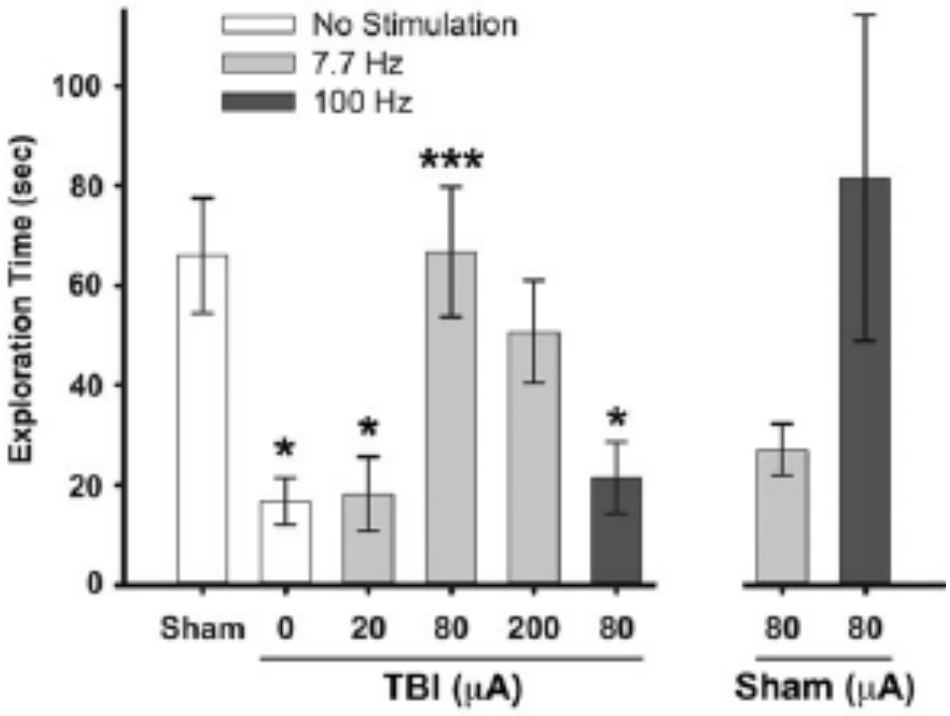

Figure 4-2 Dose response curve of MSN theta stimulation on an object exploration task. Here, we stimulated the MSN with theta (7.7 Hz) oscillations and evaluated a range of currents on an object exploration task. Traumatic brain injury (TBI) rats had a significant decrease in hippocampal theta oscillations that correlated with impaired object exploration compared to sham rats. Interestingly, TBI rats stimulated with 80 μA had similar behaviors to sham rats, but TBI rats receiving 20 μA of theta stimulation or 80 μA of gamma stimulation explored objects less than sham rats. Based upon these findings, we decided to use 80 μA for our stimulation current. * signifies $p<0.05$ and *** signifies $p<0.05$ comparing stimulation to TBI without stimulation.

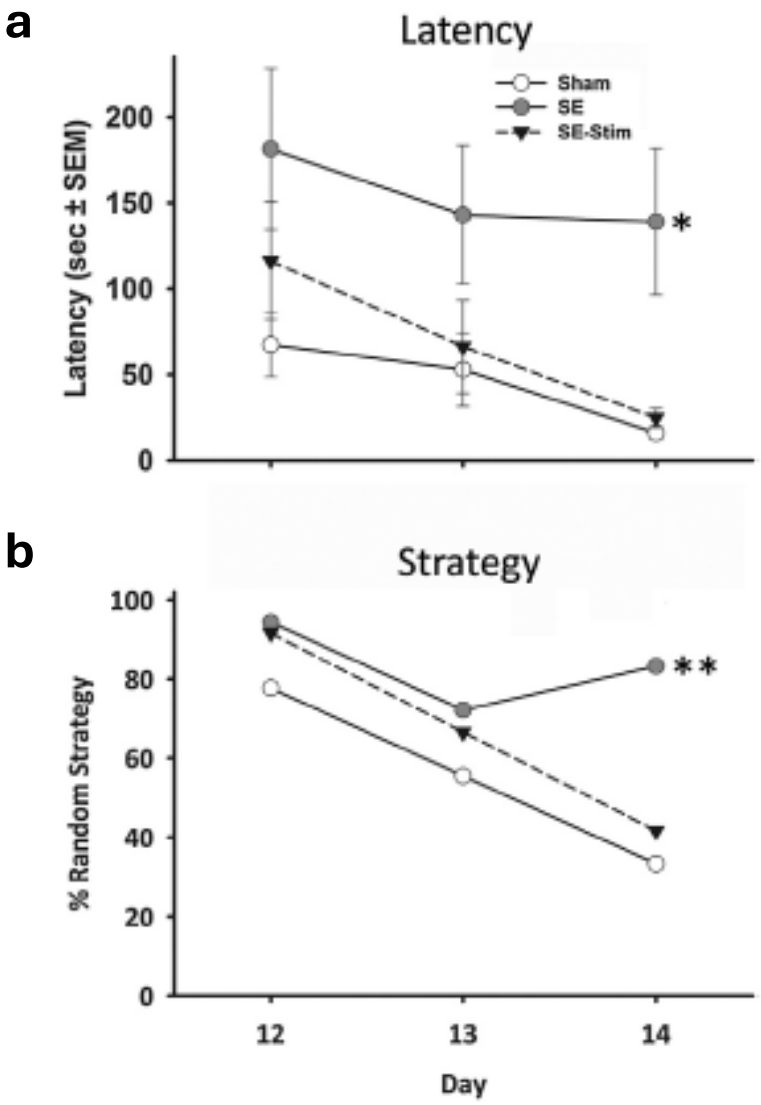

Figure 4-3 MSN theta stimulation improves hippocampal-dependent spatial working memory in a pilocarpine model of epileptogenesis. (**a**) Twelve days after pilocarpine-induced status epilepticus (SE), there was a significant increase in latency to finding the escape box on the Barnes maze (spatial memory). In SE rats, MSN theta stimulation during the Barnes maze improved latency to finding the escape box compared to SE rats without stimulation. (**b**) Similarly, MSN theta stimulation improved search strategy in pilocarpine SE rats relative to pilocarpine SE rats without stimulation improved.

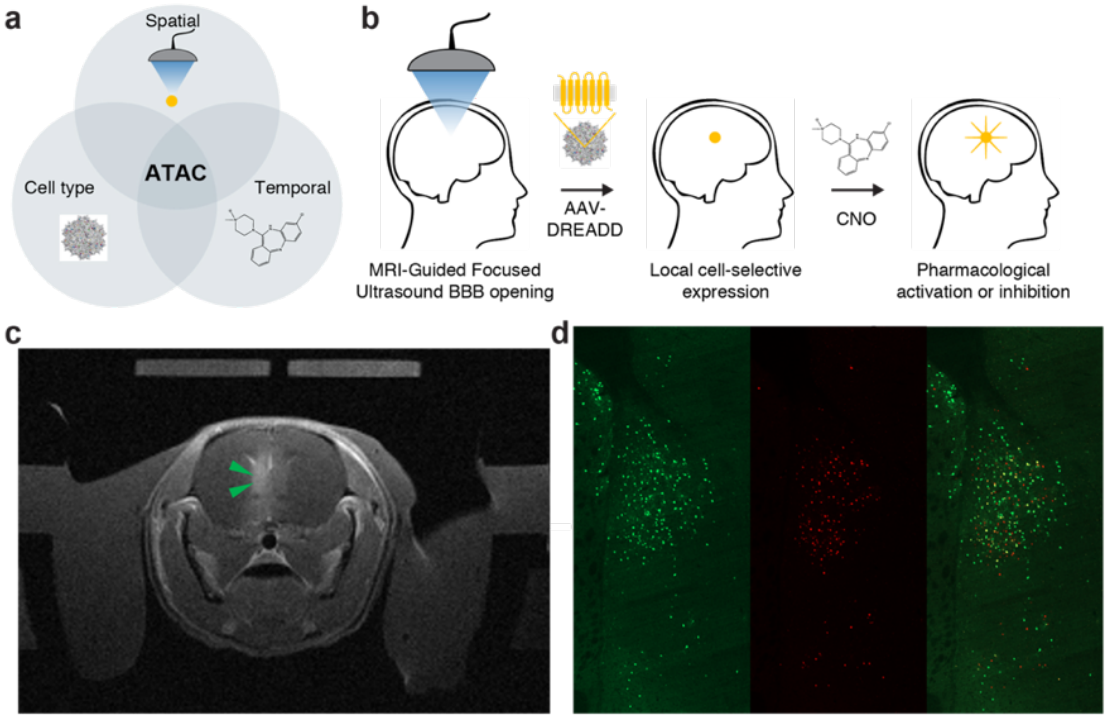

Figure 4-4 Acoustically targeted chemogenetics (ATAC) combined with engineered capsid AAV.FUS.3 paradigm for MSN neurons stimulation. (**a-b**) uses MRI-guided focused ultrasound to reversibly open the blood-brain barrier at specific brain locations (**c-d**) and deliver cell-type specific viral vectors to mouse MSN in left hemisphere (**c**) T1 weighted MRI image of post-FUS targeted left MSN (green arrows point to contrast from Gadolinium extravasation due to BBBO) (**d**) Representative images obtained from mice FUS-BBBO targeted in left hemisphere MSN, co-injected with AAV9 and a AAV.FUS.3, which encodes for mCherry and EGFP, respectively, at 1010 viral particles per gram of body weight. After 3 weeks, the mice were perfused, brains were extracted and then sectioned at 50 microns. Sections were imaged on a confocal microscope with 20x objective showing brain transduction by AAV9 (green) and AAV.FUS.3 (red).

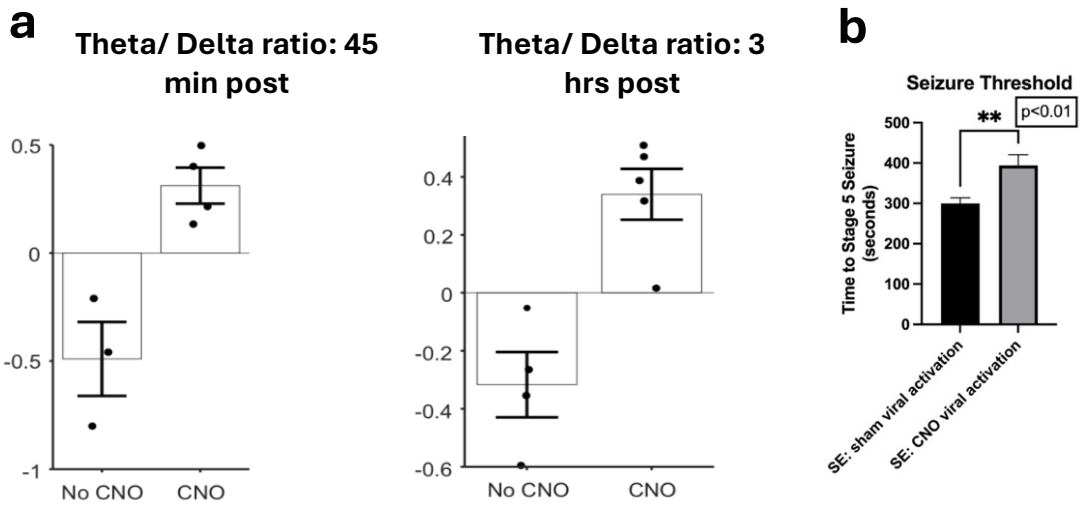

Figure 4-5 Chemogenetics activation of glutamatergic MSN neurons increases theta oscillations in pilocarpine-indicued SE animals. (**a**) 45 minutes and three hours after viral activation in SE rats (n=3) there was a significant increase in the hippocampal theta/ delta ratio compared to sham activation (saline, n=3) in the SE rats. This suggests that MSN glutamatergic viral activation can drive hippocampal theta oscillations. (**b**) Using flurothyl testing to evaluate seizure susceptibility/ threshold, pilocarpine-induced SE rats who underwent activation of excitatory neuronal populations in the MSN via adeno-associated viral (AAV9-CamKIIa-hM3D(Gq)-mcherry) vectors encoding DREADDs via intraperitoneal clozapine-N-oxide (CNO) before behavior tasks resulted in a longer latency compared to sham activation (saline) in pilocarpine-induced SE rats, p=0.004. This suggests that viral activation of glutamatergic MSN neurons has an antiepileptic effect.

together, these data demonstrate that it is possible to modulate hippocampal oscillations through MSN stimulation. Behavior on an object exploration task can be modulated in a dose-dependent fashion. Based upon our previous data, the optimal current is 80μA (**Fig. 4-2**).

We have also demonstrated that MSN theta stimulation improves hippocampal-dependent spatial working memory in a pilocarpine model of epileptogenesis (**Fig. 4-3**). Drawing from this work, we propose to utilize MSN electric and chemogenetic stimulation to restore hippocampal theta oscillations, improve cognition and increase seizure threshold in a mouse model of epilepsy.

Our work demonstrates that demonstrates that we can use MRI-guided focused ultrasound (FUS-BBBO) to open the blood-brain barrier and deliver cell type-selective viral vectors to the MSN (**Fig. 4-4**). Moreover, neuronal glutamatergic viral expression and activation of the MSN (via an AAV, promoter and Designer Receptors Exclusively Activated by Designer Drug (DREADD): CamKIIa-hM3D(Gq)-mcherry) drives hippocampal theta oscillations (**Fig. 4-5a**) and leads to increased seizure threshold in a pilocarpine-induced SE animal model (**Fig. 4-5b**).

4.3 Fentanyl Addiction Remission via Acoustically Targeted Chemogenetics

4.3.1 Introduction

Opioid use disorder (OUD) poses a significant public health challenge, characterized by high relapse rates, substantial disability, and elevated mortality (Strang et al., 2020; Centers for Disease Control and Prevention [CDC], 2019; Case & Deaton, 2015; Koob, 2020; Evans & Cahill, 2016; and Jones et al., 2018). Fentanyl, a potent synthetic opioid widely administered for anesthesia and pain management, is responsible for nearly 46% of opioid overdose fatalities (Jones, Einstein, & Compton, 2018). Unfortunately, existing treatments have only modest efficacy (Schuckit, 2016; Carley & Oesterle, 2021; Lee et al., 2024; and Gold et al., 2020). Both preclinical and human neuroimaging studies provide compelling evidence that the hallmark behaviors of fentanyl addiction—compulsive drug use, impaired self-control, and behavioral inflexibility—are rooted in dysregulation in specific neural circuits (Chang & Peters, 2023; Blackwood & Cadet, 2021; and Herlinger & Lingford-Hughes, 2022) such as the corticotropin-releasing factor (CRF) circuit in the bed nucleus of the stria terminalis (BNST), a crucial part of brain stress system (Koob & Schulkin, 2019; Carmack et al., 2019; Roberto et al., 2017; and Carmack et al., 2022) (**Fig. 4-6**). If it were possible to selectively modulate these dysfunctional neural circuits, this could effectively treat fentanyl addiction. However, current technology for neuromodulation is either too invasive or too non-specific to target these circuits and have an impact on this large, high-need, patient population. In this project, we attempt to overcome some of the major challenges constraining the successful application of neuromodulation in treating addiction disorders by combining focused ultrasound with molecular engineering and chemogenetics.

This project leverages an approach we developed to modulate neural circuits non-invasively with spatial, cell-type, and temporal specificity. This approach, which we call Acoustically Targeted Chemogenetics, or ATAC, uses transient ultrasonic opening of the blood brain barrier (BBB) to transduce neurons at specific locations in the brain with virally-encoded engineered chemogenetic receptors, which subsequently respond to systemically

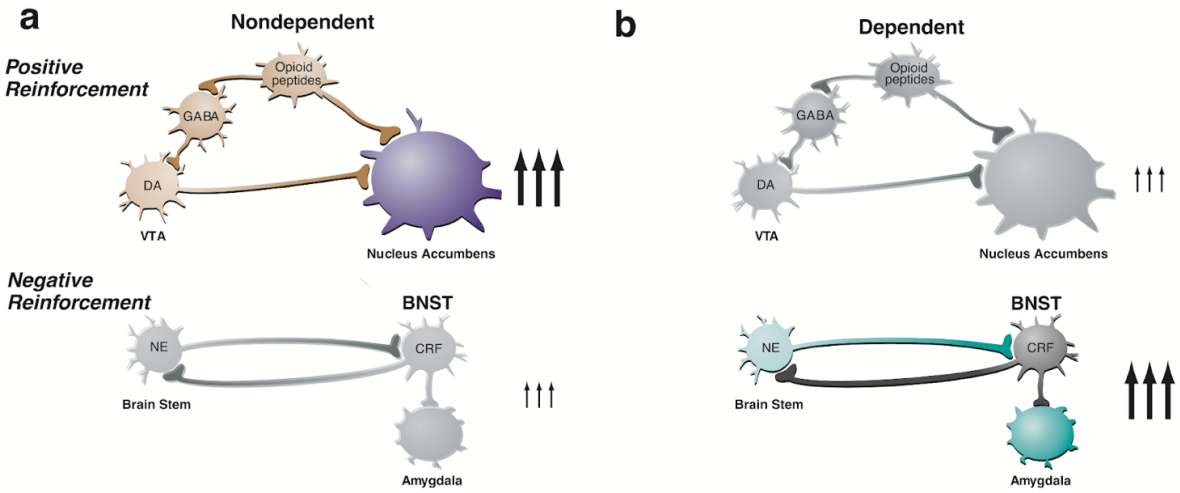

Figure 4-6 Neurocircuitry associated with the positive reinforcement of fentanyl abuse and the negative reinforcement of dependence and how it changes in the transition from nondependent drug taking to dependent drug taking. (**a**) Key elements of the reward circuit are dopamine (DA) and opioid peptide neurons that act at both the ventral tegmental area (VTA) and the nucleus accumbens and which are activated during initial alcohol use and early stages of the progression to dependence. (**b**) Key elements of the stress circuit are corticotropin-releasing factor (CRF) and norepinephrine (NE)-releasing neurons that converge on γ-aminobutyric acid (GABA) interneurons in the central nucleus of the amygdala and which are activated during the development of dependence.

administered designer compounds to activate or inhibit the activity of these neurons (**Fig. 4-7**). This technology allows a brief, non-invasive procedure to make one or more specific brain regions capable of being selectively modulated using systemically bioavailable compounds. We previously implemented this concept in mice by using ATAC to non-invasively target AAV9 viral vectors encoding a type of chemogenetic receptors, known as Designer Receptors Exclusively Activated by Designer Drugs (DREADD), to excitatory neurons in the hippocampus, and showing that this enables pharmacological inhibition of memory formation (see ***Chapter 1*** at **Fig. 1-2**) (Szablowski et al., 2018). Our study showed that this modulation can be achieved completely non-invasively and efficiently with no damage to brain tissue. Subsequently, we engineered novel AAV vectors, AAV.FUS, to substantially enhance ATAC gene delivery and cell-type tropism to the brain while reducing peripheral transduction, providing a more than ten-fold improvement in targeting specificity *in vivo* (Li et al., 2024) and enhancing the prospects for clinical translation.

In this project, we hypothesize that with ATAC, non-invasively targeting AAV.FUS encoding inhibitory chemogenetic receptors to CRF neurons in the BNST will enable us to effectively reduce the expression of stress-related neuropeptide CRF that drives excessive drug seeking during fentanyl withdrawal. As a result, hallmark symptoms of fentanyl withdrawal such as increased sensitivity to pain (hyperalgesia) and abnormal physical patterns (somatic signs) will subside and compulsive drug seeking behavior will stop, achieving fentanyl addiction remission. If successful, this work will introduce a strategy for treatment of opioid abuse through non-invasive neuromodulation for potential human clinical translation.

4.3.2 Significance

Current addiction therapies often fail to achieve long-term success due to the chronic and relapsing nature of the disorder. Even after completing rehabilitation programs, many individuals relapse, particularly in the first year of recovery (Kabisa et al., 2021; Rahman et al., 2016; Sinha, 2011). Existing treatments focus on managing withdrawal symptoms

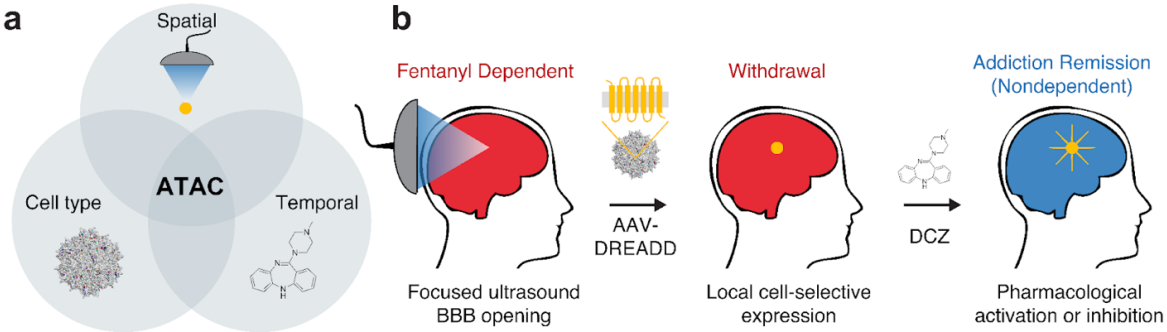

Figure 4-7 Conceptual illustration of Acoustically TArgeted Chemogenetics (ATAC) delivered via focused ultrasound and modulating localized & specific brain circuit for addiction remission

without directly targeting the dysfunctional neural circuits responsible for addictive behaviors (Srivastava, Mariani, & Levin, 2020). Moreover, current pharmacological interventions often fail to adequately address polysubstance use—for example, methadone and buprenorphine are used for opioid addiction, while disulfiram and acamprosate are for alcohol dependence—making it challenging to treat patients with multiple substance dependencies, a clinical scenario that is becoming increasingly common (Crummy et al., 2020; and John et al., 2018). Additionally, medications like methadone carry their own risk of dependency (Wakeman et al., 2020). The major concept of this proposal, ATAC, provides a long-term targeted intervention that can directly modulate neural circuits regulating stress-related neuropeptide CRF implicated in compulsive drug-seeking behaviors and heightened relapse risk commonly involved in addiction of multiple substances (Koob, 2020). We hypothesize that this therapy can provide a generalized approach to treating dependence on various drugs. Importantly, the non-invasive nature of ATAC will synergize with the growing clinical acceptance of AAV gene therapies (Ling, Herstine, Bradbury, & Gray, 2023) and the high efficiency of AAV.FUS to facilitate broad clinical application with reduced risk of complications and cost of therapy, making it accessible to patients in great need who have few other options.

4.3.3 Results

Our research strategy comprises two parts. In first part of the project, we optimize and validate the ATAC paradigm to inhibit CRF neurons in mouse BNST. First, we establish and optimize the ATAC technique with site- and cell-type specificity in the BNST in mice, assessing success using histology and non-invasive functional imaging. In second part of the project, we will evaluate the withdrawal behavioral hallmarks and functional remission in fentanyl-dependent mice upon ATAC inhibition of CRF^{BNST} neurons. We assess the optimized ATAC paradigm for treating the hyperalgesia and negative somatic effects during withdrawal, and then drug-seeking behaviors resulting from long-term fentanyl dependence, using a novel fentanyl vapor self-administration mouse model.

Optimize and validate the ATAC paradigm to inhibit CRF neurons in mouse BNST

In the first part of the project, we begin with perform FUSBBBO delivery of AAV.FUS encoding inhibitory chemogenetic receptors to the BNST of healthy CRH-Cre mice, testing viral doses, ultrasound parameters and ligand-receptor pairs. We then establish methods to visualize chemogenetic inactivation of (CRF) neuronal activity in the BNST functional ultrasound imaging, and confirm it with electrophysiology and c-Fos markers of neuronal activity. At the end of these experiments, we assess expression and tissue viability using post-mortem histology.

In demonstrating for robust FUSBBBO viral vector delivery to BNST, CRH-Cre mice was prepared for intravenous injection of AAVs encoding inhibitory DREADD and bilateral focused ultrasound BBB opening (FUSBBBO) at BNST s. As our initial parameters based on our previous ATAC study in mice, we will use Definity microbubbles injected intravenously at 1.2E5 bubbles/g and apply 10 ms sonications repeated at 2 Hz for 120 seconds by 1.5 MHz eight-element annular transducer. We perform a systemic injection of 1E10 vg/g AAV.FUS encoding a chemogenetic receptor. For our initial test of expression and function we will use the inhibitory DREADD (FLEx-hM4Di-mCherry) under the hSyn promoter. Simultaneously, we co-inject the same dose of 1E10 vg/g AAV.FUS-CAG-FLEx-eGFP to allow CRF neurons to produce GFP in the BNST s of CRH-Cre mice. The co-localization of mCherry and GFP in histology validates successful targeted expression of inhibitory DREADD in CRF neurons. We'll allow 6 weeks for gene expression before assessment. In preliminary experiments, we have demonstrated that BNST can be accurately and sufficiently transduced by AAV mediated by MRI guided FUSBBBO targeting based on histologic results (**Fig. 4-8**). To assess chemogenetic inhibition, with help from the Caltech Neurotechnology Laboratory led by Dr. Daniel Wagenaar, we will record the spiking of neurons in the FUS-targeted BNST s before and after the administration of chemogenetic ligands (DCZ) (Nagai et al., 2020). These effects will be compared with the effects of ligand administration while recording from a control area where no ultrasound was applied. In

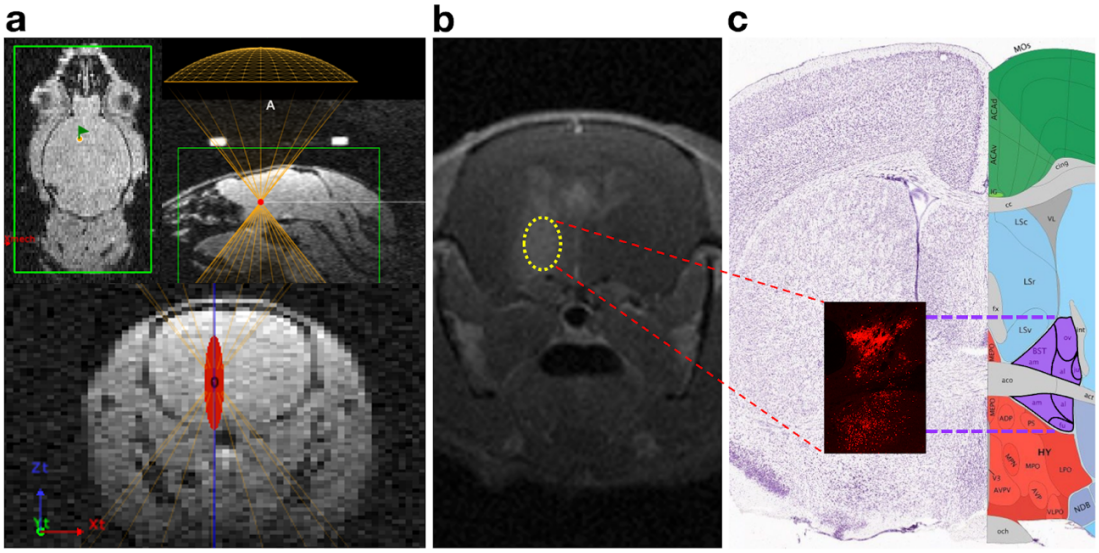

Figure 4-8 FUS-mediated delivery of AAV to BNST (**a**) Focused ultrasound targeting BNST for BBBO, pressure profile simulated as red spindle (**b**) Image from a representative T1-weighted MRI scan acquired immediately after AAV injection and FUS-BBBO, with brighter areas indicating relaxation enhancement from contrast agents extravasation, as shown by the yellow dots (BNST). (**c**) Overlaid mouse brain atlas with mCherry expression in BNST by FUS-mediated delivery of AAV

addition, we will image the effects of ATAC inhibition with functional ultrasound to verify the effect of inhibition based on differential blood flow in the region of modulation.

To determine the efficiency of FUSBBBO gene delivery for DREADD used in the initial set of CRH-Cre mice, we will euthanize the animals after evaluating ATAC functionality and examine fixed brain tissue using immunofluorescence (using antibodies against the products of transduced transgenes and activity-dependent gene product c-Fos). Evaluating ratios of total CRF neurons (labeled with eGFP from previous section) and DREADD expressing CRF neurons (labeled with mCherry from previous section), and c-Fos expression level, will allow us to optimize viral dosage, ultrasound targeting parameters, and guide our DREADD choices for later experiments of the project. Simultaneously, we will test two additional chemogenetic receptors besides hM4Di. This will allow us to find the optimal set of reagents for later experiments of the project, and provide the field with important information for future studies. This additional testing will include the alternative inhibitory DREADD KORDi and its cognate ligand salvinorin B, and the ionotropic inhibitory $PSAM^4$ -GlyR system. Each of these genetic constructs will be packaged in the AAV.FUS and introduced into the BNST using the methods described above. Animals will undergo assessments described in previous sections, using varying doses of the appropriate ligands. In the future, utilizing the KORDi and/or $PSAM^4$-GlyR system could enable orthogonal modulation of neural circuits in multiple brain regions.

(Future Plans) Evaluate the withdrawal behavioral hallmarks and functional remission in fentanyl-dependent mice upon ATAC inhibition of CRFBNST neurons

The need to avoid withdrawal symptoms is hypothesized to drive compulsive drug-taking and drug-seeking in OUD (Koob, 2020; Evans & Cahill, 2016; and Alvarez-Bagnarol et al., 2022). Thus, evaluating effects of ATAC inhibition of CRF^{BNST} neurons on protracted fentanyl withdrawal will help verify therapeutic efficacy for treating this salient aspect of dependency. We hypothesize that inhibiting CRF^{BNST} neurons alone with the ATAC paradigm will be sufficient to significantly decrease hyperalgesia and somatic effects in mice during fentanyl withdrawal; and reducing these symptoms associated with compulsive drug

seeking renders the technology's potential for treating long-term opioid dependence. As addiction-like behaviors are defined by persistent, repetitive drug seeking and taking, which may serve to alleviate or prevent distress, anxiety, or stress (American Psychiatric Association, 2022; el-Guebaly et al., 2012; and Robbins et al., 2012). We hypothesize that if ATAC inhibition of CRF^{BNST} neurons can reduce the negative effects of behavioral hallmarks during fentanyl withdrawal associated with compulsive drug seeking, then it can choke the negative reinforcement in opioid addiction and subsequently cut the drives for continued drug use to remission the long-term fentanyl dependence (Marchette, Carlson, Said, Koob, & Vendruscolo, 2023).

Utilizing a novel non-invasive operant fentanyl vapor self-administration mouse model developed by our collaborator Dr. Leandro Vendruscolo (Moussawi et al., 2020), we'll study how inhibitory ATAC targeting the CRF^{BNST} neurons affects withdrawal behavioral hallmarks and drug-seeking behavior in long-term fentanyl dependent mice. Specifically, we will assess whether and how the ATAC treatment alters hyperalgesia and somatic withdrawal effects, and drug-seeking behaviors into the following phenotypic components of increased drug seeking under progressive-ratio (PR) and -delay conditions, and continued drug seeking and taking despite aversive consequences (Moore et al., 2019). Firstly, wild type C57BL/6J mice will be randomly assigned to two groups, where one group will be treated with FUS-mediated AAV.FUS delivery of inhibitory DREADD targeting CRF^{BNST} neurons bilaterally while the other group remains untreated. After six weeks of DREADD expression (during which the mice will be shipped from Caltech to the NIH, pass quarantine and and undergo acclimatization), to train mice to self-administer fentanyl, in an airtight plexiglass chamber equipped with fentanyl vaporizer linked to levers and cue lights, both groups of mice will be exposed to a fentanyl vapor delivery triggered by active lever press on a fixed-ratio 1 (FR1) schedule of reinforcement for 1-hour sessions (Moussawi et al., 2020) (a fixed ratio refers to the number of times an action must be done in order to receive an award). After six 1-hour training sessions of fentanyl vapor self-administration, all mice will be allowed 6-hour access to fentanyl self-administration in 10 FR1 sessions to achieve the persistent addiction through escalation of fentanyl intake. Preliminary data from our collaborator Vendruscolo Lab has

demonstrated that behavioral hallmarks of withdrawal and motivation for fentanyl are inducible by the fentanyl vapor self-administration mouse model (**Fig. 4-9**).

Assessment of hyperalgesia and somatic signs during spontaneous fentanyl withdrawal upon ATAC inhibition of CRF^{BNST} neurons: After 6 weeks of DREADD expression, before self-administration conditioning, we will measure the baseline paw withdrawal thresholds for von Frey test. Subsequently the mice will receive self-administration conditioning in the fentanyl vapor device. For the mice that received ATAC treatment, they will then receive intraperitoneal (i.p.) of vehicle (saline) or Deschloroclozapine (DCZ) thirty minutes before another von Frey test. A separate group of mice without ATAC treatment (receives FUSBBBO and saline injection instead) will also be subjected to the self-administration conditioning to build dependence and then receive the same i.p. Injections of saline or DCZ before behavioral tests, whose data will serve as controls. Functional ultrasound imaging will be monitoring BNST s and the primary somatosensory areas (S1) during each paw withdrawal threshold test. We will then evaluate somatic signs during naloxone-precipitated fentanyl withdrawal with or without ATAC inhibition of CRF^{BNST} neurons. After self-administration conditioning in the fentanyl vapor device, each mouse from both groups (received AAV or saline upon FUSBBBO) will receive intraperitoneal (i.p.) of vehicle (saline) or clozapine-N-oxide (DCZ). Thirty minutes after the i.p. injections, we will precipitate withdrawal with a single i.p. injection of the preferential m-opioid receptor antagonist naloxone and record somatic signs of withdrawal for twenty minutes. We will count the number of paw tremors (i.e., “clapping” front paws), jumps, and “wet-dog” shakes. We’ll assign one point per observation for each behavior. We will also assign one point per observation for the appearance of less frequent signs of withdrawal, such as abnormal posture, genital grooming, and diarrhea. We will perfuse mice one hour after the end of behavior scoring for histologic analysis of chemogenetic expression.

Assessment of fentanyl seeking under progressive-ratio (PR) and progressive-delay conditions upon ATAC inhibition of CRF^{BNST} neurons: After the escalation phase, DCZ and saline will be i.p. administered to ATAC-treated group and untreated group, respectively.

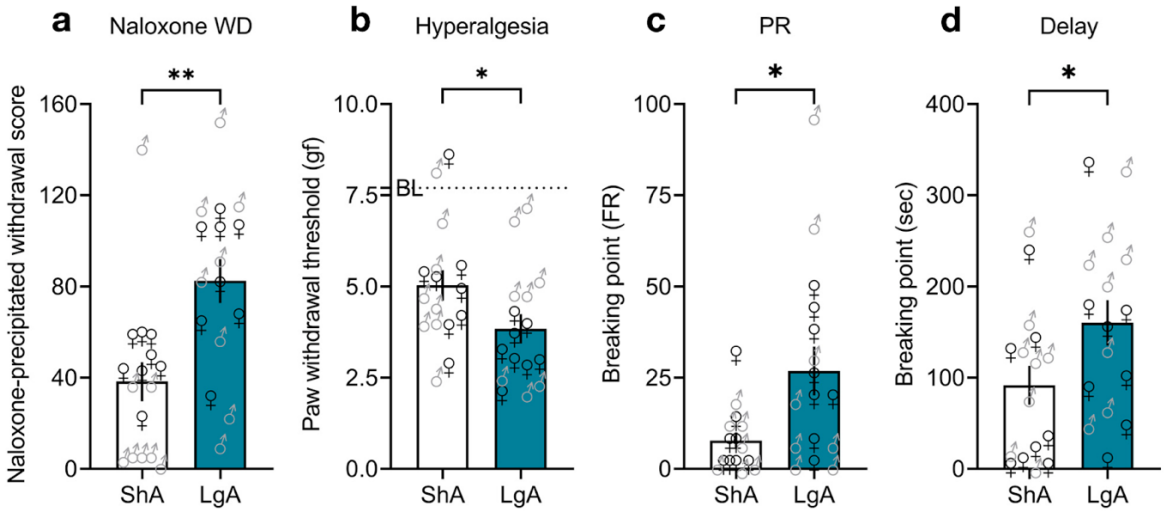

Figure 4-9 Fentanyl vapor self-administration mouse model induces addiction-like behavioral hallmarks of withdrawal and motivation for fentanyl in mice. ShA = short access to fentanyl that does NOT build dependence; LgA = escalated exposure to fentanyl that condition for long-term fentanyl dependence (**a**) Naloxone-precipitated withdrawal. Immediately after fentanyl vapor self-administration escalation phase, all mice received naloxone and were observed for signs of withdrawal. (**b**) Mechanical hyperalgesia. After a self-administration session (i.e., during spontaneous withdrawal), the mice were tested for mechanical hyperalgesia using an electronic von Frey device. The dotted line represents the average baseline measure (i.e., before fentanyl exposure) for all mice; both groups developed hyperalgesia compared with the baseline (BL) measure. (**c**) Progressive ratio test (motivation or "effort"). After escalation, all mice were tested in a progressive-ratio task (**d**) Time delay task (motivation). After escalation, all mice were tested in the delayed-reward task

Thirty minutes later, we will test both groups of mice in a PR task, in which the number of lever presses that is required for vapor delivery will be sequentially increased by six (PR 6; i.e., 1, 7, 13, 19, 25, 31, etc.). A 30-minute period without vapor delivery or a total of 6 hours will end the session. The breakpoints will be determined for both groups as the last ratio that is completed in the session, indicating the levels of "effort" in seeking fentanyl. In parallel to the progressive-ratio (PR) test, both ATAC-treated and untreated mice will be tested in a delayed-reward task. In this test, the interval between lever pressing and vapor delivery will be sequentially increased by 6 s (i.e., 1, 7, 13, 19, 25, 31, etc.) for each subsequent drug delivery. Similarly, the breakpoint will also be determined as the last ratio (in seconds; "time") that is completed in the session for both groups of mice, indicating the levels of "effort" and "perseverance" in seeking fentanyl.

Assessment of fentanyl seeking and taking despite aversive consequences upon ATAC inhibition of CRF^{BNST} neurons: After the escalation phase, DCZ and saline will be i.p. administered to ATAC-treated group and untreated group, respectively. Thirty minutes later, to model punished drug seeking, we will test both groups for the self-administration of capsaicin alone (i.e., vehicle without fentanyl). The mice will be exposed to four concentrations of capsaicin (0, 0.01, 0.03, and 0.1%, w/v) in 1-hour sessions. To model punished drug taking, the fentanyl solution will be adulterated with increasing concentrations of capsaicin. The concentrations of capsaicin followed a log scale, starting at 0.01% (capsaicin in fentanyl [w/v]) up to 3% (Edwards & Koob, 2023). The number of deliveries of fentanyl will be recorded for both mice groups for each concentration of capsaicin.

Potential Pitfalls and Alternative Approaches

The BNST, part of the extended amygdala, has been studied extensively for its role in the negative emotional state of withdrawal during opioid addiction (Avery et al., 2016; Awasthi et al., 2020; Ch'ng et al., 2018; Lebow & Chen, 2016; Goode & Maren, 2017; and Zheng et al., 2024). We have chosen the brain region and its CRF neurons as target for ATAC inhibition due to recent findings on corticosteroid sensitization in the extended amygdala driving opioid addiction and transcriptional evidence of activation of glucocorticoid receptor

signaling in humans with a history of opioid dependence (Roberto, Spierling, Kirson, & Zorrilla, 2017; Carmack et al., 2022; and Szablowski et al., 2018). However, if we are unable remit fentanyl withdrawal with ATAC inhibition of CRFBNST neurons only, we will individually test single targeted inhibition of dorsal raphe nucleus, locus coeruleus, or targeting two or more of these brain regions combined, as these regions are showing c-Fos correlation to hyperalgesia and somatic signs of opioid withdrawal (Alvarez-Bagnarol, Marchette, Francis, and Morales, & Vendruscolo, 2022). It is worth noting that due to its non-invasive nature, ATAC is capable of multi-region targeting in animals suitable for long-term studies without tissue damage, superior to other invasive neuromodulation methods.

4.3.4 Conclusion and Future Efforts

Successful completion of this study will validate our strategy for treatment of substance abuse through non-invasive neuromodulation mediated by biomolecular ultrasound for potential human clinical translation. It is also a promising approach with the potential to transform the targeted treatment of a broad range of neurological and psychiatric diseases. Support from the Jacobs Institute will enable us to engineer and validate the technology thus allowing us to compete for larger-scale funding from the NIH or other agencies. By collaborating with colleagues from NIH and clinical agencies early in the project, we are also setting this effort up for successful future translation into the clinic.

4.4 Acoustically Targeted Delivery of Genetically Encoded Gas Vesicles Enables Deep-brain Imaging of *in situ* Gene Expression

4.4.1 Introduction

Noninvasive interrogation and modulation of the brain remain a longstanding challenge in neuroscience and neurotherapeutics. Traditional molecular imaging tools, including those based on fluorescence and bioluminescence, provide high sensitivity and specificity but suffer from poor tissue penetration, especially in deep brain structures. While magnetic resonance imaging (MRI) and positron emission tomography (PET) offer improved depth, they require specialized hardware, radiotracers, or contrast agents, limiting their scalability, spatial resolution, or temporal precision. There remains a critical need for tools that enable molecular-level imaging and control within the brain, with high resolution, deep tissue access, and minimal invasiveness.

Ultrasound has emerged as a powerful modality for both imaging and therapeutic applications in the brain due to its ability to penetrate deep tissue noninvasively, its compatibility with portable hardware, and its capacity for spatially focused energy deposition. Recent advances in focused ultrasound (FUS) have enabled temporary and localized opening of the blood-brain barrier (BBB), allowing for the targeted delivery of nanoparticles, small molecules, and gene therapy vectors. This development opens the possibility of combining ultrasound-based targeting with molecular tools for sensing and reporting biological processes in the brain.

Gas vesicles (GVs), genetically encoded protein nanostructures derived from buoyant microorganisms, have recently been introduced as acoustic reporter genes (ARGs) that produce ultrasound contrast when heterologously expressed in mammalian cells. Unlike microbubbles or exogenous contrast agents, ARGs offer the advantage of persistent, cell-specific contrast through endogenous expression, enabling long-term and cell-resolved imaging of biological processes. However, safe and effective delivery of ARGs into the

brain, particularly in a spatially resolved and noninvasive manner, remains a critical bottleneck for their *in vivo* application.

Here, we report an integrated platform for acoustically targeted gene delivery and expression of gas vesicle-based acoustic reporter genes in the brain. By combining focused ultrasound-mediated BBB opening with systemic administration of adeno-associated virus (AAV) vectors encoding GVs, we achieve spatially defined expression of acoustic reporter genes within selected brain regions of living mice. We validate this approach through ultrasound imaging of GV expression, confirming the production of robust and localized acoustic contrast corresponding to sites of ultrasound targeting.

This work represents the first demonstration of fully non-invasive, spatially resolved genetic labeling of the brain, and pertaining cells' gene expressions for ultrasound imaging. By integrating the strengths of acoustically targeted delivery with genetically encoded ultrasound reporters, our approach establishes a new paradigm for molecular-scale imaging of the neural activities and genetic expressions with deep tissue access. Beyond imaging, the same strategy could be extended to deliver and monitor therapeutic genes or to control cellular activity in a site-specific manner. Thus, acoustically targeted expression of acoustic reporter genes opens new opportunities for neuroscience research, brain–machine interfaces, and the development of non-invasive theranostic strategies.

4.4.2 Significance

Achieving noninvasive, spatially precise, and cell-type-specific gene delivery to the brain has long been a central challenge in both basic neuroscience and clinical neurotherapeutics. The brain's anatomical complexity, dense cellular heterogeneity, and protective barriers—particularly the blood–brain barrier (BBB)—have collectively limited the safe and effective deployment of gene-based tools for imaging, modulation, or therapy. Conventional methods rely on direct intracranial injection, which, despite offering precision, introduce risks of tissue damage, inflammation, and poor scalability to multiple or deep brain targets. The

development of acoustically targeted gene delivery, as demonstrated in this study, offers a transformative solution to these limitations by enabling spatially confined, noninvasive expression of genetically encoded acoustic reporter genes within the living brain.

By leveraging focused ultrasound (FUS) to transiently and reversibly open the BBB, combined with systemic administration of adeno-associated viral (AAV) vectors encoding gas vesicle (GV)-based acoustic reporter genes (ARGs), this platform enables region-specific transduction and expression without surgical intervention. The use of gas vesicles as reporter genes provides an additional layer of innovation, as GVs produce ultrasound contrast intrinsically through their nanostructure, eliminating the need for exogenous contrast agents. This introduces a new paradigm in molecular neuroimaging: one in which endogenous, persistent, and noninvasively imageable signals can be used to monitor gene expression, cellular identity, or biochemical activity over time and in real physiological contexts.

Clinically, this approach has significant implications for the diagnosis, monitoring, and treatment of neurological disorders. For instance, targeted gene delivery via FUS could enable localized expression of neuroprotective, anti-inflammatory, or gene-silencing payloads in diseases such as Alzheimer's disease, Parkinson's disease, glioblastoma, or focal epilepsy. Importantly, the GV-based ARGs introduced here allow for real-time imaging of gene delivery efficacy and duration, offering an integrated readout for optimizing therapeutic strategies on a per-patient basis. Moreover, because ultrasound is widely available, portable, and non-ionizing, the approach is highly compatible with longitudinal studies and scalable across diverse patient populations—including pediatric, geriatric, and critically ill groups who may not tolerate invasive neurosurgical procedures.

Beyond therapeutic applications, this technology introduces compelling new capabilities for the field of brain–machine interfaces (BMIs). Traditional BMI systems rely on electrical signals recorded via implanted electrodes or hemodynamic signals obtained through optical or magnetic methods. These approaches are often limited in spatial specificity, long-term stability, or noninvasiveness. The use of acoustic reporter genes offers a molecularly precise interface with neural circuits, enabling ultrasound-based imaging of genetically defined

populations, neural states, or activity-regulated promoters. Such capabilities could facilitate the development of closed-loop BMI systems in which neural activity is both monitored and modulated using the same physical modality—ultrasound—creating a seamless bridge between synthetic biology and device-based neuromodulation.

More broadly, the ability to spatially program gene expression through noninvasive external inputs represents a major step toward precision neuroengineering. It paves the way for developing fully noninvasive neural probes, synthetic neurofeedback systems, or programmable gene therapies that can be selectively activated in vivo. As genetic toolkits for neural sensing, editing, and modulation continue to expand, platforms such as the one presented here will become critical enablers of next-generation neuroscience and neurotechnology.

4.4.3 Results

Acoustically targeted gene delivery enables localized expression of gas vesicles in the mouse hippocampus

To establish a non-invasive strategy for expressing acoustic reporter genes in the brain, we employed magnetic resonance (MR) image-guided focused ultrasound (FUS) to transiently and reversibly open the blood–brain barrier (BBB) in the hippocampus of adult mice (**Fig. 4-11a, b**). Following FUS-BBBO, intravenous injection of a three-vector adeno-associated virus (AAV) system encoding the complete set of gas vesicle (GV) genes was performed. This multi-vector system was required due to the size of the GV gene cluster, which exceeds the packaging capacity of a single AAV (Shivaei et al., 2025). Two of the vectors also carried fluorescent reporters—green fluorescent protein (GFP) or red fluorescent protein (RFP)—allowing for independent verification of successful transduction and expression (**Fig. 4-10**).

The procedure was well tolerated. Animals recovered without observable behavioral or physiological abnormalities, and no gross tissue damage was noted on histological inspection at the site of BBB opening. At 4 weeks post-delivery, robust GV expression was detected in

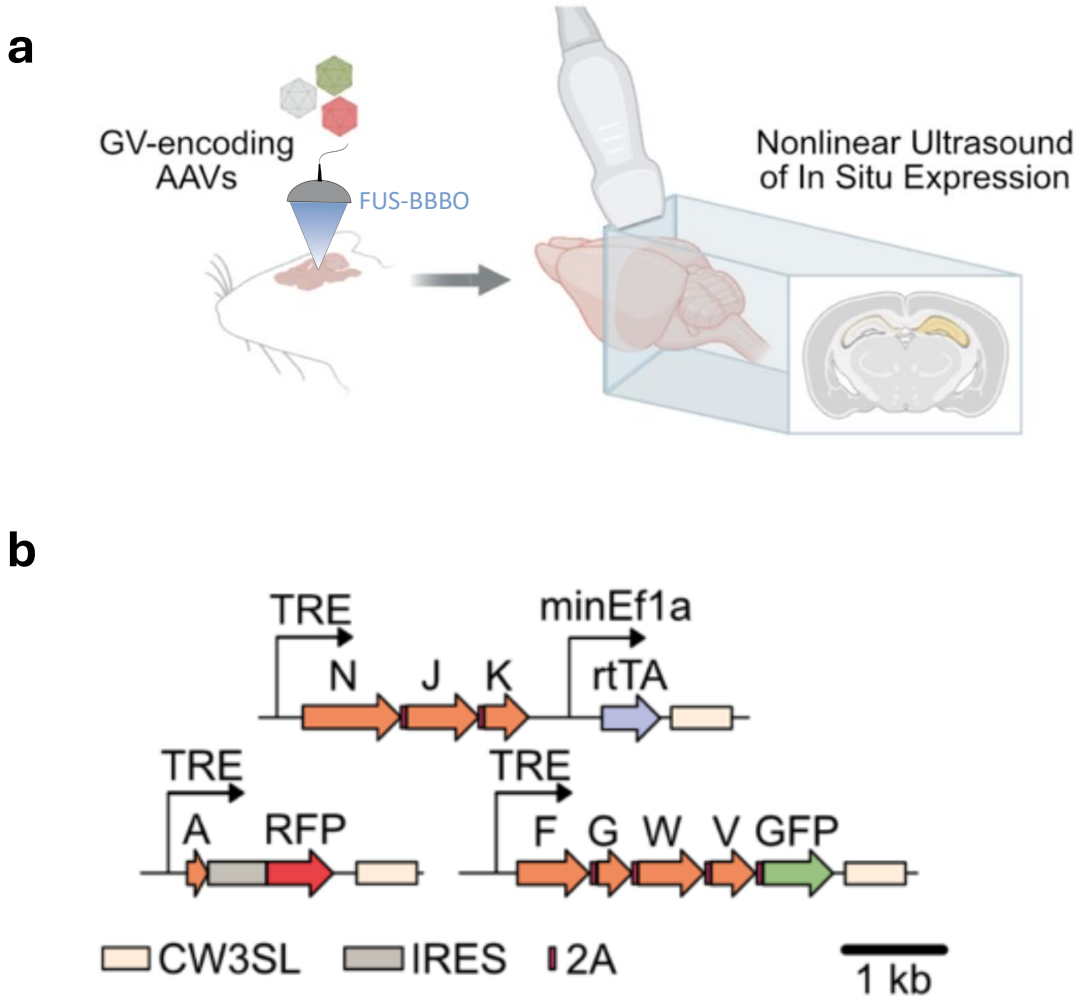

Figure 4-10 Acoustically targeted gene delivery mediated AAV delivery of GV genes into tissues enables ultrasound imaging of endogenous cellular function. (**a**) Schematic showing MRI-guided targeting of FUS-BBBO to locally deliver 3-vector AAV system encoding the GV genes into the brain, followed by nonlinear ultrasound imaging of *in situ* gene expression and downstream capabilities, including tracking activity-dependent gene expression. (**b**) The 3-vector AAV system, with the structural gene *gvpA* encoded on a separate plasmid to enable stoichiometric tuning of its expression relative to assembly factors. ***(Illustrations are adapted from Shivaei et al., 2025)***

the hippocampal region targeted by FUS, while no detectable expression was observed in contralateral or non-targeted brain regions. These results confirm that FUS enables precise, spatially confined delivery of multi-vector AAV systems across the BBB and establishes the hippocampus as a tractable site for acoustically targeted genetic labeling.

Ultrasound BURST imaging detects localized gas vesicle expression in the brain

We next sought to determine whether heterologous GV expression produced sufficient acoustic contrast for *in vivo* ultrasound imaging. To maximize sensitivity and avoid attenuation by the skull, BURST (Burst Ultrasound Repeated Short-Time) imaging was performed through a craniotomy over the hippocampal region 4 weeks after AAV administration.

BURST imaging revealed strong, localized acoustic contrast in the hippocampus of animals that had undergone acoustically targeted delivery of the 3-vector GV system (**Fig. 4-11c**). The signal was spatially coincident with the site of FUS targeting, confirming that GV expression was restricted to the BBB-opened region. Quantitative analysis demonstrated that BURST signal intensity in targeted hippocampi was significantly elevated compared to contralateral control regions. Control animals that underwent FUS without AAV administration, or AAV injection without FUS, showed no detectable ultrasound contrast, confirming that acoustic signals arose specifically from GV expression.

These results demonstrate that acoustically targeted delivery of a 3-vector GV system enables detectable and spatially confined ultrasound contrast in the mammalian brain. Although BURST imaging in this study required craniotomy, the robust acoustic signature establishes a proof of concept for molecular imaging of GV expression *in vivo*.

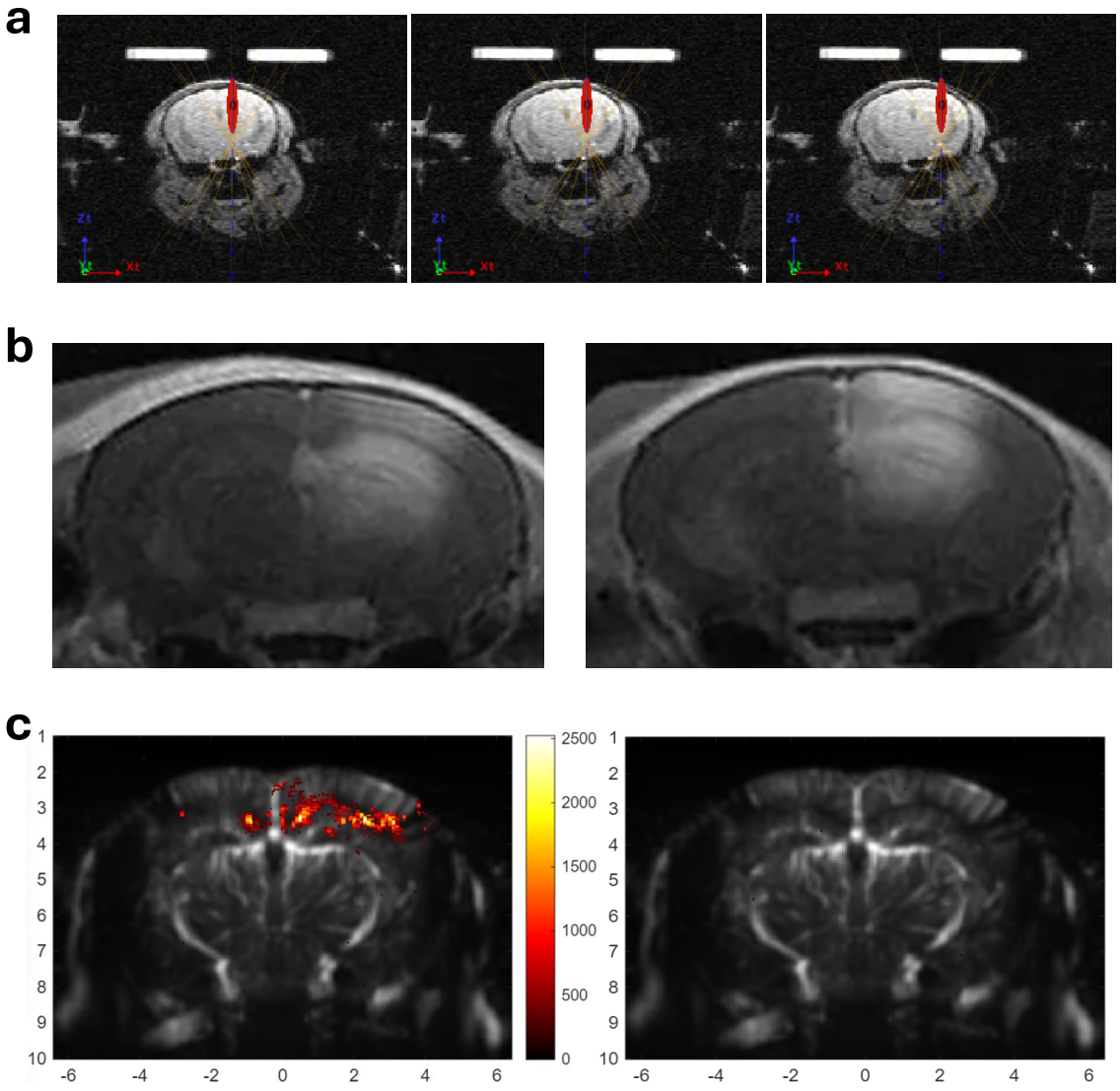

Figure 4-11 Acoustically targeted gene delivery mediated AAV delivery and longitudinal imaging of GV-expression in the mouse brain. (**a**) MRI-guided targeting of FUS in the mouse brain to disrupt blood-brain barrier, where three individual sessions of FUS adjacent in the same coronal plane were used to deliver systemically introduced AAVs encoding for GVs to unilateral hippocampus (**b**) Safe and noninvasive opening of the BBB with FUS in hippocampus which was used to deliver 3 AAV viral vectors carrying DNA encoding for GV. The BBB opening is visualized by extravasation of gadolinium contrast agent in a T1-weighted MRI. (**c**) Representative BURST images (colormap) overlaid on Doppler images (grayscale) of mouse brain administered with GV-encoding AAVs, pre- (left) or post- BURST imaging, which collapses GVs

Fluorescent histology validates gas vesicle expression and confirms targeting specificity

To verify GV expression with an orthogonal modality, we performed histological analysis of hippocampal tissue sections. Confocal fluorescence microscopy revealed strong expression of GFP and RFP in the hippocampus of animals that received the corresponding reporter-containing vectors, whereas contralateral tissue showed no detectable fluorescence. The distribution of fluorescent reporter expression matched the FUS focal zone, demonstrating spatial confinement of viral transduction.

Analysis revealed high transduction efficiencies of hippocampal neurons within the targeted zone. Regions with stronger fluorescence corresponded to sites of greatest BURST contrast, indicating that acoustic and optical readouts reported on the same underlying GV expression. Colocalization analysis confirmed that fluorescence was restricted to cells in the targeted hippocampus, and no widespread diffusion outside of the FUS-targeted zone was observed.

Integration of acoustic and fluorescent readouts establishes a multimodal validation framework

By combining BURST imaging and histological analysis, we established a robust validation framework for acoustically targeted GV expression in the brain. Ultrasound provided a noninvasive, real-time readout of GV expression following craniotomy, while fluorescence microscopy confirmed cellular-level expression with high spatial fidelity. The strong spatial correlation between the two modalities validates GV expression as the source of ultrasound contrast.

Taken together, these results provide compelling evidence that acoustically targeted delivery of genetically encoded GVs enables precise and spatially confined expression of acoustic reporter genes in the mouse brain. The demonstration of robust acoustic contrast, coupled with histological confirmation of targeted transduction, establishes this approach as a viable platform for molecular imaging and opens the door to future development of fully non-

invasive acoustic reporter strategies for monitoring brain-wide neural dynamics and genetic expressions in the mammalian brain.

The implications of this work extend beyond proof-of-concept imaging. By establishing that GV-based acoustic reporter genes can be targeted to and functionally expressed in specific brain regions, we set the stage for the development of ultrasound as a truly molecular-scale neuroimaging modality. In the future, this approach could allow us to monitor cellular and molecular processes in deep brain regions longitudinally, without reliance on optical windows or radioactive tracers. Moreover, the modularity of the GV system suggests that it could be engineered for enhanced sensitivity, multiplexed imaging, or coupling to molecular sensors, thereby expanding the repertoire of ultrasound-based functional readouts.

4.5 Discussion and Future Perspectives

Our findings establish acoustically targeted gene delivery as a versatile, non-invasive platform for the spatially precise modulation of neural circuits across a range of therapeutic and diagnostic contexts to interfacing brain. By integrating focused ultrasound with systemically administered vectors, we achieved blood–brain barrier opening and robust gene expression in targeted regions of the adult mammalian brain. We demonstrate the utility of this approach in three distinct applications: (1) chemogenetic rescue of epileptogenic circuits, (2) chemogenetic inhibition of stress neural circuits implicated in opioid addiction, and (3) delivery of gas vesicle–based acoustic reporter genes for real-time molecular neuroimaging. Collectively, these results underscore the potential of acoustically targeted gene delivery to enable circuit-specific, tunable, and repeatable interventions for neurological disease and brain function monitoring.

Importantly, acoustically targeted gene delivery overcomes several limitations of existing gene delivery methods. Compared to intracranial injections, our approach is minimally invasive and scalable across multiple brain regions or bilateral structures. In contrast to systemic gene therapies that lack spatial specificity, acoustically targeted gene delivery restricts transgene expression to sonicated areas, thereby reducing off-target effects. Moreover, our use of chemogenetic actuators offers temporal control over neural modulation, while gas vesicle reporters allow for longitudinal and non-invasive readouts of gene expression dynamics using ultrasound imaging. These complementary features position acoustically targeted gene delivery as a promising toolkit for both therapeutic intervention and functional brain mapping; both as a means of writing-in to modulate and neural activities and a facilitator of reading-out of brain-wide dynamics.

Despite these advances, several challenges must be addressed to accelerate clinical translation. First, while adeno-associated virus (AAV) vectors remain the most widely used vehicles for CNS gene delivery, their immunogenicity, payload size constraints, and limited cell-type specificity warrant the development of improved viral and nonviral platforms. Second, precise control over acoustic parameters is essential to ensure consistent and safe

blood-brain barrier opening without tissue damage. Future work should incorporate real-time acoustic feedback and adaptive focusing to enhance delivery fidelity. Third, although our current results demonstrate efficacy in rodent models, further validation in non-human primates will be critical to assess translatability across species with thicker skulls and more complex neuroanatomy.

Beyond its therapeutic potential, acoustically targeted gene delivery opens new frontiers in non-invasive neuroengineering by enabling the remote and precise installation of synthetic genetic programs into the brain. This capability allows researchers to modulate neural activity, monitor molecular states, or even rewire circuit function without the need for implanted hardware or surgical intervention. For instance, acoustically targeted gene delivery can be harnessed to deliver opto-, chemo-, or magnetogenetic tools that respond to exogenous stimuli, enabling on-demand control of specific neural ensembles with high spatiotemporal resolution. Moreover, coupling acoustically targeted gene delivery with activity-dependent promoters or engineered feedback loops could facilitate the creation of self-regulating neural interfaces that dynamically adapt to endogenous brain states. As synthetic biology continues to generate sophisticated genetic payloads—ranging from logic-gated effectors to programmable RNA devices— acoustically targeted gene delivery stands to become a critical delivery mechanism for deploying these tools *in vivo*. The ability to iteratively and non-invasively program brain function across time and space represents a paradigm shift in how we interface with the nervous system, offering a powerful alternative to electrode-based systems in both research and clinical settings.

Looking ahead, the integration of acoustically targeted gene delivery with brain–machine interface (BMI) systems offer a compelling direction for next-generation neurotechnologies. One envisioned application is the use of acoustically targeted gene delivery to deliver activity-dependent genetic programs—such as calcium- or voltage-sensitive acoustic reporting sensors and/or modulatory receptors—in closed-loop systems where neural decoding algorithms trigger gene expression in response to specific brain states. Such platforms could enable adaptive neuromodulation for conditions like epilepsy, depression,

or chronic pain. Moreover, combining acoustic reporter genes with neural signal acquisition may offer a dual-modality interface, linking molecular events to electrophysiological or hemodynamic signatures. This convergence of molecular targeting and neural interfacing could transform our ability to read from and write to the brain with unprecedented specificity and reversibility.

Finally, the ethical dimensions of acoustically targeted gene delivery-enhanced BMIs must be carefully considered. As these technologies approach levels of intervention that may influence cognition, emotion, or volition, frameworks for consent, privacy, and long-term monitoring must evolve in parallel. Future studies should incorporate neuroethical design principles alongside technical development to ensure responsible deployment of acoustically targeted gene delivery-enabled brain interfaces.

In summary, acoustically targeted gene delivery offers a powerful and flexible approach for region-specific, noninvasive gene delivery to the brain, with immediate relevance to therapeutic neuromodulation, molecular imaging, and functional brain interfacing. Continued interdisciplinary work across ultrasound physics, gene therapy, systems neuroscience, and neural engineering will be essential to fully realize its potential.

BIBLIOGRAPHY

Li, H. R., Harb, M., Heath, J. E., Trippett, J. S., Shapiro, M. G., & Szablowski, J. O. (2024). Engineering viral vectors for acoustically targeted gene delivery. *Nature Communications*, 15(1). https://doi.org/10.1038/s41467-024-48974-y

Rabut, C., Yoo, S., Hurt, R. C., Jin, Z., Li, H. R., Guo, H., Ling, B., & Shapiro, M. G. (2020). Ultrasound technologies for imaging and modulating neural activity. *Neuron*, 108(1), 93–110. https://doi.org/10.1016/j.neuron.2020.09.003

Rabut, C., Daghlian, G. H., Barturen-Larrea, P., Li, H. R., Bruegge, R. V., Jones, R. M., Malounda, D., Pinton, G. F., & Shapiro, M. G. (2024). Acoustic Tumor Paint for Real-Time Imaging, Surgical Guidance and Recurrence Monitoring of Brain Tumors with Ultrasound. *bioRxiv*. https://doi.org/10.1101/2024.12.22.629782

Vassallo, R., Ling, B., Criado-Hidalgo, E., Robinson, N., Schrunk, E., Liu, A., Daghlian, G., Li, H. R., Swift, M. B., Mannar, D., Malounda, D., Goldenberg, S. L., Salcudean, S. E., Shapiro, M. G., Black, P. C., & Cox, M. E. (2025). A modular method for rapidly prototyping targeted gas vesicle protein nanoparticles (p. 2025.08.06.668980). *bioRxiv*. https://doi.org/10.1101/2025.08.06.668980

Pisanello, F., Mandelbaum, G., Pisanello, M., Oldenburg, I., Sileo, L., Markowitz, J., … & Sabatini, B. (2017). Dynamic illumination of spatially restricted or large brain volumes via a single tapered optical fiber. *Nature Neuroscience*, 20(8), 1180-1188. https://doi.org/10.1038/nn.4591

Lin, J., Knutsen, P., Muller, A., Kleinfeld, D., & Tsien, R. (2013). Reachr: a red-shifted variant of channelrhodopsin enables deep transcranial optogenetic excitation. *Nature Neuroscience*, 16(10), 1499-1508. https://doi.org/10.1038/nn.3502

Eriksson, D., Schneider, A., Thirumalai, A., Alyahyay, M., Crompe, B., Sharma, K., … & Diester, I. (2022). Multichannel optogenetics combined with laminar recordings for ultra-controlled neuronal interrogation. *Nature Communications*, 13(1). https://doi.org/10.1038/s41467-022-28629-6

Stujenske, J., Spellman, T., & Gordon, J. (2015). Modeling the spatiotemporal dynamics of light and heat propagation for in vivo optogenetics. *Cell Reports*, 12(3), 525-534. https://doi.org/10.1016/j.celrep.2015.06.036

Zaaimi, B., Turnbull, M., Hazra, A., Wang, Y., Gándara, C., McLeod, F., … & Jackson, A. (2022). Closed-loop optogenetic control of the dynamics of neural activity in non-human primates. *Nature Biomedical Engineering*, 7(4), 559-575. https://doi.org/10.1038/s41551-022-00945-8

Armbruster, B. N., Holmes, A., & Roth, B. L. (2007). Evolving the lock to fit the key: The development of DREADD technology. *Nature Methods*, 4(12), 931-933. https://doi.org/10.1038/nmeth1113

Weston, M., Kaserer, T., Wu, A., Mouravlev, A., Carpenter, J., Snowball, A., … & Lieb, A. (2019). Olanzapine: a potent agonist at the hm4d(gi) dreadd amenable to clinical translation of chemogenetics. *Science Advances*, 5(4). https://doi.org/10.1126/sciadv.aaw1567

Auffenberg, E., Jurik, A., Mattusch, C., Stoffel, R., Genewsky, A., Namendorf, C., … & Thoeringer, C. (2016). Remote and reversible inhibition of neurons and circuits by small molecule induced potassium channel stabilization. *Scientific Reports*, 6(1). https://doi.org/10.1038/srep19293

Podewin, T., Ast, J., Broichhagen, J., Fine, N., Nasteska, D., Leippe, P., … & Hodson, D. (2018). Conditional and reversible activation of class a and b g protein-coupled receptors using tethered pharmacology. *Acs Central Science*, 4(2), 166-179. https://doi.org/10.1021/acscentsci.7b00237

Vardy, E., Robinson, J., Li, C., Olsen, R., DiBerto, J., Giguère, P., … & Roth, B. (2015). A new dreadd facilitates the multiplexed chemogenetic interrogation of behavior. *Neuron*, 86(4), 936-946. https://doi.org/10.1016/j.neuron.2015.03.065

Upright, N. and Baxter, M. (2020). Effect of chemogenetic actuator drugs on prefrontal cortex-dependent working memory in nonhuman primates. *Neuropsychopharmacology*, 45(11), 1793-1798. https://doi.org/10.1038/s41386-020-0660-9

Magnus, C., Lee, P., Bonaventura, J., Zemla, R., Gomez, J., Ramirez, M., … & Sternson, S. (2019). Ultrapotent chemogenetics for research and potential clinical applications. *Science*, 364(6436). https://doi.org/10.1126/science.aav5282

Yoo, S., Mittelstein, D., Hurt, R., Lacroix, J., & Shapiro, M. (2022). Focused ultrasound excites cortical neurons via mechanosensitive calcium accumulation and ion channel amplification. *Nature Communications*, 13(1). https://doi.org/10.1038/s41467-022-28040-1

Song, M., Zhang, M., He, S., Li, L., & Hu, H. (2023). Ultrasonic neuromodulation mediated by mechanosensitive ion channels: current and future. *Frontiers in Neuroscience*, 17. https://doi.org/10.3389/fnins.2023.1232308

Lee, W., Croce, P., Margolin, R., Cammalleri, A., Yoon, K., & Yoo, S. (2018). Transcranial focused ultrasound stimulation of motor cortical areas in freely-moving awake rats. *BMC Neuroscience*, 19(1). https://doi.org/10.1186/s12868-018-0459-3

Kamimura, H., Wang, S., Chen, H., Wang, Q., Aurup, C., Acosta, C., … & Konofagou, E. (2016). Focused ultrasound neuromodulation of cortical and subcortical brain structures using 1.9 mhz. *Medical Physics*, 43(10), 5730-5735. https://doi.org/10.1118/1.4963208

Sato, T., Shapiro, M. G., & Tsao, D. Y. (2018). Ultrasonic neuromodulation causes widespread cortical activation via an indirect auditory mechanism. *Neuron*, 98(5), 1031-1041.e5. https://doi.org/10.1016/j.neuron.2018.05.009

Todd, N., Zhang, Y., Power, C., Becerra, L., Borsook, D., Livingstone, M., … & McDannold, N. (2019). Modulation of brain function by targeted delivery of gaba through the disrupted blood-brain barrier. *Neuroimage*, 189, 267-275. https://doi.org/10.1016/j.neuroimage.2019.01.037

Airan, R., Meyer, R., Ellens, N., Rhodes, K., Farahani, K., Pomper, M., … & Green, J. (2017). Noninvasive targeted transcranial neuromodulation via focused ultrasound gated drug release from nanoemulsions. *Nano Letters*, 17(2), 652-659. https://doi.org/10.1021/acs.nanolett.6b03517

Yang, Y., Pacia, C. P., Ye, D., Zhu, L., Baek, H., Yue, Y., Yuan, J., Miller, M. J., Cui, J., Culver, J. P., Bruchas, M. R., & Chen, H. (2021). Sonothermogenetics for noninvasive and cell-type specific deep brain neuromodulation. *Brain Stimulation*, 14(4), 790–800. https://doi.org/10.1016/j.brs.2021.04.021

Hernández‐Morales, M., Morales-Weil, K., Han, S., Han, V., Tran, T., Benner, E., ⋯ & Liu, C. (2024). Electrophysiological mechanisms and validation of ferritin-based magnetogenetics for remote control of neurons. *Journal of Neuroscience*, 44(30), e1717232024. https://doi.org/10.1523/jneurosci.1717-23.2024

Unda, S. R., Pomeranz, L. E., Marongiu, R., Yu, X., Kelly, L., Hassanzadeh, G., Molina, H., Vaisey, G., Wang, P., Dyke, J. P., Fung, E. K., Grosenick, L., Zirkel, R., Antoniazzi, A. M., Norman, S., Liston, C. M., Schaffer, C., Nishimura, N., Stanley, S. A., . . . Kaplitt, M. G. (2024). Bidirectional regulation of motor circuits using magnetogenetic gene therapy. *Science Advances*, 10(41). https://doi.org/10.1126/sciadv.adp9150

Duret, G., Polali, S., Anderson, E., Bell, A., Tzouanas, C., Avants, B., … & Robinson, J. (2019). Magnetic entropy as a proposed gating mechanism for magnetogenetic ion channels. *Biophysical Journal*, 116(3), 454-468. https://doi.org/10.1016/j.bpj.2019.01.003

Munshi, R., Qadri, S., & Pralle, A. (2018). Magnetothermal deep brain neuromodulation in awake, freely moving mice. *Biophysical Journal*, 114(3), 670a. https://doi.org/10.1016/j.bpj.2017.11.3614

Marblestone, A. H., Zamft, B. M., Maguire, Y. G., Shapiro, M. G., Cybulski, T. R., Glaser, J. I., Amodei, D., Stranges, P. B., Kalhor, R., Dalrymple, D. A., Seo, D., Alon, E., Maharbiz, M. M., Carmena, J. M., Rabaey, J. M., Boyden, E. S., Church, G. M., & Kording, K. P. (2013). Physical principles for scalable neural recording. *Frontiers in Computational Neuroscience*, 7. https://doi.org/10.3389/fncom.2013.00137

Piraner, D. I., Farhadi, A., Davis, H. C., Wu, D., Maresca, D., Szablowski, J. O., & Shapiro, M. G. (2017). Going deeper: biomolecular tools for acoustic and magnetic imaging and control of cellular function. *Biochemistry*, 56(39), 5202–5209. https://doi.org/10.1021/acs.biochem.7b00443

Ntziachristos, V. Going deeper than microscopy: the optical imaging frontier in biology. *Nat Methods* 7, 603–614 (2010). https://doi.org/10.1038/nmeth.1483

Maresca, D., Lakshmanan, A., Abedi, M., Bar-Zion, A., Farhadi, A., Lu, G. J., Szablowski, J. O., Wu, D., Yoo, S., & Shapiro, M. G. (2018). Biomolecular ultrasound and sonogenetics. *Annual Review of Chemical and Biomolecular Engineering*, 9(1), 229–252. https://doi.org/10.1146/annurev-chembioeng-060817-084034

Escoffre, J. M., & Bouakaz, A. (Eds.). (2016). *Therapeutic ultrasound* (Vol. 880, p. 465). Cham, Switzerland: Springer International Publishing.

Dromi, S., Frenkel, V., Luk, A., Traughber, B., Angstadt, M., Bur, M., Poff, J., Xie, J., Libutti, S. K., Li, K. C., & Wood, B. J. (2007). Pulsed-High intensity focused ultrasound and Low Temperature–Sensitive liposomes for enhanced targeted drug delivery and antitumor effect. *Clinical Cancer Research*, 13(9), 2722–2727. https://doi.org/10.1158/1078-0432.ccr-06-2443

Rapoport, N. Y.; Kennedy, A. M.; Shea, J. E.; Scaife, C. L.; Nam, K.-H. Controlled and targeted tumor chemotherapy by ultrasoundactivated nanoemulsions/microbubbles. *J. Controlled Release* 2009, 138, 268−276. https://doi.org/10.1016/j.progpolymsci.2007.05.009

Nelson, J. L., Roeder, B. L., Carmen, J. C., Roloff, F., & Pitt, W. G. (2002). Ultrasonically activated chemotherapeutic drug delivery in a rat model. PubMed, 62(24), 7280–7283. https://pubmed.ncbi.nlm.nih.gov/12499270

Schoellhammer, C. M., Schroeder, A., Maa, R., Lauwers, G. Y., Swiston, A., Zervas, M., Barman, R., DiCiccio, A. M., Brugge, W. R., Anderson, D. G., Blankschtein, D., Langer, R., & Traverso, G. (2015). Ultrasound-mediated gastrointestinal drug delivery. *Science Translational Medicine*, 7(310). https://doi.org/10.1126/scitranslmed.aaa5937

Zderic, V., Vaezy, S., Martin, R. W., & Clark, J. I. (2002). Ocular drug delivery using 20-kHz ultrasound. *Ultrasound in Medicine & Biology*, 28(6), 823–829. https://doi.org/10.1016/s0301-5629(02)00515-x

Dayton, P., Klibanov, A., Brandenburger, G., & Ferrara, K. (1999). Acoustic radiation force in vivo: a mechanism to assist targeting of microbubbles. *Ultrasound in Medicine & Biology*, 25(8), 1195–1201. https://doi.org/10.1016/s0301-5629(99)00062-9

Hynynen, K., McDannold, N., Vykhodtseva, N., & Jolesz, F. A. (2001). *Noninvasive MR imaging–guided focal opening of the Blood-Brain barrier in rabbits.* Radiology, 220(3), 640–646. https://doi.org/10.1148/radiol.2202001804

Escoffre, J.-M.; Bouakaz, A. Therapeutic ultrasound; *Springer*, 2015; Vol. 880.

Mullick Chowdhury, S.; Lee, T.; Willmann, J. K. Ultrasoundguided drug delivery in cancer. *Ultrasonography* 2017, 36, 171−184.

Lochhead, J. J., & Thorne, R. G. (2011). Intranasal delivery of biologics to the central nervous system. *Advanced Drug Delivery Reviews*, 64(7), 614–628. https://doi.org/10.1016/j.addr.2011.11.002

Patel, T., Zhou, J., Piepmeier, J. M., & Saltzman, W. M. (2011). Polymeric nanoparticles for drug delivery to the central nervous system. *Advanced Drug Delivery Reviews*, 64(7), 701–705. https://doi.org/10.1016/j.addr.2011.12.006

Curtis, C., Zhang, M., Liao, R., Wood, T., & Nance, E. (2016). Systems‐level thinking for nanoparticle‐mediated therapeutic delivery to neurological diseases. *Wiley Interdisciplinary Reviews Nanomedicine and Nanobiotechnology*, 9(2). https://doi.org/10.1002/wnan.1422

Moyaert, P., Padrela, B. E., Morgan, C. A., Petr, J., Versijpt, J., Barkhof, F., Jurkiewicz, M. T., Shao, X., Oyeniran, O., Manson, T., Wang, D. J. J., Günther, M., Achten, E., Mutsaerts, H. J. M. M., & Anazodo, U. C. (2023). Imaging blood-brain barrier dysfunction: A state-of-the-art review from a clinical perspective. *Frontiers in Aging Neuroscience*, 15. https://doi.org/10.3389/fnagi.2023.1132077

Alonso, A., Reinz, E., Leuchs, B., Kleinschmidt, J., Fatar, M., Geers, B., Lentacker, I., Hennerici, M. G., De Smedt, S. C., & Meairs, S. (2013). Focal delivery of AAV2/1-transgenes into the rat brain by localized ultrasound-induced BBB opening. Molecular Therapy — Nucleic Acids, 2, e73. https://doi.org/10.1038/mtna.2012.64

Szablowski, J. O., Lee-Gosselin, A., Lue, B., Malounda, D., & Shapiro, M. G. (2018). Acoustically targeted chemogenetics for the non-invasive control of neural circuits. Nature Biomedical Engineering, 2(7), 475–484. https://doi.org/10.1038/s41551-018-0258-2

Thévenot, E., Jordão, J. F., O'Reilly, M. A., Markham, K., Weng, Y., Foust, K. D., Kaspar, B. K., Hynynen, K., & Aubert, I. (2012). Targeted delivery of Self-Complementary Adeno-Associated virus serotype 9 to the brain, using magnetic resonance Imaging-Guided focused ultrasound. Human Gene Therapy, 23(11), 1144–1155. https://doi.org/10.1089/hum.2012.013

Wang, S., Olumolade, O. O., Sun, T., Samiotaki, G., & Konofagou, E. E. (2014). Noninvasive, neuron-specific gene therapy can be facilitated by focused ultrasound and recombinant adeno-associated virus. Gene Therapy, 22(1), 104–110. https://doi.org/10.1038/gt.2014.91

Rezai, A. R., Ranjan, M., D'Haese, P., Haut, M. W., Carpenter, J., Najib, U., Mehta, R. I., Chazen, J. L., Zibly, Z., Yates, J. R., Hodder, S. L., & Kaplitt, M. (2020). Noninvasive hippocampal blood−brain barrier opening in Alzheimer's disease with focused ultrasound. *Proceedings of the National Academy of Sciences*, 117(17), 9180–9182. https://doi.org/10.1073/pnas.2002571117

Lipsman, N., Meng, Y., Bethune, A. J., Huang, Y., Lam, B., Masellis, M., Herrmann, N., Heyn, C., Aubert, I., Boutet, A., Smith, G. S., Hynynen, K., & Black, S. E. (2018). Blood–brain barrier opening in Alzheimer's disease using MR-guided focused ultrasound. *Nature Communicati*ons, 9(1). https://doi.org/10.1038/s41467-018-04529-6

Upright, N. A., & Baxter, M. G. (2020). Effect of chemogenetic actuator drugs on prefrontal cortex-dependent working memory in nonhuman primates. *Neuropsychopharmacology*, 45(11), 1793–1798. https://doi.org/10.1038/s41386-020-0660-9

Eldridge, M. a. G., Lerchner, W., Saunders, R. C., Kaneko, H., Krausz, K. W., Gonzalez, F. J., Ji, B., Higuchi, M., Minamimoto, T., & Richmond, B. J. (2015). Chemogenetic disconnection of monkey orbitofrontal and rhinal cortex reversibly disrupts reward value. *Nature Neuroscience*, 19(1), 37–39. https://doi.org/10.1038/nn.4192

Chan, K. Y., Jang, M. J., Yoo, B. B., Greenbaum, A., Ravi, N., Wu, W., Sánchez-Guardado, L., Lois, C., Mazmanian, S. K., Deverman, B. E., & Gradinaru, V. (2017). Engineered AAVs for efficient noninvasive gene delivery to the central and peripheral nervous systems. *Nature Neuroscience*, 20(8), 1172–1179. https://doi.org/10.1038/nn.4593

Carpentier, A., Canney, M., Vignot, A., Reina, V., Beccaria, K., Horodyckid, C., Karachi, C., Leclercq, D., Lafon, C., Chapelon, J., Capelle, L., Cornu, P., Sanson, M., Hoang-Xuan, K., Delattre, J., & Idbaih, A. (2016). Clinical trial of blood-brain barrier disruption by pulsed ultrasound. *Science Translational Medicine*, 8(343). https://doi.org/10.1126/scitranslmed.aaf6086

Burgess, A., Dubey, S., Nhan, T., Aubert, I., & Hynynen, K. (2015). Therapeutic effects of focused ultrasound-mediated blood-brain barrier opening in a mouse model of Alzheimer's disease. *Journal of Therapeutic Ultrasound*, 3(S1). https://doi.org/10.1186/2050-5736-3-s1-o16

Baseri, B., Choi, J. J., Deffieux, T., Samiotaki, G., Tung, Y., Olumolade, O., Small, S. A., Morrison, B., & Konofagou, E. E. (2012). Activation of signaling pathways following localized delivery of systemically administered neurotrophic factors across the blood–brain barrier using focused ultrasound and microbubbles. *Physics in Medicine and Biology*, 57(7), N65–N81. https://doi.org/10.1088/0031-9155/57/7/n65

Sternson, S. M., & Roth, B. L. (2014). Chemogenetic tools to interrogate brain functions. *Annual Review of Neuroscience*, 37(1), 387–407. https://doi.org/10.1146/annurev-neuro-071013-014048

Dittgen, T., Nimmerjahn, A., Komai, S., Licznerski, P., Waters, J., Margrie, T. W., Helmchen, F., Denk, W., Brecht, M., & Osten, P. (2004). Lentivirus-based genetic manipulations of cortical neurons and their optical and electrophysiological monitoring in vivo. *Proceedings of the National Academy of Sciences*, 101(52), 18206–18211. https://doi.org/10.1073/pnas.0407976101

Karakatsani, M. E., Blesa, J., & Konofagou, E. E. (2019). Blood–brain barrier opening with focused ultrasound in experimental models of Parkinson's disease. *Movement Disorders*, 34(9), 1252–1261. https://doi.org/10.1002/mds.27804

High-dose AAV gene therapy deaths. (2020). *Nature Biotechnology*, 38(8), 910. https://doi.org/10.1038/s41587-020-0642-9

Sun, T., Samiotaki, G., Wang, S., Acosta, C., Chen, C. C., & Konofagou, E. E. (2015). Acoustic cavitation-based monitoring of the reversibility and permeability of ultrasound-induced blood-brain barrier opening. P*hysics in Medicine and Biology*, 60(23), 9079–9094. https://doi.org/10.1088/0031-9155/60/23/9079

Li, C., & Samulski, R. J. (2020). Engineering adeno-associated virus vectors for gene therapy. *Nature Reviews Genetics*, 21(4), 255–272. https://doi.org/10.1038/s41576-019-0205-4

Maheshri, N., Koerber, J. T., Kaspar, B. K., & Schaffer, D. V. (2006). Directed evolution of adeno-associated virus yields enhanced gene delivery vectors. *Nature Biotechnology*, 24(2), 198–204. https://doi.org/10.1038/nbt1182

Tervo, D. G. R., Hwang, B., Viswanathan, S., Gaj, T., Lavzin, M., Ritola, K. D., Lindo, S., Michael, S., Kuleshova, E., Ojala, D., Huang, C., Gerfen, C. R., Schiller, J., Dudman, J. T., Hantman, A. W., Looger, L. L., Schaffer, D. V., & Karpova, A. Y. (2016). A designer AAV variant permits efficient retrograde access to projection neurons. *Neuron*, 92(2), 372–382. https://doi.org/10.1016/j.neuron.2016.09.021

Gray, S. J., Kalburgi, S. N., McCown, T. J., & Samulski, R. J. (2013). Global CNS gene delivery and evasion of anti-AAV-neutralizing antibodies by intrathecal AAV administration in non-human primates. *Gene Therapy*, 20(4), 450–459. https://doi.org/10.1038/gt.2012.101

Russell, S. et al. (2017). Efficacy and safety of voretigene neparvovec (AAV2-hRPE65v2) in patients with RPE65-mediated inherited retinal dystrophy: a randomised, controlled, open-label, phase 3 trial. *Lancet* 390, 849–860. https://doi.org/10.1016/S0140-6736(17)31868-8

Mendell, J. R. et al. (2017). Single-dose gene-replacement therapy for spinal muscular atrophy. *N. Engl. J. Med*. 377, 1713–1722. DOI: 10.1056/NEJMoa1706198

Gaudet, D. et al. (2013). Efficacy and long-term safety of alipogene tiparvovec (AAV1-LPL S447X) gene therapy for lipoprotein lipase deficiency: an open-label trial. *Gene Ther*. 20, 361–369. https://doi.org/10.1038/gt.2012.43

Duque, S. et al. (2009). Intravenous administration of self-complementary AAV9 enables transgene delivery to adult motor neurons. *Mol. Ther*. 17, 1187–1196. https://doi.org/10.1038/mt.2009.71

Chan, K. Y. et al. (2017). Engineered AAVs for efficient noninvasive gene delivery to the central and peripheral nervous systems. *Nat. Neurosci*. 20, 1172–1179. https://doi.org/10.1038/nn.4593

Deverman, B. E. et al. (2016). Cre-dependent selection yields AAV variants for widespread gene transfer to the adult brain. *Nat. Biotechnol*. 34, 204–209. https://doi.org/10.1038/nbt.3440

Gray, S. J., Kalburgi, S. N., McCown, T. J. & Samulski, R. J. (2013). Global CNS gene delivery and evasion of anti-AAV-neutralizing antibodies by intrathecal AAV administration in non-human primates. *Gene Ther*. 20, 450–459. https://doi.org/10.1038/gt.2012.101

Alonso, A., Reinz, E., Leuchs, B., Kleinschmidt, J., Fatar, M., Geers, B., Lentacker, I., Hennerici, M. G., De Smedt, S. C., & Meairs, S. (2013). Focal delivery of AAV2/1-transgenes into the rat brain by localized ultrasound-induced BBB opening. *Molecular Therapy — Nucleic Acids*, *2*, e73. https://doi.org/10.1038/mtna.2012.64

Alves, S., Bode, J., Bemelmans, A., Von Kalle, C., Cartier, N., & Tews, B. (2016). Ultramicroscopy as a novel tool to unravel the tropism of AAV gene therapy vectors in the brain. *Scientific Reports*, *6*(1). https://doi.org/10.1038/srep28272

Baseri, B., Choi, J. J., Tung, Y., & Konofagou, E. E. (2010). Multi-Modality Safety Assessment of Blood-Brain Barrier Opening using focused ultrasound and Definity Microbubbles: A Short-Term Study. *Ultrasound in Medicine & Biology*, *36*(9), 1445–1459. https://doi.org/10.1016/j.ultrasmedbio.2010.06.005

Bhardwaj, D., Youssef, I., Imphean, D., Holmes, S. K., Krishnan, V., Estill-Terpack, S. J., Diamond, M., Chopra, R., Bailey, R. M., & Shah, B. R. (2025). Nitrous oxide enhances MR-guided focused ultrasound delivery of gene therapy to the murine hippocampus. *Gene Therapy*. https://doi.org/10.1038/s41434-025-00530-z

Blesa, J., Pineda-Pardo, J. A., Inoue, K., Gasca-Salas, C., Balzano, T., Del Rey, N. L., Reinares-Sebastián, A., Esteban-García, N., Rodríguez-Rojas, R., Márquez, R., Ciorraga, M., Del Álamo, M., García-Cañamaque, L., De Aguiar, S. R., Rachmilevitch, I., Trigo-Damas, I., Takada, M., & Obeso, J. A. (2023). BBB opening with focused ultrasound in nonhuman primates and Parkinson's disease patients: Targeted AAV vector delivery and PET imaging. *Science Advances*, *9*(16). https://doi.org/10.1126/sciadv.adf4888

Burr, A., Erickson, P., Bento, R., Shama, K., Roth, C., & Parekkadan, B. (2022). Allometric-like scaling of AAV gene therapy for systemic protein delivery. *Molecular Therapy — Methods & Clinical Development*, *27*, 368–379. https://doi.org/10.1016/j.omtm.2022.10.011

Buss, N., Lanigan, L., Zeller, J., Cissell, D., Metea, M., Adams, E., Higgins, M., Kim, K. H., Budzynski, E., Yang, L., Liu, Y., Butt, M., Danos, O., & Fiscella, M. (2022). Characterization of AAV-mediated dorsal root ganglionopathy. *Molecular Therapy — Methods & Clinical Development*, *24*, 342–354. https://doi.org/10.1016/j.omtm.2022.01.013

Chen, H., & Konofagou, E. E. (2014). The Size of Blood–Brain Barrier Opening Induced by Focused Ultrasound is Dictated by the Acoustic Pressure. *Journal of Cerebral Blood Flow & Metabolism*, *34*(7), 1197–1204. https://doi.org/10.1038/jcbfm.2014.71

Choi, J. J., Pernot, M., Small, S. A., & Konofagou, E. E. (2006). Noninvasive, transcranial and localized opening of the blood-brain barrier using focused ultrasound in mice. *Ultrasound in Medicine & Biology*, *33*(1), 95–104. https://doi.org/10.1016/j.ultrasmedbio.2006.07.018

Choi, J. J., Selert, K., Gao, Z., Samiotaki, G., Baseri, B., & Konofagou, E. E. (2010). Noninvasive and Localized Blood—Brain Barrier Disruption using Focused Ultrasound can be Achieved at Short Pulse Lengths and Low Pulse Repetition Frequencies. *Journal of Cerebral Blood Flow & Metabolism*, *31*(2), 725–737. https://doi.org/10.1038/jcbfm.2010.155

Dalkara, D., Byrne, L. C., Klimczak, R. R., Visel, M., Yin, L., Merigan, W. H., Flannery, J. G., & Schaffer, D. V. (2013). In Vivo–Directed Evolution of a New Adeno-Associated Virus for Therapeutic Outer Retinal Gene Delivery from the Vitreous. *Science Translational Medicine*, *5*(189). https://doi.org/10.1126/scitranslmed.3005708

Day, J. W., Finkel, R. S., Chiriboga, C. A., Connolly, A. M., Crawford, T. O., Darras, B. T., Iannaccone, S. T., Kuntz, N. L., Peña, L. D. M., Shieh, P. B., Smith, E. C., Kwon, J. M., Zaidman, C. M., Schultz, M., Feltner, D. E., Tauscher-Wisniewski, S., Ouyang, H., Chand, D. H., Sproule, D. M., . . . Mendell, J. R. (2021). Onasemnogene abeparvovec gene therapy for symptomatic infantile-onset spinal muscular atrophy in patients with two copies of SMN2 (STR1VE): an open-label, single-arm, multicentre, phase 3 trial. *The Lancet Neurology*, *20*(4), 284–293. https://doi.org/10.1016/s1474-4422(21)00001-6

Eldridge, M. a. G., Lerchner, W., Saunders, R. C., Kaneko, H., Krausz, K. W., Gonzalez, F. J., Ji, B., Higuchi, M., Minamimoto, T., & Richmond, B. J. (2015). Chemogenetic disconnection of monkey orbitofrontal and rhinal cortex reversibly disrupts reward value. *Nature Neuroscience*, *19*(1), 37–39. https://doi.org/10.1038/nn.4192

Felix, M., Borloz, E., Metwally, K., Dauba, A., Larrat, B., Matagne, V., Ehinger, Y., Villard, L., Novell, A., Mensah, S., & Roux, J. (2021). Ultrasound-Mediated Blood-Brain barrier opening improves whole brain gene delivery in mice. *Pharmaceutics*, *13*(8), 1245. https://doi.org/10.3390/pharmaceutics13081245

Gaudet, D., Méthot, J., Déry, S., Brisson, D., Essiembre, C., Tremblay, G., Tremblay, K., De Wal, J., Twisk, J., Van Den Bulk, N., Sier-Ferreira, V., & Van Deventer, S. (2012). Efficacy and long-term safety of alipogene tiparvovec (AAV1-LPLS447X) gene therapy for lipoprotein lipase deficiency: an open-label trial. *Gene Therapy*, *20*(4), 361–369. https://doi.org/10.1038/gt.2012.43

Gong, Y., Mu, D., Prabhakar, S., Moser, A., Musolino, P., Ren, J., Breakefield, X. O., Maguire, C. A., & Eichler, F. S. (2015). Adenoassociated virus Serotype 9-Mediated gene therapy for X-Linked adrenoleukodystrophy. *Molecular Therapy*, *23*(5), 824–834. https://doi.org/10.1038/mt.2015.6

Harrison, P. T., & Friedmann, T. (2023). Cost of gene therapy. *Gene Therapy*, *30*(10–11), 737. https://doi.org/10.1038/s41434-023-00408-y

High, K. A., George, L. A., Eyster, M. E., Sullivan, S. K., Ragni, M. V., Croteau, S. E., Samelson-Jones, B. J., Evans, M., Joseney-Antoine, M., Macdougall, A., Kadosh, J., Runoski, A. R., Campbell-Baird, C., Douglas, K., Tompkins, S., Hait, H., Couto, L. B., Bassiri, A. E., Valentino, L. A., . . . Reape, K. B. (2018). A phase 1/2 trial of investigational SPK-8011 in hemophilia A demonstrates durable expression and prevention of bleeds. *Blood*, *132*(Supplement 1), 487. https://doi.org/10.1182/blood-2018-99-115495

High-dose AAV gene therapy deaths. (2020). *Nature Biotechnology*, *38*(8), 910. https://doi.org/10.1038/s41587-020-0642-9

Hinderer, C., Katz, N., Buza, E. L., Dyer, C., Goode, T., Bell, P., Richman, L. K., & Wilson, J. M. (2018). Severe toxicity in nonhuman primates and piglets following High-Dose Intravenous administration of an Adeno-Associated virus vector expressing human SMN. *Human Gene Therapy*, *29*(3), 285–298. https://doi.org/10.1089/hum.2018.015

Hordeaux, J., Wang, Q., Katz, N., Buza, E. L., Bell, P., & Wilson, J. M. (2018). The neurotropic properties of AAV-PHP.B are limited to C57BL/6J mice. *Molecular Therapy*, *26*(3), 664–668. https://doi.org/10.1016/j.ymthe.2018.01.018

Hsu, P., Wei, K., Huang, C., Wen, C., Yen, T., Liu, C., Lin, Y., Chen, J., Shen, C., & Liu, H. (2013). Noninvasive and Targeted Gene Delivery into the Brain Using Microbubble-Facilitated Focused Ultrasound. *PLoS ONE*, *8*(2), e57682. https://doi.org/10.1371/journal.pone.0057682

Hudry, E., & Vandenberghe, L. H. (2019). Therapeutic AAV gene transfer to the nervous system: a clinical reality. *Neuron*, *101*(5), 839–862. https://doi.org/10.1016/j.neuron.2019.02.017

Jun-Ichi, M., Satoshi, T., Kimi, A., Fumi, T., Akira, T., Kiyoshi, T., & Ken-Ichi, Y. (1989). Expression vector system based on the chicken β-actin promoter directs efficient production of interleukin-5. *Gene*, *79*(2), 269–277. https://doi.org/10.1016/0378-1119(89)90209-6

Karakatsani, M. E., Blesa, J., & Konofagou, E. E. (2019). Blood–brain barrier opening with focused ultrasound in experimental models of Parkinson's disease. *Movement Disorders*, *34*(9), 1252–1261. https://doi.org/10.1002/mds.27804

Kishimoto, T. K., & Samulski, R. J. (2022). Addressing high dose AAV toxicity – 'one and done' or 'slower and lower'? *Expert Opinion on Biological Therapy*, *22*(9), 1067–1071. https://doi.org/10.1080/14712598.2022.2060737

Kofoed, R. H., Dibia, C. L., Noseworthy, K., Xhima, K., Vacaresse, N., Hynynen, K., & Aubert, I. (2022). Efficacy of gene delivery to the brain using AAV and ultrasound depends on serotypes and brain areas. *Journal of Controlled Release*, *351*, 667–680. https://doi.org/10.1016/j.jconrel.2022.09.048

Kumar, S. R., Miles, T. F., Chen, X., Brown, D., Dobreva, T., Huang, Q., Ding, X., Luo, Y., Einarsson, P. H., Greenbaum, A., Jang, M. J., Deverman, B. E., & Gradinaru, V. (2020). Multiplexed Cre-dependent selection yields systemic AAVs for targeting distinct brain cell types. *Nature Methods*, *17*(5), 541–550. https://doi.org/10.1038/s41592-020-0799-7

Li, C., & Samulski, R. J. (2020). Engineering adeno-associated virus vectors for gene therapy. *Nature Reviews Genetics*, *21*(4), 255–272. https://doi.org/10.1038/s41576-019-0205-4

Lipsman, N., Meng, Y., Bethune, A. J., Huang, Y., Lam, B., Masellis, M., Herrmann, N., Heyn, C., Aubert, I., Boutet, A., Smith, G. S., Hynynen, K., & Black, S. E. (2018). Blood–brain barrier opening in Alzheimer's disease using MR-guided focused ultrasound. *Nature Communications*, *9*(1). https://doi.org/10.1038/s41467-018-04529-6

Lock, M., McGorray, S., Auricchio, A., Ayuso, E., Beecham, E. J., Blouin-Tavel, V., Bosch, F., Bose, M., Byrne, B. J., Caton, T., Chiorini, J. A., Chtarto, A., Clark, K. R., Conlon, T., Darmon, C., Doria, M., Douar, A., Flotte, T. R., Francis, J. D., . . . Snyder, R. O. (2010). Characterization of a recombinant Adeno-Associated virus Type 2 reference standard material. *Human Gene Therapy*, *21*(10), 1273–1285. https://doi.org/10.1089/hum.2009.223

Lukashchuk, V., Lewis, K. E., Coldicott, I., Grierson, A. J., & Azzouz, M. (2016). AAV9-mediated central nervous system–targeted gene delivery via cisterna magna route in mice. *Molecular Therapy — Methods & Clinical Development*, *3*, 15055. https://doi.org/10.1038/mtm.2015.55

Maguire, A. M., Russell, S., Wellman, J. A., Chung, D. C., Yu, Z., Tillman, A., Wittes, J., Pappas, J., Elci, O., Marshall, K. A., McCague, S., Reichert, H., Davis, M., Simonelli, F., Leroy, B. P., Wright, J. F., High, K. A., & Bennett, J. (2019). Efficacy, safety, and durability of Voretigene Neparvovec-RZYL in RPE65 Mutation–Associated inherited retinal dystrophy. *Ophthalmology*, *126*(9), 1273–1285. https://doi.org/10.1016/j.ophtha.2019.06.017

Maheshri, N., Koerber, J. T., Kaspar, B. K., & Schaffer, D. V. (2006). Directed evolution of adeno-associated virus yields enhanced gene delivery vectors. *Nature Biotechnology*, *24*(2), 198–204. https://doi.org/10.1038/nbt1182

Marsic, D., Govindasamy, L., Currlin, S., Markusic, D. M., Tseng, Y., Herzog, R. W., Agbandje-McKenna, M., & Zolotukhin, S. (2014). Vector Design Tour de Force: Integrating Combinatorial and Rational Approaches to Derive Novel Adeno-associated Virus Variants. *Molecular Therapy*, *22*(11), 1900–1909. https://doi.org/10.1038/mt.2014.139

McDannold, N., Vykhodtseva, N., & Hynynen, K. (2006). Targeted disruption of the blood–brain barrier with focused ultrasound: association with cavitation activity. *Physics in Medicine and Biology*, *51*(4), 793–807. https://doi.org/10.1088/0031-9155/51/4/003

McMahon, D., Bendayan, R., & Hynynen, K. (2017). Acute effects of focused ultrasound-induced increases in blood-brain barrier permeability on rat microvascular transcriptome. *Scientific Reports*, *7*(1). https://doi.org/10.1038/srep45657

McMahon, D., O'Reilly, M. A., & Hynynen, K. (2021). Therapeutic agent delivery across the Blood–Brain barrier using focused ultrasound. *Annual Review of Biomedical Engineering*, *23*(1), 89–113. https://doi.org/10.1146/annurev-bioeng-062117-121238

Mingozzi, F., & High, K. A. (2013). Immune responses to AAV vectors: overcoming barriers to successful gene therapy. *Blood*, *122*(1), 23–36. https://doi.org/10.1182/blood-2013-01-306647

Nouraein, S., Lee, S., Saenz, V. A., Del Mundo, H. C., Yiu, J., & Szablowski, J. O. (2023). Acoustically targeted noninvasive gene therapy in large brain volumes. *Gene Therapy*, *31*(3–4), 85–94. https://doi.org/10.1038/s41434-023-00421-1

Ojala, D. S., Sun, S., Santiago-Ortiz, J. L., Shapiro, M. G., Romero, P. A., & Schaffer, D. V. (2017). In vivo selection of a computationally designed SCHEMA AAV library yields a novel variant for infection of adult neural stem cells in the SVZ. *Molecular Therapy*, *26*(1), 304–319. https://doi.org/10.1016/j.ymthe.2017.09.006

O'Reilly, M. A., & Hynynen, K. (2012). Blood-Brain barrier: real-time feedback-controlled focused ultrasound disruption by using an acoustic emissions–based controller. *Radiology*, *263*(1), 96–106. https://doi.org/10.1148/radiol.11111417

Pipe, S., Leebeek, F. W., Ferreira, V., Sawyer, E. K., & Pasi, J. (2019). Clinical Considerations for CAPSID choice in the development of Liver-Targeted AAV-Based Gene Transfer. *Molecular Therapy — Methods & Clinical Development*, *15*, 170–178. https://doi.org/10.1016/j.omtm.2019.08.015

Pipe, S. W., Leebeek, F. W., Recht, M., Key, N. S., Castaman, G., Miesbach, W., Lattimore, S., Peerlinck, K., Van Der Valk, P., Coppens, M., Kampmann, P., Meijer, K., O'Connell, N., Pasi, K. J., Hart, D. P., Kazmi, R., Astermark, J., Hermans, C. R., Klamroth, R., . . . Monahan, P. E. (2023). Gene Therapy with Etranacogene Dezaparvovec for Hemophilia B. *New England Journal of Medicine*, *388*(8), 706–718. https://doi.org/10.1056/nejmoa2211644

Poon, C., McMahon, D., & Hynynen, K. (2016). Noninvasive and targeted delivery of therapeutics to the brain using focused ultrasound. *Neuropharmacology*, *120*, 20–37. https://doi.org/10.1016/j.neuropharm.2016.02.014

Powell, S. K., Khan, N., Parker, C. L., Samulski, R. J., Matsushima, G., Gray, S. J., & McCown, T. J. (2016). Characterization of a novel adeno-associated viral vector with preferential oligodendrocyte tropism. *Gene Therapy*, *23*(11), 807–814. https://doi.org/10.1038/gt.2016.62

Rezai, A. R., Ranjan, M., D'Haese, P., Haut, M. W., Carpenter, J., Najib, U., Mehta, R. I., Chazen, J. L., Zibly, Z., Yates, J. R., Hodder, S. L., & Kaplitt, M. (2020). Noninvasive hippocampal blood−brain barrier opening in Alzheimer's disease with focused ultrasound. *Proceedings of the National Academy of Sciences*, *117*(17), 9180–9182. https://doi.org/10.1073/pnas.2002571117

Rubin, J. D., Nguyen, T. V., Allen, K. L., Ayasoufi, K., & Barry, M. A. (2019). Comparison of gene delivery to the kidney by adenovirus, Adeno-Associated virus, and lentiviral vectors after intravenous and direct kidney injections. *Human Gene Therapy*, *30*(12), 1559–1571. https://doi.org/10.1089/hum.2019.127

Sabatino, D. E., Bushman, F. D., Chandler, R. J., Crystal, R. G., Davidson, B. L., Dolmetsch, R., Eggan, K. C., Gao, G., Gil-Farina, I., Kay, M. A., McCarty, D. M., Montini, E., Ndu, A., & Yuan, J. (2022). Evaluating the state of the science for adeno-associated virus integration: An integrated perspective. *Molecular Therapy*, *30*(8), 2646–2663. https://doi.org/10.1016/j.ymthe.2022.06.004

Sheikov, N., McDannold, N., Vykhodtseva, N., Jolesz, F., & Hynynen, K. (2004). Cellular mechanisms of the blood-brain barrier opening induced by ultrasound in presence of microbubbles. *Ultrasound in Medicine & Biology*, *30*(7), 979–989. https://doi.org/10.1016/j.ultrasmedbio.2004.04.010

Sun, C., Wu, T., Chen, C., Wu, P., Shih, Y., Tsuneyama, K., & Tao, M. (2013). Studies of efficacy and liver toxicity related to Adeno-Associated Virus–Mediated RNA interference. *Human Gene Therapy*, *24*(8), 739–750. https://doi.org/10.1089/hum.2012.239

Szablowski, J. O., Lee-Gosselin, A., Lue, B., Malounda, D., & Shapiro, M. G. (2018). Acoustically targeted chemogenetics for the non-invasive control of neural circuits. *Nature Biomedical Engineering*, *2*(7), 475–484. https://doi.org/10.1038/s41551-018-0258-2

Tervo, D. G. R., Hwang, B., Viswanathan, S., Gaj, T., Lavzin, M., Ritola, K. D., Lindo, S., Michael, S., Kuleshova, E., Ojala, D., Huang, C., Gerfen, C. R., Schiller, J., Dudman, J. T., Hantman, A. W., Looger, L. L., Schaffer, D. V., & Karpova, A. Y. (2016). A designer AAV variant permits efficient retrograde access to projection neurons. *Neuron*, *92*(2), 372–382. https://doi.org/10.1016/j.neuron.2016.09.021

Thévenot, E., Jordão, J. F., O'Reilly, M. A., Markham, K., Weng, Y., Foust, K. D., Kaspar, B. K., Hynynen, K., & Aubert, I. (2012). Targeted delivery of Self-Complementary Adeno-Associated virus serotype 9 to the brain, using magnetic resonance Imaging-Guided focused ultrasound. *Human Gene Therapy*, *23*(11), 1144–1155. https://doi.org/10.1089/hum.2012.013

Upright, N. A., & Baxter, M. G. (2020). Effect of chemogenetic actuator drugs on prefrontal cortex-dependent working memory in nonhuman primates. *Neuropsychopharmacology*, *45*(11), 1793–1798. https://doi.org/10.1038/s41386-020-0660-9

Wang, S., Kugelman, T., Buch, A., Herman, M., Han, Y., Karakatsani, M. E., Hussaini, S. A., Duff, K., & Konofagou, E. E. (2017). Non-invasive, focused Ultrasound-Facilitated gene delivery for optogenetics. *Scientific Reports*, *7*(1). https://doi.org/10.1038/srep39955

Wang, S., Olumolade, O. O., Sun, T., Samiotaki, G., & Konofagou, E. E. (2014). Noninvasive, neuron-specific gene therapy can be facilitated by focused

ultrasound and recombinant adeno-associated virus. *Gene Therapy*, *22*(1), 104–110. https://doi.org/10.1038/gt.2014.91

Weber, T. (2021). Anti-AAV antibodies in AAV gene therapy: current challenges and possible solutions. *Frontiers in Immunology*, *12*. https://doi.org/10.3389/fimmu.2021.658399

Weitzman, M. D., & Linden, R. M. (2011). Adeno-Associated Virus Biology. *Methods in Molecular Biology*, 1–23. https://doi.org/10.1007/978-1-61779-370-7_1

White, J., Clement, G., & Hynynen, K. (2005). Transcranial ultrasound focus reconstruction with phase and amplitude correction. *IEEE Transactions on Ultrasonics Ferroelectrics and Frequency Control*, *52*(9), 1518–1522. https://doi.org/10.1109/tuffc.2005.1516024

Yue, Y., Ghosh, A., Long, C., Bostick, B., Smith, B. F., Kornegay, J. N., & Duan, D. (2008). A single intravenous injection of adeno-associated virus serotype-9 leads to whole body skeletal muscle transduction in dogs. *Molecular Therapy*, *16*(12), 1944–1952. https://doi.org/10.1038/mt.2008.207

Zincarelli, C., Soltys, S., Rengo, G., & Rabinowitz, J. E. (2008). Analysis of AAV serotypes 1–9 Mediated gene expression and tropism in mice after systemic injection. *Molecular Therapy*, *16*(6), 1073–1080. https://doi.org/10.1038/mt.2008.76

Arjomandnejad, M., Dasgupta, I., Flotte, T., & Keeler, A. (2023). Immunogenicity of recombinant adeno-associated virus (aav) vectors for gene transfer. *Biodrugs*, 37(3), 311-329. https://doi.org/10.1007/s40259-023-00585-7

Armbruster, N., Lattanzi, A., Jeavons, M., Wittenberghe, L., Gjata, B., Marais, T., … & Buj-Bello, A. (2016). Efficacy and biodistribution analysis of intracerebroventricular administration of an optimized scaav9-smn1 vector in a mouse model of spinal muscular atrophy. *Molecular Therapy — Methods & Clinical Development*, 3, 16060. https://doi.org/10.1038/mtm.2016.60

Au, H., Isalan, M., & Mielcarek, M. (2022). Gene therapy advances: a meta-analysis of aav usage in clinical settings. *Frontiers in Medicine*, 8. https://doi.org/10.3389/fmed.2021.809118

Chen, Z., Yang, L., Zhang, Y., Li, Y., Chen, G., Wang, Z., … & Guo, Y. (2024). A drug-elicitable alternative-splicing module (dream) for tunable aav expression and controlled myocardial regeneration.. https://doi.org/10.1101/2024.07.01.601517

García-Olloqui, P., Rodriguez-Madoz, J., Scala, M., Abizanda, G., Vales, Á., Olagüe, C., … & Pelacho, B. (2019). Effect of heart ischemia and administration route on biodistribution and transduction efficiency of aav9 vectors. *Journal of Tissue Engineering and Regenerative Medicine*, 14(1), 123-134. https://doi.org/10.1002/term.2974

Kuranda, K., Jean-Alphonse, P., Leborgne, C., Hardet, R., Collaud, F., Marmier, S., … & Mingozzi, F. (2018). Exposure to wild-type aav drives distinct capsid immunity profiles in humans. *Journal of Clinical Investigation*, 128(12), 5267-5279. https://doi.org/10.1172/jci122372

Mullagulova, A., Shaimardanova, A., Solovyeva, V., Mukhamedshina, Y., Chulpanova, D., Kostennikov, A., … & Rizvanov, A. (2023). Safety and efficacy of intravenous and intrathecal delivery of aav9-mediated arsa in minipigs. *International Journal of Molecular Sciences*, 24(11), 9204. https://doi.org/10.3390/ijms24119204

Watano, R., Ohmori, T., Hishikawa, S., Sakata, A., & Mizukami, H. (2020). Utility of microminipigs for evaluating liver-mediated gene expression in the presence of neutralizing antibody against vector capsid. *Gene Therapy*, 27(9), 427-434. https://doi.org/10.1038/s41434-020-0125-0

Xu, Y., Bai, X., Lin, J., Wu, Y., Weng, S., Li, H., … & Li, W. (2024). Antibodies against the capsid induced after intracranial aav administration limits second administration in a dose dependent manner.. https://doi.org/10.1101/2024.09.15.612566

Zhang, Y., Li, H., Min, Y., Sanchez-Ortiz, E., Huang, J., Mireault, A., … & Olson, E. (2020). Enhanced crispr-cas9 correction of duchenne muscular dystrophy in mice by a self-complementary aav delivery system. *Science Advances*, 6(8). https://doi.org/10.1126/sciadv.aay6812

Castle, M., Baltanás, F., Kovács, I., Nagahara, A., Barba, D., & Tuszynski, M. (2020). Postmortem analysis in a clinical trial of aav2-ngf gene therapy for alzheimer's disease identifies a need for improved vector delivery. *Human Gene Therapy*, 31(7-8), 415-422. https://doi.org/10.1089/hum.2019.367

Hang, Y., Aburidi, M., Husain, B., Hickman, A., Poehlman, W., & Feltus, F. (2020). Exploration into biomarker potential of region-specific brain gene co-expression networks. *Scientific Reports*, 10(1). https://doi.org/10.1038/s41598-020-73611-1

Kofoed, R., Noseworthy, K., Wu, K., Vecchio, L., Dibia, C., Sivadas, S., … & Aubert, I. (2024). Focused ultrasound increases gene delivery to deep brain structure following the administration of a recombinant adeno-associated virus in the cerebrospinal fluid.. https://doi.org/10.1101/2024.02.09.579587

Leib, D., Chen, Y., Tecedor, L., Ranum, P., Keiser, M., Lewandowski, B., … & Davidson, B. (2024). Optimized aav capsids for diseases of the basal ganglia show robust potency and distribution in adult nonhuman primates.. https://doi.org/10.1101/2024.05.02.592211

Noroozian, Z., Xhima, K., Huang, Y., Kaspar, B., Kügler, S., Hynynen, K., … & Aubert, I. (2019). Mri-guided focused ultrasound for targeted delivery of raav to the brain., 177-197. https://doi.org/10.1007/978-1-4939-9139-6_10

Raghunathan, R., Polinski, N., Klein, J., Hogan, J., Chun, S., Khatri, K., … & Zaia, J. (2018). Glycomic and proteomic changes in aging brain nigrostriatal pathway. *Molecular & Cellular Proteomics*, 17(9), 1778-1787. https://doi.org/10.1074/mcp.ra118.000680

Seo, J., Trippett, J., Huang, Z., Wang, R., Lee, S., & Szablowski, J. (2023). Acoustically-targeted measurement of transgene expression in the brain.. https://doi.org/10.1101/2023.05.23.541868

Torregrosa, T., Lehman, S., Hana, S., Marsh, G., Xu, S., Koszka, K., … & Lo, S. (2021). Use of crispr/cas9-mediated disruption of cns cell type genes to profile transduction of aav by neonatal intracerebroventricular delivery in mice. *Gene Therapy*, 28(7-8), 456-468. https://doi.org/10.1038/s41434-021-00223-3

Tuszynski, M., Yang, J., Barba, D., Hoi-Sang, U., Bakay, R., Pay, M., … & Nagahara, A. (2015). Nerve growth factor gene therapy. *Jama Neurology*, 72(10), 1139. https://doi.org/10.1001/jamaneurol.2015.1807

Research, C. F. B. E. A. (2024, November 21). Frequently asked questions — Developing potential cellular and gene therapy products. U.S. Food And Drug Administration. https://www.fda.gov/regulatory-information/search-fda-guidance-documents/frequently-asked-questions-developing-potential-cellular-and-gene-therapy-products

Ngugi AK, Bottomley C, Kleinschmidt I, Sander JW and Newton CR. (2010). Estimation of the burden of active and life-time epilepsy: a meta-analytic approach. Epilepsia. 51:883-890. https://doi.org/10.1111/j.1528-1167.2009.02481.x

Lee DJ, Gurkoff GG, Izadi A, Seidl SE, Echeverri A, Melnik M, Berman RF, Ekstrom AD, Muizelaar JP, Lyeth BG and Shahlaie K. (2015). Septohippocampal Neuromodulation Improves Cognition after Traumatic Brain Injury. J Neurotrauma. 32:1822-1832. https://doi.org/10.1089/neu.2015.3948

Lee DJ, Izadi A, Melnik M, Seidl S, Echeverri A, Shahlaie K and Gurkoff GG. (2017). Stimulation of the medial septum improves performance in spatial learning following pilocarpine-induced status epilepticus. Epilepsy Res. 130:53-63. https://doi.org/10.1016/j.eplepsyres.2017.01.010

Lee DJ, Gurkoff GG, Izadi A, Berman RF, Ekstrom AD, Muizelaar JP, Lyeth BG and Shahlaie K. (2013). Medial septal nucleus theta frequency deep brain stimulation improves spatial working memory after traumatic brain injury. J Neurotrauma. 30:131-139. https://doi.org/10.1089/neu.2012.2530

Ponds RW and Hendriks M. (2006). Cognitive rehabilitation of memory problems in patients with epilepsy. Seizure. 15:267-273. https://doi.org/10.1016/j.seizure.2006.02.008

Salanova V, Witt T, Worth R, Henry TR, Gross RE, Nazzaro JM, Labar D, Sperling MR, Sharan A, Sandok E, Handforth A, Stern JM, Chung S, Henderson JM, French J, Baltuch G, Rosenfeld WE, Garcia P, Barbaro NM, Fountain NB, Elias WJ, Goodman RR, Pollard JR, Troster AI, Irwin CP, Lambrecht K, Graves N, Fisher R and Group SS. (2015). Long-term efficacy and safety of thalamic stimulation for drug-resistant partial epilepsy. Neurology. 84:1017-1025. https://doi.org/10.1212/WNL.0000000000001334

Yang JC, Bullinger KL, Isbaine F, Alwaki A, Opri E, Willie JT and Gross RE. (2022). Centromedian thalamic deep brain stimulation for drug-resistant epilepsy: single-center experience. Journal of neurosurgery. 137:1591-1600. https://doi.org/10.3171/2021.10.JNS211372

Vertes RP. (2005). Hippocampal theta rhythm: a tag for short-term memory. Hippocampus. 15:923-935. https://doi.org/10.1002/hipo.20118

Zepeda NC, Crown LM, Medvidovic S, Choi W, Sheth M, Bergosh M, Gifford R, Folz C, Lam P, Lu G, Featherstone R, Liu CY, Siegel SJ and Lee DJ. (2022). Frequency-specific medial septal nucleus deep brain stimulation improves spatial memory in MK-801-treated male rats. Neurobiol Dis. 170:105756. https://doi.org/10.1016/j.nbd.2022.105756

Izadi A, Pevzner A, Lee DJ, Ekstrom AD, Shahlaie K and Gurkoff GG. (2019). Medial septal stimulation increases seizure threshold and improves cognition in epileptic rats. Brain Stimul. 12:735-742. https://doi.org/10.1016/j.brs.2018.12.225

Izadi A, Schedlbauer A, Ondek K, Disse G, Ekstrom AD, Cowen SL, Shahlaie K and Gurkoff GG. (2021). Early Intervention via Stimulation of the Medial Septal Nucleus Improves Cognition and Alters Markers of Epileptogenesis in Pilocarpine-Induced Epilepsy. Front Neurol. 12:708957. https://doi.org/10.3389/fneur.2021.708957

Chauviere L, Rafrafi N, Thinus-Blanc C, Bartolomei F, Esclapez M and Bernard C. (2009). Early deficits in spatial memory and theta rhythm in experimental temporal lobe epilepsy. J Neurosci. 29:5402-5410. https://doi.org/10.1523/JNEUROSCI.4699-08.2009

Szablowski JO, Lee-Gosselin A, Lue B, Malounda D and Shapiro MG. (2018). Acoustically targeted chemogenetics for the non-invasive control of neural circuits. Nat Biomed Eng. 2:475-484. https://doi.org/10.1038/s41551-018-0233-8

Carpentier A, Canney M, Vignot A, Reina V, Beccaria K, Horodyckid C, Karachi C, Leclercq D, Lafon C, Chapelon JY, Capelle L, Cornu P, Sanson M, Hoang-Xuan K, Delattre JY and Idbaih A. (2016). Clinical trial of blood-brain barrier disruption by pulsed ultrasound. Science Translational Medicine. 8:343re342. https://doi.org/10.1126/scitranslmed.aaf6086

Elias WJ, Lipsman N, Ondo WG, Ghanouni P, Kim YG, Lee W, Schwartz M, Hynynen K, Lozano AM, Shah BB, Huss D, Dallapiazza RF, Gwinn R, Witt J, Ro S, Eisenberg HM, Fishman PS, Gandhi D, Halpern CH, Chuang R, Butts Pauly K, Tierney TS, Hayes MT, Cosgrove GR, Yamaguchi T, Abe K, Taira T and Chang JW. (2016). A Randomized Trial of Focused Ultrasound Thalamotomy for Essential Tremor. The New England Journal of Medicine. 375:730-739. https://doi.org/10.1056/NEJMoa1600159

Dobrakowski PP, Machowska-Majchrzak AK, Labuz-Roszak B, Majchrzak KG, Kluczewska E and Pierzchala KB. (2014). MR-guided focused ultrasound: a new generation treatment of Parkinson's disease, essential tremor and neuropathic pain. Interv Neuroradiol. 20:275-282. https://doi.org/10.15274/INR-2014-10023

Hynynen K, McDannold N, Vykhodtseva N and Jolesz FA. (2001). Noninvasive MR imaging-guided focal opening of the blood-brain barrier in rabbits. Radiology. 220:640-646. https://doi.org/10.1148/radiol.2202001804

Tung YS, Vlachos F, Feshitan JA, Borden MA and Konofagou EE. (2011). The mechanism of interaction between focused ultrasound and microbubbles in blood-brain barrier opening in mice. J Acoust Soc Am. 130:3059-3067. https://doi.org/10.1121/1.3646905

Samiotaki G, Acosta C, Wang S and Konofagou EE. (2015). Enhanced delivery and bioactivity of the neurturin neurotrophic factor through focused ultrasound-mediated blood-brain barrier opening in vivo. J Cereb Blood Flow Metab. 35:611-622. https://doi.org/10.1038/jcbfm.2014.240

O'Reilly MA and Hynynen K. (2012). Ultrasound enhanced drug delivery to the brain and central nervous system. Int J Hyperthermia. 28:386-396. https://doi.org/10.3109/02656736.2012.666709

Thevenot E, Jordao JF, O'Reilly MA, Markham K, Weng YQ, Foust KD, Kaspar BK, Hynynen K and Aubert I. (2012). Targeted delivery of self-complementary adeno-associated virus serotype 9 to the brain, using magnetic resonance imaging-guided focused ultrasound. Hum Gene Ther. 23:1144-1155. https://doi.org/10.1089/hum.2012.013

Wang S, Olumolade OO, Sun T, Samiotaki G and Konofagou EE. (2015). Non-invasive, neuron-specific gene therapy can be facilitated by focused ultrasound and recombinant adeno-associated virus. Gene Ther. 22:104-110. https://doi.org/10.1038/gt.2014.91

Nance E, Timbie K, Miller GW, Song J, Louttit C, Klibanov AL, Shih T-Y, Swaminathan G, Tamargo RJ and Woodworth GF. (2014). Non-invasive delivery of stealth, brain-penetrating nanoparticles across the blood−brain barrier using MRI-guided focused ultrasound. J Control Release. 189:123-132. https://doi.org/10.1016/j.jconrel.2014.06.018

Clement GT and Hynynen K. (2002). A non-invasive method for focusing ultrasound through the human skull. Phys Med Biol. 47:1219-1236. https://doi.org/10.1088/0031-9155/47/8/303

Hsu PH, Wei KC, Huang CY, Wen CJ, Yen TC, Liu CL, Lin YT, Chen JC, Shen CR and Liu HL. (2013). Noninvasive and targeted gene delivery into the brain using microbubble-facilitated focused ultrasound. PLoS One. 8:e57682. https://doi.org/10.1371/journal.pone.0057682

McDannold N, Arvanitis CD, Vykhodtseva N and Livingstone MS. (2012). Temporary disruption of the blood–brain barrier by use of ultrasound and microbubbles: safety and efficacy evaluation in rhesus macaques. Cancer Res. 72:3652-3663. https://doi.org/10.1158/0008-5472.CAN-12-0128

Downs ME, Buch A, Sierra C, Karakatsani ME, Teichert T, Chen SS, Konofagou EE and Ferrera VP. (2015). Long-Term Safety of Repeated Blood-Brain Barrier Opening via Focused Ultrasound with Microbubbles in Non-Human Primates Performing a Cognitive Task (vol 10, e0125911, 2015). PLoS One. 10:e0125911. https://doi.org/10.1371/journal.pone.0125911

Tung Y-S, Marquet F, Teichert T, Ferrera V and Konofagou EE. (2011). Feasibility of noninvasive cavitation-guided blood-brain barrier opening using focused ultrasound and microbubbles in nonhuman primates. Appl Phys Lett. 98:163704. https://doi.org/10.1063/1.3580763

Strang, J., Volkow, N. D., Degenhardt, L., Hickman, M., Johnson, K., Koob, G. F., et al. (2020). Opioid use disorder. Nature Reviews Disease Primers, 6(1), 3. https://doi.org/10.1038/s41572-019-0137-0

Centers for Disease Control and Prevention. (2019). Understanding the epidemic | Drug overdose | CDC injury center. https://www.cdc.gov/drugoverdose

Case, A., & Deaton, A. (2015). Rising morbidity and mortality in midlife among white non-Hispanic Americans in the 21st century. Proceedings of the National Academy of Sciences, 112(49), 15078–15083. https://doi.org/10.1073/pnas.1518393112

Koob, G. F. (2020). Neurobiology of opioid addiction: Opponent process, hyperkatifeia, and negative reinforcement. Biological Psychiatry, 87(1), 44–53. https://doi.org/10.1016/j.biopsych.2019.05.023

Evans, C. J., & Cahill, C. M. (2016). Neurobiology of opioid dependence in creating addiction vulnerability. F1000Research, 5, 1748. https://doi.org/10.12688/f1000research.8369.1

Jones, C. M., Einstein, E. B., & Compton, W. M. (2018). Changes in synthetic opioid involvement in drug overdose deaths in the United States, 2010-2016. JAMA, 319(17), 1819–1821. https://doi.org/10.1001/jama.2018.2844

Schuckit, M. A. (2016). Treatment of opioid-use disorders. New England Journal of Medicine, 375(4), 357–368. https://doi.org/10.1056/NEJMra1604339

Carley, J. A., & Oesterle, T. (2021). Therapeutic approaches to opioid use disorder: What is the current standard of care? International Journal of General Medicine, 14, 2305–2311. https://doi.org/10.2147/IJGM.S299508

Lee, Y. K., Gold, M. S., Blum, K., Thanos, P. K., Hanna, C., & Fuehrlein, B. S. (2024). Opioid use disorder: Current trends and potential treatments. Frontiers in Public Health, 11, 1274719. https://doi.org/10.3389/fpubh.2023.1274719

Gold, M. S., Baron, D., Bowirrat, A., & Blum, K. (2020). Neurological correlates of brain reward circuitry linked to opioid use disorder (OUD): Do homo sapiens acquire or have a reward deficiency syndrome? Journal of the Neurological Sciences, 418, 117137. https://doi.org/10.1016/j.jns.2020.117137

Chang, V. N., & Peters, J. (2023). Neural circuits controlling choice behavior in opioid addiction. Neuropharmacology, 226, 109407. https://doi.org/10.1016/j.neuropharm.2022.109407

Blackwood, C. A., & Cadet, J. L. (2021). The molecular neurobiology and neuropathology of opioid use disorder. Current Research in Neurobiology, 2, 100023. https://doi.org/10.1016/j.crneuro.2021.100023

Herlinger, K., & Lingford-Hughes, A. (2022). Opioid use disorder and the brain: A clinical perspective. Addiction, 117(2), 495–505. https://doi.org/10.1111/add.15692

Koob, G. F., & Schulkin, J. (2019). Addiction and stress: An allostatic view. Neuroscience & Biobehavioral Reviews, 106, 245–262. https://doi.org/10.1016/j.neubiorev.2018.09.008

Carmack, S. A., Keeley, R. J., Vendruscolo, J. C. M., Lowery-Gionta, E. G., Lu, H., Koob, G. F., et al. (2019). Addiction engages negative emotional learning brain circuits in rats. Journal of Clinical Investigation, 129(6), 2480–2484. https://doi.org/10.1172/JCI127330

Roberto, M., Spierling, S. R., Kirson, D., & Zorrilla, E. P. (2017). Corticotropin-releasing factor (CRF) and addictive behaviors. In T. E. Thiele (Ed.), International Review of Neurobiology (Vol. 136, pp. 5–51). Academic Press. https://doi.org/10.1016/bs.irn.2017.06.002

Carmack, S. A., Vendruscolo, J. C. M., McGinn, M. A., et al. (2022). Corticosteroid sensitization drives opioid addiction. Molecular Psychiatry, 27(5), 2492–2501. https://doi.org/10.1038/s41380-022-01499-5

Szablowski, J. O., Lee-Gosselin, A., Lue, B., et al. (2018). Acoustically targeted chemogenetics for the non-invasive control of neural circuits. Nature Biomedical Engineering, 2(7), 475–484. https://doi.org/10.1038/s41551-018-0236-3

Li, H. R., Harb, M., Heath, J. E., Trippett, J. S., Shapiro, M. G., & Szablowski, J. O. (2024). Acoustically controlled neural modulation. Nature Communications, 15(1), 4924. https://doi.org/10.1038/s41467-024-4924

Kabisa, E., Biracyaza, E., Habagusenga, J., et al. (2021). Determinants and prevalence of relapse among patients with substance use disorders: Case of Icyizere Psychotherapeutic Centre. Substance Abuse Treatment, Prevention, and Policy, 16(1), 13. https://doi.org/10.1186/s13011-021-00355-3

Rahman, M. M., Rahaman, M., Hamadani, J., Mustafa, K., et al. (2016). Psycho-social factors associated with relapse to drug addiction in Bangladesh. Journal of Substance Use, 21(2), 2–7. https://doi.org/10.3109/14659891.2014.994211

Sinha, R. (2011). New findings on biological factors predicting addiction relapse vulnerability. Current Psychiatry Reports, 13(5), 398–405. https://doi.org/10.1007/s11920-011-0224-0

Srivastava, A. B., Mariani, J. J., & Levin, F. R. (2020). New directions in the treatment of opioid withdrawal. The Lancet, 395(10241), 1938–1948. https://doi.org/10.1016/S0140-6736(20)30852-7

Crummy, E. A., O'Neal, T. J., Baskin, B. M., & Ferguson, S. M. (2020). One is not enough: Understanding and modeling polysubstance use. Frontiers in Neuroscience, 14, 569. https://doi.org/10.3389/fnins.2020.00569

John, W. S., Zhu, H., Mannelli, P., Schwartz, R. P., Subramaniam, G. A., & Wu, L. T. (2018). Prevalence, patterns, and correlates of multiple substance use disorders among adult primary care patients. Drug and Alcohol Dependence, 187, 79–87. https://doi.org/10.1016/j.drugalcdep.2018.02.012

Wakeman, S. E., Larochelle, M. R., Ameli, O., et al. (2020). Comparative effectiveness of different treatment pathways for opioid use disorder. JAMA Network Open, 3(2), e1920622. https://doi.org/10.1001/jamanetworkopen.2019.20622

Alvarez-Bagnarol, Y., Marchette, R., Francis, C., Morales, M., & Vendruscolo, L. F. (2022). Neuronal correlates of hyperalgesia and somatic signs of heroin withdrawal in male and female mice. eNeuro, 9(4), ENEURO.0106-22. https://doi.org/10.1523/ENEURO.0106-22.2022

Moussawi, K., Ortiz, M. M., Gantz, S. C., Tunstall, B. J., Marchette, R. C. N., Bonci, A., Koob, G. F., & Vendruscolo, L. F. (2020). Fentanyl vapor self-administration model in mice to study opioid addiction. Science Advances, 6(32), eabc0413. https://doi.org/10.1126/sciadv.abc0413

American Psychiatric Association. (2022). Diagnostic and statistical manual of mental disorders (5th ed., text rev.). American Psychiatric Association Publishing.

el-Guebaly, N., Mudry, T., Zohar, J., Tavares, H., & Potenza, M. N. (2012). Compulsive features in behavioural addictions: The case of pathological gambling. Addiction, 107(10), 1726–1734. https://doi.org/10.1111/j.1360-0443.2011.03776.x

Robbins, T., Curran, H., & de Wit, H. (2012). Special issue on impulsivity and compulsivity. Psychopharmacology, 219(2), 251–252. https://doi.org/10.1007/s00213-011-2555-3

Moore, C. F., Sabino, V., Koob, G. F., & Cottone, P. (2019). Dissecting compulsive eating behavior into three elements. In Compulsive Eating Behavior and Food Addiction (pp. 41–81). Academic Press. https://doi.org/10.1016/B978-0-12-815760-7.00003-7

Marchette, R. C. N., Carlson, E. R., Said, N., Koob, G. F., & Vendruscolo, L. F. (2023). Extended access to fentanyl vapor self-administration leads to addiction-like behaviors in mice. Addiction Neuroscience, 5, 100057. https://doi.org/10.1016/j.addicn.2023.100057

Edwards, S., & Koob, G. F. (2023). Escalation of drug self-administration as a hallmark of persistent addiction liability. Behavioural Pharmacology, 24(5–6), 356–362. https://doi.org/10.1097/FBP.0000000000000112

Avery, S. N., Clauss, J. A., et al. (2016). The human BNST: Functional role in anxiety and addiction. Neuropsychopharmacology, 41(1), 126–141. https://doi.org/10.1038/npp.2015.185

Awasthi, S., Pan, H., LeDoux, J. E., et al. (2020). The bed nucleus of the stria terminalis and functionally linked neurocircuitry modulate emotion processing and HPA axis dysfunction in posttraumatic stress disorder. NeuroImage: Clinical, 28, 102442. https://doi.org/10.1016/j.nicl.2020.102442

Ch'ng, S., Fu, J., et al. (2018). The intersection of stress and reward: BNST modulation of aversive and appetitive states. Progress in Neuro-Psychopharmacology and Biological Psychiatry, 87(Pt A), 108–125. https://doi.org/10.1016/j.pnpbp.2017.10.005

Lebow, M. A., & Chen, A. (2016). Overshadowed by the amygdala: The bed nucleus of the stria terminalis emerges as key to psychiatric disorders. Molecular Psychiatry, 21(4), 450–463. https://doi.org/10.1038/mp.2015.1

Goode, T. D., & Maren, S. (2017). Role of the bed nucleus of the stria terminalis in aversive learning and memory. Learning & Memory, 24(9), 480–491. https://doi.org/10.1101/lm.044206.116

Zheng, X., et al. (2024). The role and mechanism of 5-HTDRN-BNST neural circuit in anxiety and fear lesions. Frontiers in Neuroscience, 18, 1362899. https://doi.org/10.3389/fnins.2024.1362899

Nagai, Y., Miyakawa, N., Takuwa, H., et al. (2020). Deschloroclozapine, a potent and selective chemogenetic actuator enables rapid neuronal and behavioral modulations in mice and monkeys. Nature Neuroscience, 23(9), 1157–1167. https://doi.org/10.1038/s41593-020-0655-9

Ling, Q., Herstine, J. A., Bradbury, A., & Gray, S. J. (2023). AAV-based in vivo gene therapy for neurological disorders. Nature Reviews Drug Discovery, 22(10), 789–806. https://doi.org/10.1038/s41573-023-00781-3